# Investigation of the Role of BCR/ABL1 in Neutrophil Extracellular Trap (NET) Formation in Chronic Myeloid Leukemia (CML)

**Emilia Wold Poleo**

This thesis is submitted in partial fulfilment of the requirements for the degree of Master in Biomedical Sciences

Department of Biomedicine and Department of Clinical Science

University of Bergen

June 2022

# Acknowledgements

Firstly, I would like to express my sincere gratitude to my supervisors Maria Omsland and Vibeke Andresen for their continuous support with my master's project. Maria, for all the hours she spent with me in the lab teaching me everything I know about lab work and for her caring and support during this year. Thank you for always answering my questions and helping me all the times I was lost. Vibeke, for her generous contribution and feedback throughout this year, for sharing her immense scientific knowledge, and for being so calm and motivating during the stressful last months. I truly appreciate all the feedback and help she has given me, especially with the writing of this thesis. Thank you both for your everlasting help and encouragement and for showing faith in me.

I would also express a big thank to Bjørn Tore Gjertsen, for showing such interest in my project and for sharing his expertise and enthusiasm for science. I highly appreciate the opportunity I have been given, to do my master's project in his research group. A big thanks to all the people in the Gjertsen group for their constant help, support, and kindness.

I am truly thankful to my family and friends for their love and encouragement. A special thanks to my roommates, Thea and Liv, for being such good company and providing a nice place to come home to after long and tiring days, with lots of laughter and support that have been extremely important for me this year. Finally, my deepest gratitude to my mother for her endless love, help, and support, for her everlasting patience listening to all my engagements and frustrations about this thesis, and for always being there for me.

Again, thank you all, these achievements would not be possible without you.

Bergen, May 2022

Emilia Wold Poléo

# Table of contents

# Abbreviations

| | |
|---|---|
| ATRA | All-trans retinoic acid |
| BC | Blast crisis |
| CD | Cluster of differentiation |
| CitH3 | Citrullinated histone H3 |
| CML | Chronic myeloid leukemia |
| DMF | Dimethyl formamide |
| DMSO | Dimethyl sulfoxide |
| ELISA | Enzyme linked immunosorbent assay |
| ETs | Extracellular traps |
| HBSS | Hanks` Balanced Salt Solution |
| IO | Ionomycin |
| MCETs | Mast cell extracellular traps |
| MFI | Median fluorescence intensity |
| MGG | May-Grunwald Giemsa |
| MPO | Myeloperoxidase |
| NADPH | Nicotinamide adenine dinucleotide phosphate |
| NE | Neutrophil elastase |
| NETs | Neutrophil extracellular traps |
| NOX | NADPH oxidase |
| PAD4 | Protein-arginine deiminase type-4 |
| PMA | Phorbol 12-myristate 13-acetate |
| PMNs | Polymorphonuclear leukocytes |
| ROS | Reactive oxygen species |
| RT-PCR | Reverse transcription polymerase chain reaction |
| SDS-PAGE | Sodium dodecyl sulfate- polyacrylamide gel electrophoresis |
| TKI | Tyrosine kinase inhibitor |

# Summary

Neutrophil extracellular traps (NETs) represent a rather newly discovered antimicrobial mechanism first described by Brinkmann and co-workers in 2004. NETs are extracellular structures composed of decondensed chromatin decorated with granule proteins released from neutrophils to trap and kill invading microorganisms. In addition to their role in defense, excessive NET formation has been linked to the pathogenesis of several diseases including cardiovascular diseases, autoimmune diseases (e.g. lupus erythematous), infectious diseases (e.g. sepsis and covid-19), and cancer. However, the role of NETs in chronic myeloid leukemia (CML) has been sparsely explored. More information about the involvement of NETs in CML may provide increased understanding with respect to disease development and response to current therapy consisting of tyrosine kinase inhibitors (TKIs). Also, additional knowledge about NETs in general could facilitate potential development of novel anti-NET therapeutics. In this thesis, the NET forming capabilities of a CML cell line model and neutrophils isolated from CML patients together with the effects of tyrosine kinase inhibitors were investigated.

The CML cell line Kcl-22 was intended used as a model system for NET formation in CML. First for the generation of neutrophils through cell differentiation followed by induction of these differentiated cells to produce NETs. However, it was discovered that the Kcl-22 cells did not differentiate towards neutrophils, although, subsequent detection of NET-like structures was observed in the Kcl-22 cell line after exposure to various differentiation agents and the NET stimulation compounds PMA and ionomycin. Successful induction of extracellular traps (ETs), decreased expression of CD15, and increased expression of CD33, together with an overall lack of segmented nuclei, suggested that these cells most likely had differentiated towards mast cells and that the ETs observed were mast cell extracellular traps (MCETs).

In primary neutrophils, isolated from the peripheral blood of CML patients, NETs were observed *ex vivo*, both with and without exposure to stimulating agents. NET formation capacity of primary neutrophils derived from CML patients was compared to neutrophils derived from healthy individuals. Through immunofluorescence and fluorescence microscopy NETs formed by neutrophils from CML patients appeared increased in number and size compared to neutrophils from healthy donors. In addition, attempts to quantify NETs in primary neutrophils, by ELISA and manual counting, were performed comparing NET

formation in neutrophils from CML patients to neutrophils from healthy donors to detect differences.

BCR-ABL1 is the hallmark and oncogenic driver of CML and was investigated for a potential role in NET formation. The BCR-ABL1 activity, measured by phospho-BCR-ABL1, was demonstrated to be completely inhibited by treatment with the TKIs ponatinib and ABL001 in Kcl-22 cells, however, their capability to form ETs was not affected. Additionally, no altered NET formation was observed in primary neutrophils derived from one CML patient after TKI treatment. Together, this indicated that BCR-ABL1 does not play a direct role in NET formation. In conclusion, this thesis has shown that CML cells can form extracellular traps and that BCR-ABL1 does not seem to influence the amount of NET formation in CML primary neutrophils or ET formation in the Kcl-22 cell line.

# 1. Introduction

## 1.1 Neutrophil granulocytes

When a pathogen enters the human body a series of processes are set in action. The innate immune system provides a rapid and indispensable defence mechanism against invading pathogens. An essential part of the innate immune system is the neutrophil granulocytes (neutrophils). These terminally differentiated myeloid cells are the most abundant population of leukocytes (50-70%) in the human body [1]. As a part of the first-line defence, they migrate to the site of infection to eliminate the invading microorganism. Neutrophils possess several strategies to eliminate pathogenic sources including phagocytosis, production of reactive oxygen species (ROS), degranulation of antimicrobials, and production of chemokines and cytokines recruiting other immune cells [2-4]. In 2004, Brinkmann and co-workers described a novel antimicrobial strategy performed by neutrophils which included a meshwork of chromatin fibers extruded from the cell to trap, disarm and kill bacteria extracellularly [5]. These extracellular fibers were called neutrophil extracellular traps (NETs).

Neutrophils are one of four types of granulocytes together with eosinophils, basophils, and mast cells. Granulocytes are characterized by the presence of specific granules in their cytoplasm, hence the name granulocytes (Fig. 1.1 A). Eosinophils, basophils, and neutrophils are also characterized by their nuclear morphology showing a distinct lobed appearance as if they have multiple nuclei (Fig. 1.1) [6]. In fact, these cells are sometimes referred to as polymorphonuclear leukocytes (PMNs). The term PMNs is also occasionally referred to neutrophils only since they are significantly more abundant compared to eosinophils and basophils [1].

Although neutrophils can be visually identified based on nuclear morphology and cytoplasmic granularity, the usage of cell surface-expressed cluster of differentiation (CD) markers is more specific and allows for distinguishing neutrophils from the other types of granulocytes and monocytes [7]. Neutrophils are distinguished from eosinophils and monocytes based on CD15 and CD16 expression and lack of CD14. In addition, CD11b, CD66b, CD33, and the cytoplasmic marker, myeloperoxidase (MPO), are common markers used to identify human neutrophils [1, 7, 8].

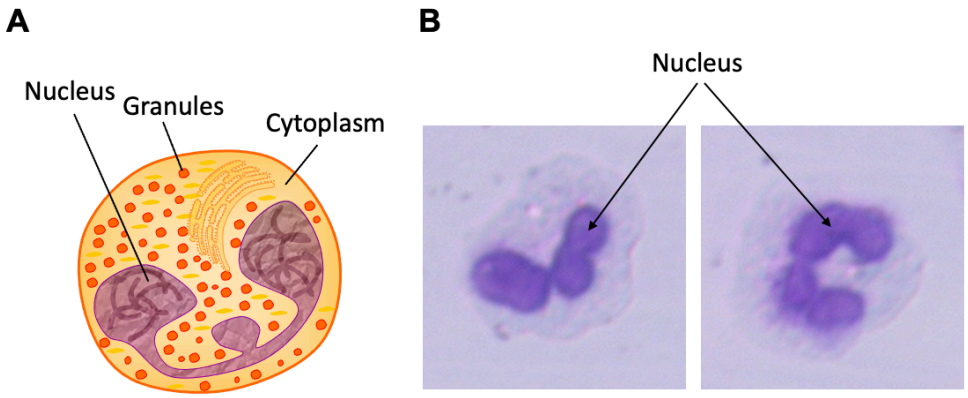


**Figure 1.1. Neutrophil granulocyte. (A)** Cartoon illustrating a neutrophil with a segmented nucleus and cytoplasmic granules. **(B)** May-Grunwald Giemsa (MGG) stained neutrophils isolated from peripheral blood of a healthy individual. Arrows indicate segmented nuclei (dark purple). Images were obtained by light microscopy (Zeiss Axio Vert. A1).

## 1.2 Neutrophil extracellular traps (NETs)

NETs are extracellular structures composed of decondensed chromatin decorated with granule proteins released from neutrophils to trap, neutralize and kill invading microorganisms, first described in 2004 by Brinkmann and co-workers in a publication in Science [5, 9]. The extruded chromatin fibers consist mainly of DNA and histones. These have antimicrobial properties, by providing a sticky meshwork of DNA that traps and immobilizes the pathogen, and by the antimicrobial activity of histones involving disruption of bacterial membrane potential and inhibition of bacterial transcription by reorganization of bacterial chromosomal DNA, a mechanism that until recently was largely unknown [10-13]. In addition, the chromatin fibers are armed with broadly effective antimicrobials. These granule-derived antimicrobials like neutrophil elastase (NE), cathepsin G, and myeloperoxidase (MPO) are enzymes and peptides that contribute to the elimination of invading pathogens such as bacteria, viruses, fungi, and parasites [5].

Although NETs originally were described as a defence strategy of mammalian neutrophil granulocytes, the mechanism of forming extracellular traps (ETs) is not limited to this cell type. Extracellular traps have been described in other types of cells such as eosinophils (EETs), basophils (BETs), mast cells (MCETs), macrophages (METs), and in other species and multicellular organisms such as protozoans, plants, fish and birds, demonstrating an evolutionary conserved antimicrobial mechanism [14, 15]. In addition, different microbes

have developed defence mechanisms against NETs, which further supports an evolutionarily conserved mechanism. This includes some bacteria (e.g. *S. aureus, S. pneumoniae*), parasites (e.g. *Plasmodium falciparum*, the malaria parasite), and fungi (e.g. *Aspergillus*) where microbial strategies against NETs include preventing capture, neutralize the effect and inhibiting or degrading the traps [16, 17].

Microbes can mask themselves with a capsule or change their surface charge to prevent capture. Most microbial surfaces are negatively charged, and the binding of NETs relies heavily upon electrostatic affinity [18]. Some pathogens can reduce this affinity by incorporating positively charged residues to their surface and thereby evade entrapment. This has been observed for Group A *Streptococcus* [19] and *S. aureus* [20]. Many bacteria are protected against eliminating factors like phagocytosis by a polysaccharide capsule that lies outside the cell wall. In addition, it has been shown that the capsule protects *S. pneumonae* from being trapped and killed by NETs [21].

Some microbes can also, after being trapped, actively degrade the DNA of NETs by the production and release of nucleases to be freed from the traps. Nucleases are enzymes that can cleave the phosphodiester bonds between nucleotides of nucleic acids and play a key role in the repair of genetic material. Some pathogens can produce extracellular nucleases as a strategy to escape NETs thereby degrading the chromatin fibers. There has been described that nuclease enzymes expressed and secreted by several bacteria, including *S. pneumoniae* [12] and *S. aureus* [22] can degrade NETs *in vitro*. It has also been demonstrated that the bacterium *V. cholerae* uses the activity of two extracellular nucleases to degrade NETs and thereby evade entrapment [23].

### 1.2.1 NET formation

Today, two main distinct models of NET release, shown in Figure 1.2, have been proposed [24]. The one mostly described is a form of active cell death termed NETosis (Fig. 1.2 A). In general, after stimulation, drastic morphological changes occur due to chromatin decondensation. As the chromatin decondense, the nuclear envelope disassembles, and the chromatin expands into the cytoplasm where it mixes with cytoplasmic and granule components [25]. The plasma membrane then permeabilizes and a net-like structure embedded with antimicrobials expands into the extracellular space where it can trap and kill invading microorganisms.

The second model, termed non-lytic NETosis (Fig 1.2 B), involves more rapid extrusion of NETs from intact neutrophils via the secretion of chromatin and granule proteins without disintegrating the plasma membrane [26, 27]. Yipp and co-workers showed that neutrophils continued to crawl and phagocytose both during and after this form of NET release [27].

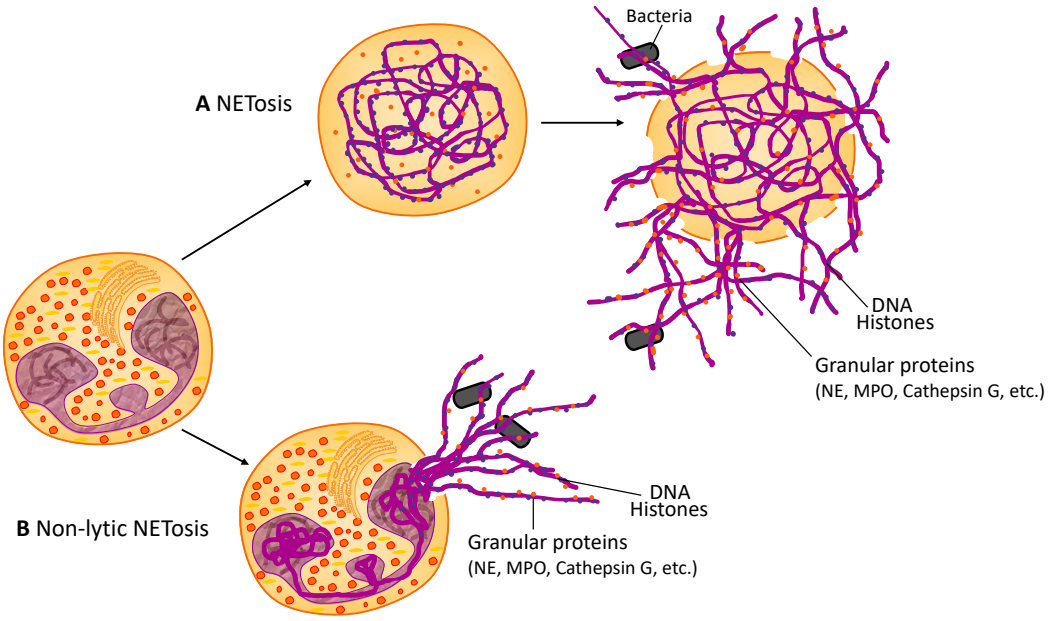


**Figure 1.2. The two main models of NET formation. (A)** NETosis: chromatin expands gradually, followed initially by nuclear disassembly ending in plasma membrane rupture releasing the NET into the extracellular space to trap and kill pathogens. **(B)** Non-lytic NETosis: rapid extrusion of chromatin NET without disintegrating the plasma membrane where pathogens are trapped, and the neutrophils can continue to crawl and phagocytose. Adapted and modified from [9].

Therefore, although NETs were first described in 2004, the detailed mechanisms behind the formation are still incompletely understood. However, some of the molecular mechanisms of NETosis have been revealed and described. The formation of NETs occurs as a response to a variety of stimuli, including bacteria, viruses, fungi, parasites, crystals, activated platelets, cytokines, the chemokine interleukin 8 (IL-8), ionophores and the mitogen phorbol 12-myristate 13-acetate (PMA) [5, 15]. In fact, the molecular mechanisms of NETosis seem to vary depending on the activating stimulus.

### ROS-dependent NETosis

The best described mechanism of NETosis is reactive oxygen species (ROS)-dependent. ROS are highly reactive chemicals, formed as bi-products of the normal metabolism of oxygen [28]. As neutrophils are stimulated with the NET inducers PMA or lipopolysaccharide (LPS), the

intracellular ROS levels rapidly increase [29]. This occurs through the activation of the enzyme complex nicotinamide adenine dinucleotide phosphate oxidase (NADPH oxidase (NOX)). When NOX is activated, it catalyses the electron transfer from NADPH to oxygen, creating reactive oxygen species like hydrogen peroxide ($H_2O_2$) and superoxide ($O_2^-$) [3]. In the presence of ROS, an optimal environment for NE and MPO is created where MPO can mediate the oxidative activation of NE [9]. NE and MPO are azurophilic granular proteins stored in the primary granules of neutrophils in association with azurocidin, defensin, cathepsin G, eosinophil cationic protein, lactoferrin, and lysosome as a complex called the azurosome [30]. It is thought that NE escapes from the azurophilic granules and translocates to the nucleus where it assists in the decondensation of chromatin by degrading the histones H1, H2B, and H4 [31, 32]. Recently, Sprenkeler and colleagues described that actin polymerization and actin cytoskeleton rearrangement is required in the formation of NETs by the translocation of NE to the nucleus. They showed that upon inhibition of actin dynamics, there is a lack of NE translocation, resulting in impaired NET formation [33]. In addition, chromatin decondensation is also promoted by caspase-1 that cleaves histone H3, and MPO [9, 34]. The role of MPO and NE is supported by studies on neutrophils from patients with chronic granulomatous disease (CGD) that show defects in NET formation. These patients have mutations in genes encoding NADPH oxidase, consequently disrupting the ability to generate ROS [35, 36].

**NOX-independent NETosis**

Upon stimulation with calcium ionophores, like ionomycin (IO), NETosis can occur in the absence of NOX activity [37, 38]. Studies show that NET formation after treatment with the NOX inhibitor diphenyleneiodonium (DPI) requires extracellular calcium influx through calcium ionophores [37, 38]. This NOX-independent NETosis could be explained by the post-translational modification citrullination of histones. It has also been described that NETosis induced by ionophores is mediated by mitochondrial ROS instead of NOX, providing a possible explanation of the molecular mechanism of NOX-independent NETosis [39].

In the nucleus, DNA is associated with histones, very tightly packaged into condensed chromatin. Histones are prone to several post-translational modifications. These modifications are linked to changes in the density of chromatin and are thus believed to be involved in NET formation. The most common described post-translational modification in NETs is histone citrullination (or deimination), mediated by the enzyme peptidyl arginine deiminase 4 (PAD4)

[3]. As calcium levels increase in the cytoplasm, PAD4 forms a complex with calcium and becomes activated [40]. Activated PAD4 then rapidly translocates to the nucleus where it catalyses the conversion of arginine into citrulline on histone H3 [41]. This results in disruptions of ionic interactions in the chromatin, causing it to decondense. Citrullinated histones, therefore, represent a biomarker for NETs.

### 1.2.2 NETs in disease

Since the discovery of NETs in 2004 it has been established that they are fundamental to the innate immune defence against pathogens. Unfortunately, as with many other immune responses, NETs have a dark side and appear to be part of the pathogenesis of several diseases. The role of NETs in disease includes cell and tissue damage, inflammation, vaso-occlusion, cancer promotion, and sources of autoantibodies contributing to autoimmunity [9]. The release of NETs leaves behind a meshwork of DNA with histones and granular proteins, with damaging properties not only to pathogens but also to the host. NET proteins such as defensins permeabilize eukaryotic cells, and NE targets the extracellular matrix and disrupts cell junctions contributing to tissue damage [42, 43]. Free circulating histones can compromise cell membrane integrity, thus having cytotoxic effects. These effects can promote the pathogenesis of sepsis and lung injury [44-46]. Another pathological role of NETs is that they can induce a strong procoagulant response by binding and activating platelets and by the proteolytic activity of NE in the setting of deep vein thrombosis [47, 48].

Uncontrolled inflammation is known to cause disease, and NETs can be modulators of inflammation by directly regulating cytokines or indirectly modulate other immune cells [49]. This modulation effect on other immune cells can also play a role in autoimmune disease development. Neutrophils have been defined as a major source of autoantigens in some autoimmune diseases. In systemic lupus erythematous, autoantibodies against double-stranded DNA (dsDNA), histones, and MPO are thought to be produced. This makes NETs a source of self-antigens promoting autoimmune and inflammatory processes [50].

Excessive NET formation has been linked to the poor outcome for some coronavirus disease 2019 (Covid-19) patients. Covid-19 is an infectious disease caused by severe acute respiratory syndrome coronavirus 2 (SARS-CoV-2). The poor outcome for some covid-19 patients is due to acute lung injury (ALI) and the progression to acute respiratory distress syndrome (ARDS) [51, 52]. It has been reported that serum from patients with covid-19 contains elevated levels

of histones, cell-free DNA and MPO-DNA, which all are markers for NETs, compared to healthy individuals, and additionally that patients with severe covid-19 disease, receiving mechanical ventilation, had higher levels of cell-free DNA and MPO-DNA compared to patients with less severe covid-19 disease [53]. Extracellular histones are toxic to cells and have been shown to be elevated in the bronchoalveolar lavage fluid and plasma of ARDS patients, which could suggest that NETs, as a source of extracellular histones, contribute to ARDS [51].

## 1.3 Chronic myeloid leukemia (CML)

Chronic myeloid leukemia (CML), also called chronic myelogenous leukemia, is a rare type of cancer that originates in the bone marrow hematopoietic stem cells. CML is a clonal myeloproliferative disorder where precursor and mature myeloid cells in the bone marrow have uncontrolled proliferation [54]. The increased and unregulated growth of myeloid cells in the bone marrow leads to the accumulation of these cells in the blood (Fig. 1.3). The word “chronic” points to the fact that the disease develops slowly, usually remaining in a chronic phase over an extended period where the patients experience little to no symptoms. CML cells are in general more mature and functional compared to acute myeloid leukemia (AML) cells, which possess almost zero function due to the lack of maturation [55]. The annual incidence of CML in Europe is 0.7-1.0/100,000 with a median age at diagnosis of 57-60 years and a male to female ratio of 1.2 to 1.7 [56].

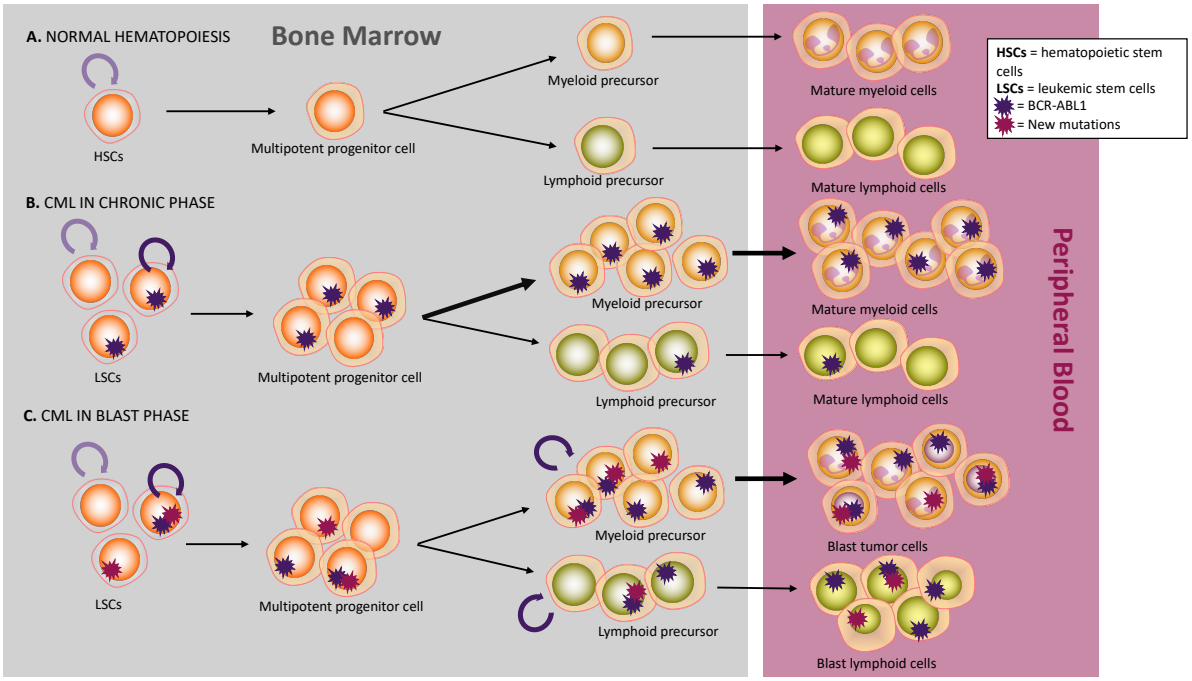


**Figure 1.3. Phases of chronic myeloid leukemia. (A)** Normal hematopoiesis where the hematopoietic stem cells (HSCs) renewal and multipotency capabilities are highly regulated resulting in a strict and balanced myeloid and lymphoid distribution. **(B)** Chronic phase of CML where a BCR-ABL1 mutation in the HSCs results in leukemic stem cells (LSCs) and an unbalanced expansion of myeloid cells. **(C)** Blast crisis phase of CML is characterized by additional mutations in the LSCs resulting in maturation arrest and increased production of immature cells (blast) in both myeloid and lymphoid lineage. Adapted and modified from [57].

### 1.3.1 Staging of CML

CML has a triphasic course, where the chronic phase, the accelerated phase, and blast crisis (BC) constitute the three phases of the disease. Most patients present in the chronic phase and are asymptomatic at diagnosis. Typically, patients are diagnosed when a blood test is taken for other reasons. However, the most frequent signs and symptoms in the chronic phase are fatigue, night sweats, weight loss, left upper quadrant pain, and splenomegaly [58]. The chronic phase is associated with the best outcome. However, if left untreated or if the patient does not respond to treatment, the cancer could progress to the accelerated phase and eventually to BC [59]. The definition of the accelerated phase and blast crisis is largely dependent on the percentage of blasts (precursor cells to mature blood cells) in the bone marrow [59]. In the accelerated phase the number of blasts in blood and bone marrow is between 10-19%. If the disease progresses further to BC, the number of blasts increases to over 20%. In this phase, the CML cells often have additional genetic changes and result in a lymphoblastic (acute lymphoblastic leukemia phenotype), myeloblastic (acute myeloid leukemia phenotype) or biphenotypic disease (Fig. 1.3) [60]. The median survival of patients

in BC is only 12 months, even with the use of tyrosine kinase inhibitors representing the standard treatment for CML patients [61].

### 1.3.2 The Philadelphia chromosome

In 1960, in the state of Philadelphia (US), Nowell and Hungerford discovered what was then called a minute chromosome, in blood samples from patients with chronic myeloid leukemia [62]. This discovery was later identified as a balanced reciprocal translocation between chromosome 9 and 22 (t(9;22) (q34;q11)). This translocation results in an abnormal, shortened chromosome 22, named the Philadelphia chromosome (Fig. 1.4 A), after the state it was first discovered [63, 64]. Today, the Philadelphia chromosome is considered the hallmark of CML.

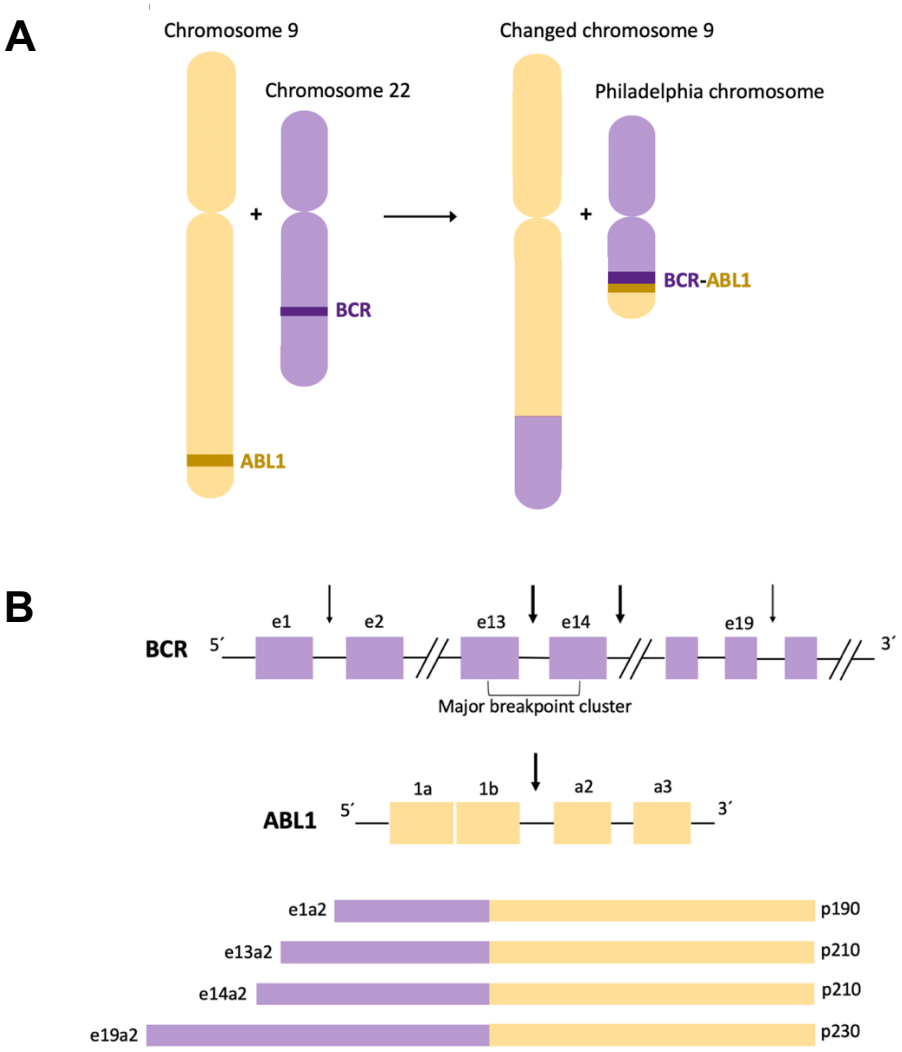


**Figure 1.4. Philadelphia chromosome. (A)** Schematic illustration of the t(9;22) (q34;q11) translocation generating the Philadelphia chromosome with the BCR-ABL1 chimeric gene. **(B)** Breakpoint locations on the BCR and ABL1 genes and the encoded proteins in the BCR-ABL1 fusion. Adapted from [57].

**BCR-ABL1**

On the Philadelphia chromosome, a new gene is created. When the *ABL1* gene (also called *c-ABL*) of chromosome 9 juxtaposes onto the breakpoint cluster region (*BCR*) of chromosome 22, the *BCR-ABL1* chimeric gene is formed [65]. The regular *ABL1* gene encodes the protein of a non-receptor tyrosine kinase. A non-receptor tyrosine kinase phosphorylates tyrosine (transfers a phosphate group from ATP to tyrosine) of specific proteins upon binding of ATP, and this activity is normally very tightly regulated [66]. The ABL1 protein is negatively regulated by its SRC Homology 3 (SH3) domain [67]. However, when the *BCR-ABL1* fusion is generated, it results in the elimination of a myristoyl group in the SH3 domain of *ABL1*, leading to the production of a constitutively active non-receptor tyrosine kinase [61]. The activity of the BCR-ABL1 protein is capable of autophosphorylation and uncontrolled signalling to a plethora of downstream proteins [58]. The constitutively active signalling causes cell reprogramming and leads to malignant transformation due to uncontrolled proliferation, lack of response to apoptotic signalling, independence of growth factors, alteration in cell adhesion, and impaired differentiation [68-70].

**The different breakpoints**

The *BCR-ABL1* gene can vary in size depending on different breakpoints between the two loci. In most patients with CML, the breakpoint at the *ABL* locus occurs in the DNA region housing exon 2, spanning more than 200 kb, and the breakpoint at the *BCR* locus occur within the major breakpoint cluster region that includes exon 13 and exon 14 (Fig. 1.4 B) [71]. Alternative splicing gives most commonly rise to two fusion mRNA transcripts with either e13a2 (formerly called b2a2) or e14a2 (b3a2) junctions [72]. The mRNA junction of e13a2 is approximately 310 bp long, while the e14a2 is approximately 385 base pairs. Both transcripts generate a 210 kDa protein. Occasionally, other fusion transcripts occur, such as e1a2 and e19a2 which translate into proteins of 190 kDa and 230 kDa, respectively [61].

Studies have reported that the e14a2 fusion is associated with a better outcome of disease by achieving complete cytogenic response more frequently compared to the e13a2 after treatment with TKIs [73, 74]. Complete cytogenic response means that no or less than 1% of the cells in the bone marrow have the Philadelphia chromosome [75].

### 1.3.3 Treatment of CML

Today, with few exceptions, the first line of treatment for CML is a tyrosine kinase inhibitor (TKI) [76]. Since the activity of the BCR-ABL1 tyrosine kinase by itself is sufficient for the development and progression of CML, targeting this protein by blocking its activity, significantly reduce the proliferation of the CML [77]. In 1996, Druker and co-workers reported the first data on the effects of a TKI, then known as signal transduction inhibitor 571 (STI571), on CML cell lines [78]. This TKI, today known as imatinib (Gleevec®, Novartis), has revolutionized the management of chronic myeloid leukemia by inducing complete cytogenic remission at a high rate [79]. Imatinib functions through competitive binding in the ATP-binding site of the BCR-ABL1 tyrosine kinase, leading to the inhibition of tyrosine phosphorylation of proteins in the BCR-ABL1 signal transduction pathway [80]. Soon after imatinib was approved for clinical use in 2001, it became clear that some patients suffered from resistance to the drug [81]. The second-generation TKIs, dasatinib, bosutinib, and nilotinib, were developed to overcome imatinib resistance. However, some patients exhibit resistance to these drugs as well or unacceptable side effects. These TKIs also bind competitively to the ATP-binding site [61]. Approximately half of the clinical resistance against TKIs is associated with the acquisition of mutations in the region of the ATP-binding site [82]. This includes the T315I mutation which is present in approximately 20% of patients with BCR-ABL1 mutations, associated with resistance to all first- and second-generation TKIs [83]. This shortcoming led to the development of ponatinib, a so-called third-generation TKI, with activity against both unmutated BCR-ABL1 and most common mutations, including T315I [61]. In October 2021, asciminib (ABL001), was approved for clinical use in the United States [84]. This TKI works through allosteric inhibition, making it distinct from all the other BCR-ABL1 tyrosine kinase inhibitors. It binds a myristoyl site of the BCR-ABL1 protein thereby locking it into an inactive conformation [85].

Despite the superiority of TKIs, allogenic bone marrow transplantation has retained a place in CML treatment. Bone marrow transplantation can provide long-term remission and a possible cure for some patients. However, since the discovery of TKIs, it is rarely the first-line treatment [61]. The European LeukemiaNet recommends assessment for transplantation when there is resistance to second-generation TKIs [86]. Disease stage, donor availability, and patient characteristics are important factors to consider before going through with

transplantation, in addition to side effects that may occur, like graft versus host disease (GvHD) [61, 76].

Some patients may have a benefit from using other drugs in addition to TKIs. One example is hydroxyurea, which is a type of chemotherapy drug that lower the number of leukocytes. Some patients may benefit from this drug to reduce symptoms while a diagnosis of CML is pending [76]. In the 1970s interferon-alpha was introduced in CML treatment. Interferon-alpha is a biological compound with immunomodulatory, antiviral, and antiproliferative properties, and has been shown to have clinical responses for some types of cancers [87]. When it first was used in CML treatment, interferon-alpha induced complete cytogenic remission in 10-15% of patients [88]. However, most patients had to discontinue treatment due to serious side effects, causing them to relapse. Today, a growing interest to re-introduce interferon-alpha in combination with TKIs for treating CML is occurring. Using interferon-alpha together with TKIs is being investigated, and the hope is that a combination of the two will increase the proportion of patients achieving treatment-free remission [86].

Since they were first approved for clinical use in 2001, TKIs have revolutionized the treatment of CML, giving most patients (around 87%) a near-normal life expectancy. Despite the success of TKIs, there are still obstacles to overcome. One major concern is that TKIs do not fully eliminate the cause of CML. While the drug is present, TKIs efficiently block the activity of BCR-ABL1 for many patients but remaining leukemic stem cells (LSCs) can regain oncogenic activity when treatment is stopped [89]. Therefore, lifelong treatment is necessary for most patients. However, long-term use facilitates adverse effects, and 10% become resistant to their initial TKI [90]. In addition, an increasing number of CML patients develop long-term side effects like cardiovascular, pulmonary, gastrointestinal, and endocrine toxicities with the use of TKIs [91].

## 1.4 NETs in CML

Cardiovascular complications are associated with the use of some TKIs, specially ponatinib, where 31% of patients experience vein or artery blood clots called thrombosis [92]. NET formation can contribute to the development of cardiovascular complications, therefore, understanding the correlation between CML, TKIs and NETs are, from a clinical point of view, of great importance. In December 2021, Telerman and colleagues described that

neutrophils isolated from CML patients demonstrated increased NET formation after *in vitro* stimulation with ionomycin compared to neutrophils from healthy controls [93]. This was associated with increased expression of PAD4 and its downstream biomarker citrullinated histone H3 in neutrophils from CML patients compared to age- and gender-matched healthy controls. In addition, increased ROS generation by NADPH oxidase was significantly increased in the neutrophils derived from CML patients.

In the study, they also investigated the impact of TKIs on NET formation in CML. By exposing primary CML neutrophils to clinically relevant concentrations of TKIs they observed an increase in markers of NET formation after *ex vivo* exposure to ponatinib. Previously it has been demonstrated that ponatinib impairs the function of the respiratory chain, thereby increasing ROS production, possibly promoting NET formation due to increased ROS levels in neutrophils [94]. This reveals a potential novel mechanism between ponatinib and vascular toxicity.

# 2. Aims

The overall aim of this project is to investigate the capability of chronic myeloid leukemia (CML) cells to form neutrophil extracellular traps (NETs) and elucidate the role of BCR-ABL1 in NET formation.

Specific aims are:

1) To utilize the CML cell line Kcl-22 as a model system to study NET formation. Thus, to investigate the potential of Kcl-22 cells to differentiate towards neutrophils and to form NETs.

2) To study the effect of specific BCR-ABL1 tyrosine kinase inhibitors (TKIs) on NET formation in KCL-22 cells.

3) To isolate neutrophils from the peripheral blood of healthy donors and CML patients for comparison of NET forming capabilities.

4) To examine the effect of specific BCR-ABL1 TKIs on primary neutrophils isolated from peripheral blood of CML patients.

# 3. Material and Methods

## 3.1 Cells

### 3.1.1 Human primary cells and cell lines

In this thesis, both human primary cells and cell lines have been used. The primary cells were derived from the blood of patients with chronic myeloid leukemia (CML) and from healthy individuals as blood donors. The study was conducted in accordance with the Declaration of Helsinki and approved by the local Ethics Committee (Regional Ethics Committee West projects 2012/2245 and 2016/253). Blood samples from three newly diagnosed CML patients included in the Bosupeg clinical trial (ClinicalTrials.gov Identifier: NCT0381776) and two healthy blood donors from the Blood bank at Haukeland University Hospital, were collected after informed and written consent.

The cell lines used in this thesis were mainly Kcl-22 (DSMZ) and HL-60 (ATCC). The Kcl-22 cell line is established from the pleural effusion of a 32-year-old woman with Philadelphia chromosome-positive CML in blast crisis. The HL-60 cell line is an acute promyelocytic leukemia (APL) cell line established from the peripheral blood leukocytes of a 35-year-old Caucasian female. Molm-13 (DSMZ), an acute myeloid leukemia cell line, and KU-812 (DSMZ), a chronic myeloid leukemia cell line were also used in this thesis. Detailed information about the primary cells and cell lines is summarized in Table 4.2 in the results section.

### 3.1.2 Cell tissue culture

The Kcl-22 and HL-60 cell lines were cultured in Roswell Park Memorial Institute (RPMI)-1640 medium (Sigma-Aldrich) supplemented with 10% heat-inactivated Fetal Bovine Serum (FBS) (PA Laboratories GmbH), 50 IU/mL Penicillin – 50 µg/mL Streptomycin (Sigma-Aldrich) and 2 mM L-glutamine (Sigma-Aldrich), and kept in a 5% $CO_2$ humidified incubator at 37°C.

All cell culture work was performed under sterile conditions. The cells were grown in cell tissue suspension flasks (TC Flask, Susp., Vent. Cap) (Sarstedt) and frequently observed by a

light microscope (Nikon Eclipse TS100) to ensure that the cells were alive, proliferating, and bacteria-free. The cell lines were in general passaged every second to third day. Kcl-22 cells were split to a density of 0.2-0.3 x $10^6$ cell/mL, and HL-60 to a density of 0.5-1 x $10^6$ cells/mL. Before and during experiments, live cells were counted using a Bürker chamber (Marienfeld Superior, Germany) mixed 1:1 with trypan blue stain 0.4% (Invitrogen).

### 3.1.3 Thawing of cryopreserved cells

Cryopreserved cells were thawed in a 37°C water bath until almost defrosted. Cells were carefully resuspended in 1 mL of 37°C preheated medium and transferred to a 15 mL tube containing 9 mL of medium. The tube was centrifuged for 5 min at 1100 rotations per minute (RPM) (Eppendorf centrifuge 5810 R, Eppendorf). The supernatant was removed, and the pellet was resuspended in fresh media. The cell suspension was then transferred to a 25 mL cell tissue suspension flask (Sarstedt). Cells were kept under normal growth conditions and the medium was changed the day after. For thawing of cryopreserved neutrophils, cells were centrifuged for 10 min at 200 x g (Eppendorf centrifuge 5810 R, Eppendorf) and Hanks` Balanced Salt Solution (HBSS) (Sigma-Aldrich) was used instead of media, otherwise, the same protocol was used.

## 3.2 Isolation of neutrophils from blood

Polymorphprep™ is a ready-made solution containing 13.8% (w/v) sodium diatrizoate and 8% (w/v) polysaccharide for the isolation of pure polymorphonuclear (PMN) leukocytes directly from blood. To separate the neutrophils from venous blood, the high osmolarity of Polymorphprep causes the erythrocytes to lose water and thus increasing their buoyant densities allowing them to sediment through the medium. As they sediment through the medium the osmolarity gradient between the medium and the erythrocytes declines. This leads to a continuous density gradient (from low to high) in the medium. The PMNs band will be within this density gradient while the mononuclear cells remain at the medium interface [95] as shown in Figure 3.1.

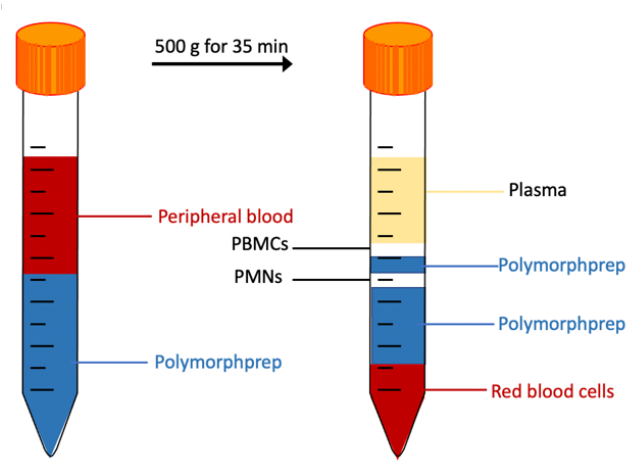


**Figure 3.1. Isolation of PMNs using Polymorphprep™.** PBMCs = peripheral blood mononuclear cells, PMNs = polymorphonuclear leukocytes.

All solutions were brought to room temperature before use. Venous blood from human healthy individuals and CML patients were collected in tubes with EDTA (final concentration 1.5-2.0 mM) within 2 h before isolation. 5 mL of density gradient media (Polymorphprep™) (Produced by Serumwerk Bernburg AG for Alere Technologies AS, Norway) was added to a 15 mL tube. Using a plastic Pasteur pipette, 5 mL of human venous blood with EDTA was carefully layered on top of the polymorphprep. The cells were separated by centrifugation at 500 x g (Eppendorf centrifuge 5810 R, Eppendorf) for 35 min at room temperature without brake, to prevent cross-contamination between the two bands of cells and swirling of the loosely packed erythrocytes (red blood cells).

After centrifugation, the plasma layer (Fig. 3.1) was removed and both bands of cells, upper containing peripheral blood mononuclear cells (PBMCs) and lower containing PMNs were collected in separate 15 mL tubes. Then, 0.85% NaCl was diluted with equal amount of autoclaved MilliQ water and mixed with equal amount of the PMNs or mononuclear cell suspensions before centrifuged at 400g (Eppendorf centrifuge 5810 R, Eppendorf) for 10 min. To remove any residual erythrocyte contamination, the pellet was resuspended in 3 mL of BD Pharm Lyse Lysing Buffer (10X concentration, BD Bioscience) diluted in distilled water to a final concentration of 1X and incubated for 7 min at 37°C in the dark. Cells were then harvested by centrifugation for 5 min at 200 x g (Eppendorf centrifuge 5810 R, Eppendorf) and resuspended in BD Pharmingen™ Stain Buffer (Dulbecco´s Phosphate-Buffered Saline, pH 7.4, 2% Fetal Bovine Serum, 0.09% Sodium Azide) (BD Bioscience).

## 3.3 Differentiation of cells

### 3.3.1 Differentiation of cell lines

To differentiate HL-60 cells or Kcl-22 cells to granulocyte-like cells, the cells were incubated for 5 days with 1.25% DMSO (Sigma Life Science), 12.9 M DMF or 1μM ATRA diluted in RPMI-1640 medium. A total of 2 x $10^6$ cells at 0.25 x $10^6$ cells/mL cell density were seeded in 8 mL in 25 $cm^2$ cell culture suspension flasks (Sarstedt) and 100 μL of 1.25% DMSO, 70 μM DMF, 1 μM ATRA or extra medium (for control) were added.

Cells were counted after 24 h (day 1), 48 h (day 2), and 120 h (day 5) after adding the differentiation agents. At day 2 (48 h after start) cells were centrifuged, counted, and added fresh medium with differentiation agent. After 120h of incubation with ATRA, DMSO or DMF cells were counted, collected, and distributed for further experiments.

## 3.4 Cellular morphology

### 3.4.1 Staining of cells for morphological visualization and quantification of differentiated cells

After treatment for 5 days with compounds known to result in cellular differentiation, treated and untreated control cells were stained with May-Grunwald Giemsa (MGG) staining and morphological inspection and differential counting of cells was performed. MGG stain is a mixture of azure, methylene blue, and eosin dye. Azure and eosin are acidic dyes that stain basic components of the cells, like the cytoplasm and granules giving them a pink cytoplasm. Methylene blue acts as the basic dye staining acidic components, especially the nucleus giving it a purple color [96].

Cells were first deposited onto an objective glass using the cytospin method. This method includes a special setup with Shandon filter paper (Thermo Scientific) placed on top of the objective glass, and a Shandon cytofunnel (Thermo Scientific) attached on top of filter paper and locked in place using a Shandon Cytoclip Stainless-steel Slide Clip (Thermo Scientific). Cells (0.06 x $10^6$) were pipetted into the Shandon cytofunnel and centrifugated at 400 RPM in

the Thermo Shandon Cytospin 3 centrifuge (Thermo Scientific) for 4 min, allowing the cells to be cytospun onto the objective glass as a flat monolayer of cells.

Cells were then fixed, first by drawing a circle around the cell layer using a Liquid blocker super pap pen (Baido Sangyo Co., Ltd. Tokyo, Japan) to make sure that liquid will be retained inside this circle and then a few droplets of methanol were added and allowed to evaporate in the chemical hood before the start of staining. After fixation, cells were first stained with May-Grunwald eosine-methylene blue solution modified (Merck) diluted 1:1 in Sørensens phosphate buffer (pH 6.8) (0.46% $Na_2HPO_4$, 0.58% $KH_2PO_4$ in $dH_2O$) (Sykehusapoteket in Bergen) for 15 min, before excess liquid was removed. Then, cells were stained with Giemsa´s azur eosine methylene blue solution (Merck) diluted 1:10 in Sørensens phosphate buffer for 5 min, followed by removal of excess liquid. After staining, the objective glasses were washed twice with distilled water, one brief wash, followed by a second wash for 5 min, and then examined using light microscopy with a color camera (Zeiss Axio Vert.A1, Zeiss). Quantification of differentiated cells was performed by manual counting of cells using light microscopy. A total of 100 cells were counted and scored based on the nuclear morphology resembling different stages in granulopoiesis.

### 3.4.2 Flow cytometry

Flow cytometry was performed to investigate expression of cell surface markers associated with differentiation and for verification of cell surface markers following isolation of human primary cells. Cells analyzed by flow cytometry were either collected after 5 days of treatment with compounds inducing differentiation (cell lines) or after isolation of neutrophils and mononuclear cells from human peripheral blood (primary cells). After collection, cells were fixed with 16% paraformaldehyde diluted directly in the medium to a final concentration of 4% for 15 min at room temperature in the dark. Cells were then washed twice by removing the supernatant after centrifugation at 400 x g for 5 min (Eppendorf centrifuge 5427 R, Eppendorf) and the pellet was resuspended in 1000 µL 1X PBS. After the final wash, the pellet was resuspended in 500 µl of 1X PBS and stored at -80°C until used.

To prepare cells for staining by flow cytometry, cells were thawed on ice and then centrifuged at 350 x g for 5 min (Eppendorf centrifuge 5427 R, Eppendorf). The supernatant was removed before the cells were resuspended in 80 µL of cell staining buffer (0.5% BSA in 1X PBS) and 20 µL of FcR Blocking Reagent human (Miltenyi Biotec B.V. & Co. KG) was added to the

cell suspension and incubated for 10 min at 4°C for blocking of unspecific binding to the FcR receptors. After blocking, 100 µL of cell staining buffer was added to the suspension and 75 µL was transferred to a new Eppendorf tube for staining. An antibody cocktail with a volume of 25 µL was added to the 75 µL resulting in a total volume of 100µL. The antibody cocktail consisted of a pre-titrated volume of APC Cyanine7 anti-human CD33 antibody (400 µg/mL) (Clone: P67.6) (BioLegend) (7.5 µL), Alexa Fluor® 647 anti-human CD15 (SSEA-1) antibody (120 µg/mL) (Clone: W6D3) (7.5 µL), Alexa Fluor® 488 anti-human CD14 antibody (400 µg/mL) (Clone: 63D3) (5 µL) and Anti-Hu CD11b PE antibody (Clone: ICRF44) (Exbio) (5 µL). The remaining cell suspension represented the unstained control. Cells and antibody cocktail were incubated for 20 min at room temperature in the dark followed by washing two times with 1000 µL cell staining buffer and centrifugation at 350 x g for 5 min. The pellet was resuspended in 500 µL cell staining buffer after the last wash, transferred to a flow tube, and cells were acquired using the BD Accuri™ C6 Plus Flow Cytometer and data analyzed by FlowJo™ v.10.8 Software (BD Life Science).

**Compensation beads**

For compensation, the AbC™ Total Antibody Compensation Bead Kit (Invitrogen) was used. The beads were resuspended before use by gentle vortex for 10 sec. One sample tube for each fluorochrome-conjugated antibody was labeled and 1 droplet of AbC™ Total Antibody Compensation Bead Component A was added to each tube. A pre-titrated amount of each antibody was deposited directly to the bead suspension in the designated tube, mixed well, and incubated for 15 min at room temperature protected from light, followed by addition of 3 mL of cell staining buffer and centrifugation for 5 min at 250 x g. The supernatant was carefully removed, and the pellet was resuspended in 500 µL of cell staining buffer and one droplet of negative beads (Component B) was added to the tubes and mixed well.

## 3.5 Visualization and quantification of NETs

### 3.5.1 NET induction

To induce NET formation cells were seeded on 12 mm in diameter glass coverslips added to a 24-well plate. Prior to adding the cells, the plate with coverslips was incubated for 1 min in the microwave at 1000 Watt for sterilization. Coverslips were then coated with 400 µL of

Poly-L-Lysine (0.01% solution) (Sigma) and incubated for 5 min at room temperature, following removal of the solution and sterile air drying.

To each Poly-L-Lysine coated coverslip, 0.3 x $10^6$ cells were added and then the plate was centrifuged at 450 RPM (Eppendorf centrifuge 5810 R, Eppendorf) with acceleration 4 and break 0, by pushing the stop button when the centrifuge reached 450 RPM. This was followed by changing the orientation of the plate and a second centrifugation at 650 RPM using the same steps and settings. Cells were then incubated for 30-60 min in 5% $CO_2$ atmosphere at 37°C, allowing the cells to attach to the coverslips before cells were stimulated to induce neutrophil extracellular trap formation. Cells were stimulated for 3 h with 100 nM phorbol 12-myristate 13-acetate (PMA) or 4 µM Ionomycin calcium salt (Ready-made solution, from *Streptomyces conglobatus,* 1 mM in DMSO, Sigma Life Science) diluted in Hanks` Balanced Salt Solution (HBSS) (Sigma-Aldrich).

### 3.5.2 Visualization of NETs by immunofluorescence

After 3 h of incubation, PMA and IO were removed, and cells were fixed with 4% paraformaldehyde (PFA) for 15 min in the dark at room temperature. The PFA was removed and coverslips with fixed cells were washed two times with 500 µL of 1X PBS. Coverslips were transferred to a parafilm in a plastic humid chamber inverted with the cell side facing down onto 30 µL droplets of 0.2% Triton-100 in 1X PBS for permeabilization and incubated at room temperature for 10 minutes. After permeabilization a droplet of 30 µL 1X PBS was added above and the coverslip was moved to this fresh droplet for washing. The cells were washed for a total of 3 times, 5 min each. Cells were blocked for 1 h at room temperature with Blocking Buffer (1X PBS, 5% goat normal serum, 0.3% Triton X-100 buffer) (Normal serum from the same species as the secondary antibody). After blocking of cells, coverslips were incubated on 30 µL droplets of primary antibodies diluted 1:100 in antibody dilution buffer (1X PBS, 1% BSA, 0.3% Triton X-100) at 4°C overnight. Primary antibodies used for identification of NETs were rabbit polyclonal antibody anti-Histone H3 (citrulline R2 + R8 + R17) (ab5103, 79 mg/mL, Abcam) and monoclonal mouse anti-human neutrophil elastase (Clone NP57, 42 mg/L, Dako).

The day after, cells on coverslips were washed three times, 5 min each, on 30 µL droplets of 1X PBS at room temperature. After washing, coverslips were incubated on 30 µL droplets with secondary antibodies diluted 1:1000 in antibody dilution buffer for 1-2 h protected from

light. The secondary antibodies used were Alexa Fluor 568 goat anti-rabbit IgG (2 mg/mL) (H+L) (Cat. No. A-110011, Invitrogen) and Alexa Fluor 594 goat anti-mouse IgG (2 mg/mL) (H+L) (Cat. No. A-11005, Invitrogen). Coverslips were again washed three times on 30 µL droplets of 1X PBS for 5 min, protected from light. Lastly, coverslips were mounted on 5 µL droplets of mounting media containing DAPI (SlowFade® Diamond Antifade Mountant with DAPI, Life Technologies) and sealed with non-coloured nail polish before analyzation using Zeiss Axio Observer Z1 with AxioVision 4.8.2 or Zen software using a 63x1.4 NA Oil DICIII objective under standard air conditions.

### 3.5.3 Visualization of NET formation by live cell imaging

For live cell imaging and counting/quantification of NETs, 0.1 x $10^6$ cells were seeded onto a 1 µ-Slide 8 Well (IBIDI GmbH) tray, pre-coated with 200 µL of Poly-L-Lysine for 5 min, and incubated under normal cell culture conditions (5% $CO_2$, 95% $O_2$, and 37°C) for 1 h for cell attachment. The supernatant was then carefully removed from each well, and NET stimulant (PMA or IO diluted in HBSS or only HBSS for control) were carefully added together with 10 µL SYTOX™ Green nucleic acid stain (5 mM solution in DMSO) with a final concentration of 2 µM and 10 µL Hoechst 33342 (1 µg/mL). Live cell imaging was performed by acquiring images every 5 min for a total of 3 h.

### 3.5.4 Quantification of NETs

After 3 h of live imaging, cells were fixed by replacing 100 µL from each well with 100 µL of hoechst fixation solution, containing 4% formaldehyde, 10 µg/mL Hoechst 33342 diluted in 1X PBS. Hoechst 33342 is a fluorescent dye that binds to DNA. Using the 10x lens on a fluorescent microscope (Zeiss Axio Observer Z1) 4 images were acquired from different areas of each well. The number of NETs and total number of cells were counted using ImageJ (Fiji) by the multi-point tool. In the green channel (SYTOX green, DNA/impermeant to live cells), every enlarged and diffuse structure was counted as one NET as exemplified in Figure 3.2, and in the blue channel all nuclei were counted (Hoechst/DNA/nuclei/permeable into live cells) to provide the total number of cells.

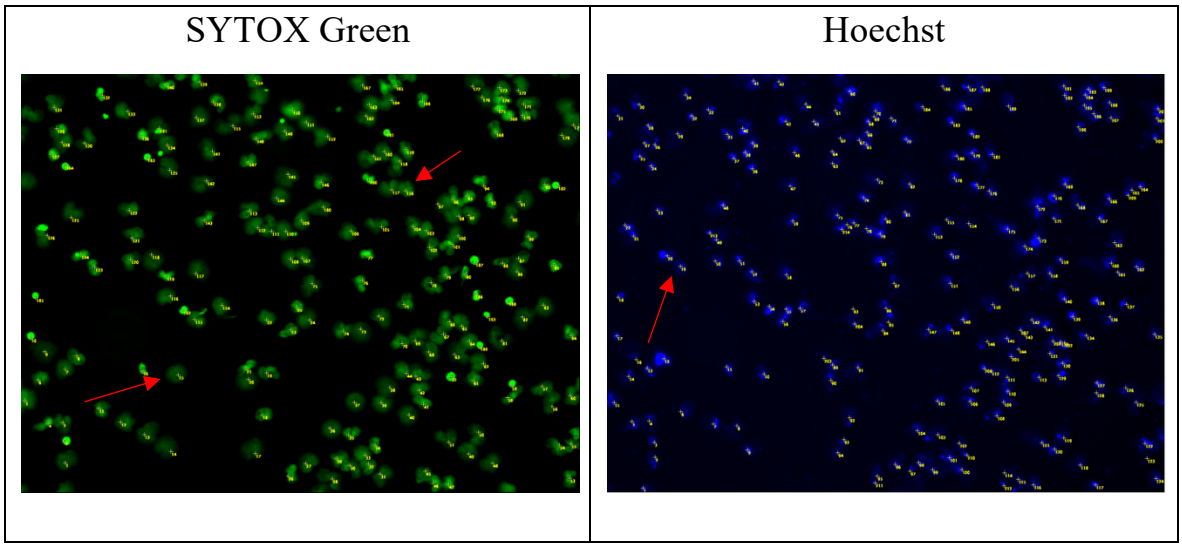


**Figure 3.2. Quantification of NETs.** Primary neutrophils were stimulated with PMA or ionomycin (here PMA) for 3 h and stained with hoechst and SYTOX Green. NET structures and total cell number were counted in ImageJ as pointed out.

### 3.5.5 Quantitative determination of NET components by enzyme-linked immunosorbent assay (ELISA)

For quantification of myeloperoxidase (MPO) in supernatants after stimulation, R&D Systems® Quantikine ELISA for Human Myeloperoxidase Immunoassay (Cat. No. DMYE00B) kit was used. The kit employed the quantitative sandwich enzyme immunoassay (antigen capturing) technique using plates precoated with a monoclonal antibody specific for MPO. Pre-coated plates and all reagents needed were supplied in the kits and the execution of the methods followed the exact step-by-step protocols provided.

**Collection and preparation of cell supernatant**

Cell supernatant used for the ELISA were either directly collected from the 24-well plate after 3 h stimulation with PMA or IO or cell on coverslips were treated with deoxyribonuclease I (DNAse I) (337.06 U/µL) (Invitrogen) after stimulation. For the supernatants collected directly from the 24-well plate, 500 µL of supernatant were collected from each well to 24 designated Eppendorf tubes. These tubes were centrifuged at 2000 RPM (Eppendorf centrifuge 5810 R, Eppendorf) for 5 min and 450 µL of the supernatant was transferred to new Eppendorf tubes before being stored at -80°C. For the DNAse I (Invitrogen) treatment, supernatants were removed from the 24-well plate, and cells on coverslips were washed two times with HBSS. Next, 5 µL of DNAse I diluted in HBSS to a final concentration of 100 U/mL was pipetted directly onto the coverslips followed by 500 µL of HBSS and then incubated for 15 min at 37°C. After incubation, 500 µL from each well were transferred to

Eppendorf tubes and 10 µL of EDTA was added to each tube. The tubes were centrifuged at 300 x g for 5 min and 450 µL of the supernatant was transferred to new tubes. All supernatants were stored at -80°C.

## 3.6 BCR-ABL1 expression

### 3.6.1 Reverse-transcription polymerase chain reaction (RT-PCR)

Reverse transcription polymerase chain reaction (RT-PCR) is a technique primarily used to measure the amount of a specific RNA sequence. The technique combines reverse transcription of RNA into complementary DNA (cDNA) and amplification of a specific DNA target using polymerase chain reaction (PCR).

**RNA isolation**

The RNeasy® Plus Mini Kit (Qiagen) was used to extract total RNA following the protocol from the manufacturer. All tubes, columns, and buffers used were supplied in the kit. RNA was extracted from Kcl-22 cells harvested after 5 days of differentiation and from primary blood cells (neutrophils and mononuclear cells) harvested from human CML patients or healthy donors. Minimum 1 x $10^6$ cells were collected and centrifuged to form a pellet, stored in -80°C until use.

Cells were thawed on ice before supernatant was removed and pellet was resuspended in 350 µL of Buffer RLT Plus and vortexed for 30 sec. For elimination of non-RNA products (DNA), the lysate was transferred to a gDNA Eliminator spin column placed in a 2 mL collection tube and centrifuged for 30 sec at 12000 RPM (Eppendorf centrifuge 5427 R, Eppendorf) The column was removed and 350 µL of 70% ethanol was added to the flow-through and mixed well. This 700 µL of RNA lysate/ethanol mix was transferred to a RNeasy spin column placed in a 2 mL collection tube and centrifuged for 30 sec at 12000 RPM (Eppendorf centrifuge 5427 R, Eppendorf) for the RNA to bind to the spin column. The flow-through was discarded and 700 µL of washing buffer (Buffer PW1) was added to the spin column and centrifuged for 30 sec at 12000 RPM (Eppendorf centrifuge 5427 R, Eppendorf) for the first wash. The same steps were repeated 2 times with 50 µL of Buffer RPE, centrifuged for 30 sec, and a second time for 2 min. Finally, the RNeasy spin column was

placed in a fresh 1.5 mL collection tube and 30 µL of RNase-free water was added directly to the spin column membrane followed by centrifugation for 1 min at 12000 RPM (Eppendorf centrifuge 5427 R, Eppendorf) to elute total RNA. The concentration of total RNA yield was measured by NanoDrop ND-1000 Spectrophotometer.

**cDNA synthesis by reverse transcription**

The synthesis of cDNA from total RNA was performed using the SuperScript® III First-Strand Synthesis System for RT-PCR (Invitrogen). All components (supplied in the kit) were thawed and briefly centrifuged before use. Approximately 5 µg of total RNA, 1 µL of oligo (dT) primer (50 µM), and 1 µL of mM dNTP mix (10mM) were combined in 500 µL tubes and incubated at 65°C for 5 min. Samples were placed on ice for at least 1 min before adding 10 µL of the cDNA Synthesis Mix. The cDNA Synthesis Mix was prepared by adding the following components in the indicated order (each volume was multiplied by number of samples): 2 µL 10X RT buffer, 4 µL 25 mM $MgCl_2$, 2 µL 0.1 M DTT, 1 µL RNaseOUT$^{TM}$ (40 U/µL) and 1 µL SuperScript® III RT (200 U/µL) per sample. After adding the cDNA Synthesis Mix samples were mixed gently and collected by brief centrifugation. For the synthesis of cDNA, samples were incubated 50 min at 50°C. The reaction was then terminated at 85°C for 5 min and samples were chilled on ice before continuing with PCR.

**Amplification of cDNA by polymerase chain reaction (PCR)**

For amplification of cDNA, polymerase chain reaction (PCR) was performed using PCR SuperMix (Invitrogen) and two primers, forward and reverse, specific for BCR/ABL and beta-actin as a housekeeping gene/positive control. Information about sequence and suppliers for all primers is provided in Table 2.1. PCR SuperMix (1.1X) (Invitrogen) is a ready-to-use mixture of recombinant *Taq* DNA Polymerase, salts, magnesium ($Mg^{2+}$) and deoxyribose nucleotide triphosphate (dNTPs) for PCR amplification.

**Table 3.1. PCR primers**

| Genes | | Sequence (5´- 3´) | Name | Supplier |
|---|---|---|---|---|
| **BCR-ABL1** | Forward | GTTTCAGAAGCTTCTCCCTG | EA122 | Sigma-Aldrich |
| | Reverse | TGTGATTATAGCCTAAGACCCGGAG | EA500 | Sigma-Aldrich |
| **ß-Actin** | Forward | CTACAATGAGCTGCGTGTGG | ActinB- F | Sigma-Aldrich |
| | Reverse | AAGGAAGGCTGGAAGAGTGC | ActinB- R | Sigma-Aldrich |

100 ng of cDNA was mixed with 35 µL PCR SuperMix (Invitrogen), 2 µL EA122 (10µM) forward primer, and 2 µL EA500 (10 µM) reverse primer in a PCR reaction tube placed on ice. Equal volumes of cDNA and PCR SuperMix (Invitrogen) with beta-actin primes (10 µM) were added in separate tubes for housekeeping gene/positive control. Tubes were briefly centrifuged before amplification was carried out in an automated DNA thermal cycler (S1000™ Thermal Cycler, Bio Rad) as following: an initial denaturing step at 94°C for 15 min, then 35 cycles of 94°C for 45 sec, 60°C for 30 sec and 75°C for 1 min, and a final extension at 72°C for 7 min. PCR products were then kept at 4°C until electrophoresis was performed.

**DNA gel electrophoresis**

Agarose gels (1.5% agarose) containing a fluorescence dye binding to dsDNA were prepared by mixing 1,5 g of UltraPure™ Agarose (Invitrogen) with 100 mL of 0.5X TAE (Tris-Acetate-EDTA) buffer (50X diluted in distilled water) and 20 µL of Nancy-520 (>97.0% HPCE, Sigma Life Science, Lot#BCBX4189). 10 µL of PCR product were mixed with 1 µL of loading buffer (1X BlueJuice) and loaded into each well. 5 µL of Quick-Load® Purple 100 bp DNA Ladder (50 µg/mL, New England Bio Labs® Inc.) were used as marker for size. The gel electrophoresis was run in 0.5X TAE buffer at 100V, 100mA, and 15W for 30 min. For reliability, BCR-ABL1 positive (KU-812 and Kcl-22) and negative (Molm-13 and water) controls were used in all assays. The gels were visualized and imaged using the Gel Doc™ EZ Imager (BioRad) with the Image Lab™ (BioRad) software.

### 3.6.2 Immunoblotting

Protein immunoblot analysis was used for investigating protein expression of BCR/ABL1 and phospho-BCR-ABL1.

In general, 3 x $10^6$ cells in suspension were centrifuged for 4 min and the supernatant was replaced with 500 µL cold 0.9% NaCl before centrifuged again at 4000 RPM (Eppendorf centrifuge 5427 R, Eppendorf) for 5 min. The supernatant was removed and the pellet was resuspended in 80 µL SHIEH lysis buffer [97] (10 mM Tris HCl pH 7.5, 1 mM EDTA, 400 mM NaCl, 10% glycerol, 0.5% NP-40, 5 mM NaF, 0.5 mM Na orthovanadate, 1 mM dithiothreitol (DTT), Complete Mini Protease Inhibitor Cocktail (Boeringer Mannheim) diluted in dd$H_2O$ and lysed for minimum 15 min on ice before centrifuged for 15 min at 12000 RPM (Eppendorf centrifuge 5427 R, Eppendorf) at 4°C and stored at -80°C until further immunoblot analysis. Protein concentration was determined by the Bradford method and plates were read by a plate reader (Infinite M200 pro, Tecan) [98].

Lysates for each sample were diluted in 2X sample buffer (2% SDS, 20% Glycerol, 24 mM Tris-HCL pH 6.8, 100 mM DTT, and 0.1% Bromophenol Blue in ddH2O) to create a total protein amount of 30 µg protein for each sample or higher amount of total protein was used if 30 microgram was not enough. 1X sample buffer (1% SDS, 10% Glycerol, 12 mM Tris-HCL pH 6.8, 50 mM DTT, and 0.1% Bromophenol Blue in ddH20) was added to get a total volume of 35 µL. Samples were heated for 10 min at 100°C to denature the proteins then briefly spun prior to gel loading. Proteins were separated by size with sodium dodecyl sulfate polyacrylamide gel electrophoresis (SDS-PAGE) using 4-20% Mini-PROTEAN TGX Gels (Bio Rad) and 1X running buffer (10X Tris/Glycine/SDS Buffer diluted with distilled water to a total volume of 1 L) for approximately 1.5 h at 100V. Precision Plus Protein™ All Blue Standards (15 µL) (Bio Rad Laboratories) was used as molecular weight standard.

Following protein separation by size, the proteins were blotted onto a Polyvinylidene fluoride (PVDF) membrane (Immun-Blot® PVDF Membranes for Protein Blotting, BioRad). Prior to protein blotting, the membrane was activated for approximately 30 sec in 100% methanol followed by 10 min incubation in 1-Step™ Transfer Buffer (Thermo Scientific) before being placed on top of two filter papers soaked in 1-Step™ Transfer Buffer (Thermo Scientific). The gel was then layered on top of the membrane followed by two additional filter papers to generate the blotting sandwich. Using the Pierce G2 Fast Blotter (Thermo Scientific), with the

high molecular weight program (10 min), proteins were transferred (blotted) from the gel to the membrane.

To avoid unspecific binding of the primary or secondary antibodies, the membrane was blocked using 5% Blocking buffer (Bovine Serum Albumin (BSA)) or Skim Milk Powder (Fluka Analytics) dissolved in TBS-Tween to a final concentration of 5% for 1 h at room temperature on a shaker. Next, the membrane was incubated with primary antibody overnight at 4°C on rotation. The phospho-c-Abl antibody ((Y412) (247C7), rabbit monoclonal antibody, Cell signaling) was diluted 1:1000 in 5% FBS blocking buffer. The c-Abl antibody ((24-11) sc-23 mouse monoclonal $IgG_1$, Santa Cruz Biotechnology) was diluted 1:1000 in 1% skim milk blocking buffer (5% skim milk blocking buffer diluted in TBS-Tween to a final concentration of 1%). The COX IV antibody (ab 16056, Abcam), used as loading control, was diluted 1:2000 in 1% skim milk blocking buffer. The day after, membranes were washed for 2 x 5 min and 1 x 15 min in TBS-Tween (1L 1X TBS with 1mL Tween® 20) before incubated with secondary antibody for 1 h at room temperature. The secondary antibodies used for binding to the primary antibodies were either anti-mouse or anti-rabbit secondary antibodies (depending on the primary antibody) conjugated with horse-radish peroxidase diluted 1:10 000 in 1% skim milk blocking buffer. After incubation, membranes were washed 2 x 5 min in TBS-T and 15 min in 1X TBS before development. Proteins were visualized using SuperSignal™ West Pico PLUS Luminol/Enhancer Solution (Thermo scientific) mixed with equal volume of SuperSignal™ West Pico PLUS Stable Peroxide Solution (Thermo Scientific) and images acquired using the Amersham™ Imager 680.

## 3.7 Treatment with tyrosine kinase inhibitors (TKIs)

Kcl-22 cells and CML neutrophils were treated with two different BCR-ABL1 specific tyrosine kinase inhibitors for the investigation of the involvement of BCR-ABL1 in NET formation.

10 x $10^6$ Kcl-22 cells, incubated with ATRA for 5 days, or control Kcl-22 cells were seeded in 10 mL of media in 25 $cm^2$ cell culture suspension flasks (Sarstedt) and treated with 0.1 µM ponatinib (AP24534, Selleckchem) or 100 nM ABL001 (asciminib) (Novartis) for 1 h in a 5% $CO_2$ humidified incubator (37°C). After treatment with TKIs, cells were seeded onto coverslips in a 24-well plate (previously described) and 3 x $10^6$ cells from each condition were

lysed for immunoblot analysis (previously described). Primary CML patient-derived neutrophils (isolated and thawed as described earlier) were treated with the same TKIs for quantification and visualization of NETs after treatment. 0.1 x $10^6$ cells were seeded onto a 1 µ-Slide 8 Well (IBIDI GmbH) tray, pre-coated with 200 µL of Poly-L-Lysine for 5 min, and incubated under normal cell culturing conditions (5% $CO_2$, 95% $O_2$, and 37°C) for 30 min for cell attachment before adding 0.1 µM ponatinib or 100 nM ABL001. Cells were then incubated for 30 min before continuing with the rest of the steps for live imaging as previously described.

# 4. Results

## 4.1 Methodology training and optimization using the HL-60 cell line

Since human primary neutrophils are short-lived and easily activated by environmental factors, the study of neutrophil extracellular trap (NET) formation is challenging, and therefore cell line models are required for method optimization. Thus, a cell line that resembles the functions of peripheral blood neutrophils is useful. Manda-Handzlik and co-workers demonstrated that differentiation of HL-60 cells towards granulocyte-like cells is achieved by treatment with all-trans retinoic acid (ATRA), dimethyl sulfoxide (DMSO), or dimethyl formamide (DMF) and that these differentiated cells release NETs upon stimulation with phorbol 12-myristate 13-acetate (PMA) or ionomycin calcium salt (IO) [99].

For this reason, the HL-60 cell line was initially used in order to learn the different methods needed for the study of NET formation. This included basic cell culture techniques, followed by cell differentiation, stimulation, and visualization of NETs by immunofluorescence and microscopy. Optimization included determination of appropriate cell density for the different experiments and titrations of primary antibodies used for immunofluorescence to determine optimal concentrations needed.

### 4.1.1 Differentiation of HL-60 cells to granulocytes assessed by nuclear morphology

To successfully differentiate HL-60 cells to granulocyte-like cells they need to be exposed for five days to compounds with cell differentiating effect [99]. Therefore HL-60 cells were treated with ATRA, DMSO, or DMF for five days, where at day two, the cells were centrifuged and added fresh medium with differentiation agent. After five days, the cells were cytospun, stained with May-Grunwald Giemsa (MGG), and examined by light microscopy for changes in nuclear morphology compared to untreated cells (Ctr). All three differentiating compounds were able to induce morphological nuclear changes similar to granulocytes with characteristic band-like nuclei (Fig. 4.1 A, arrows).

To assess differentiation efficacy, the cells were morphologically counted by classifying the cells as either “differentiated” or “undifferentiated” according to their nuclear morphology.

Cells appearing like myeloblast, promyelocytes, and myelocytes, with a round nuclear morphology were scored and counted as “undifferentiated” whereas cells with a nuclear morphology similar to metamyelocytes, banded neutrophils, and mature neutrophils were counted as “differentiated” (Fig. 4.1 B).

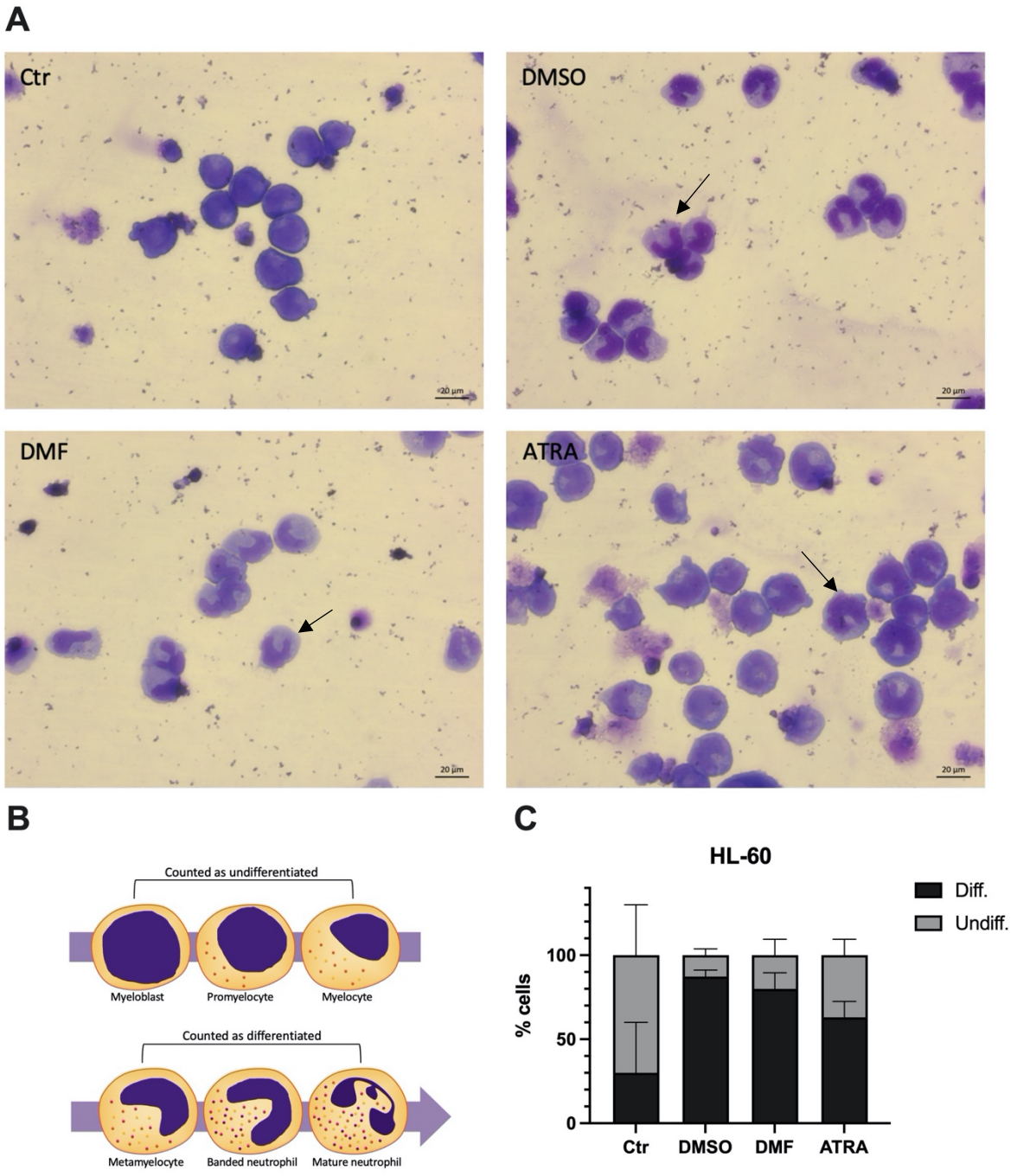


**Figure 4.1. Granulocytic differentiation of HL-60 cells. (A)** HL-60 cells were differentiated by treatment with DMSO, DMF, or ATRA for 5 days. Differentiation efficacy was assessed morphologically after May-Grunwald Giemsa (MGG) staining and light microscopy (Zeiss Axio Vert A1), 40x objective, Scale bars: 20µm. **(B)** As illustrated, cells with round shaped nuclei such as myeloblast, promyelocytes, and myelocytes were scored as undifferentiated and cells with nuclei morphologically similar to metamyelocytes, banded neutrophils, and mature neutrophils were scored as differentiated. **(C)** Quantification of differentiated (Diff) HL-60

cells versus undifferentiated (Undiff) comparing cells treated with DMSO, DMF or ATRA with untreated control cells (Ctr). 100 cells from each condition were scored and counted for three separate experiments.

The manual counting of the HL-60 cells showed that DMSO was the most potent differentiation agent followed by DMF and HL-60 cells treated by ATRA showed only around 50% differentiated cells (Fig. 4.1 C). ATRA-treated HL-60 cells appeared bigger in size compared to treatment with DMSO or DMF. Several untreated control cells were also observed with a changed nuclear morphology classified as differentiated. This could be due to high cell density and longtime culture by itself which can cause granulocytic differentiation. However, as seen in Figure 4.1 C, the standard deviation is very high for the control cells compared to ATRA, DMSO and DMF treated cells. Three counts were done, and the number of "differentiated" control cells from the three separate experiments were 19, 64, and 7, respectively, which may indicate that the control HL-60 cells had some unusual growth in experiment two compared to the other conditions and might not be representative. However, a clear differentiating effect on the HL-60 cells was found for all three compounds tested as compared to untreated cells.

### 4.1.2 Induction of NET formation visualized by immunofluorescence

Untreated HL-60 cells or HL-60 cells treated with DMSO, DMF, or ATRA were stimulated with PMA or IO for three hours and assessed for induction of NET formation. Cells were attached to poly-l-lysine pre-coated coverslips in a 24-well plate and following three hours of stimulation they were fixed and assessed by immunofluorescence. Cells were stained with primary antibodies against the NET components neutrophil elastase (NE) and citrullinated histone H3 (citH3), pre-titrated prior to this experiment, and fluorochrome-conjugated secondary antibodies against the primary antibodies. After staining, the cells were counterstained with DAPI for visualization of the nucleus/DNA and investigated by fluorescent light microscopy (Fig 4.2).

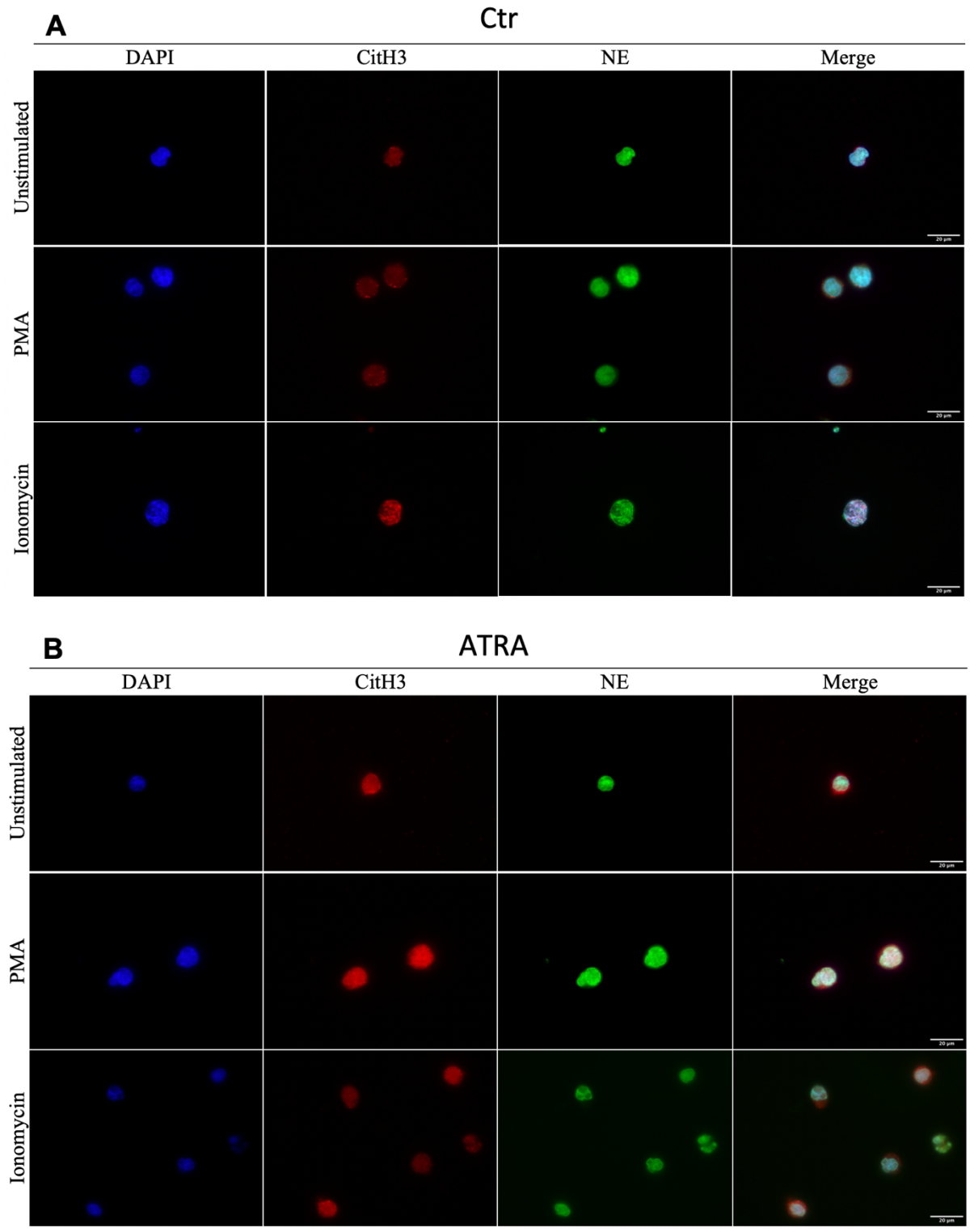
A
Ctr
DAPI
CitH3
NE
Merge
Unstimulated
PMA
Ionomycin
B
ATRA
DAPI
CitH3
NE
Merge
Unstimulated
PMA
Ionomycin

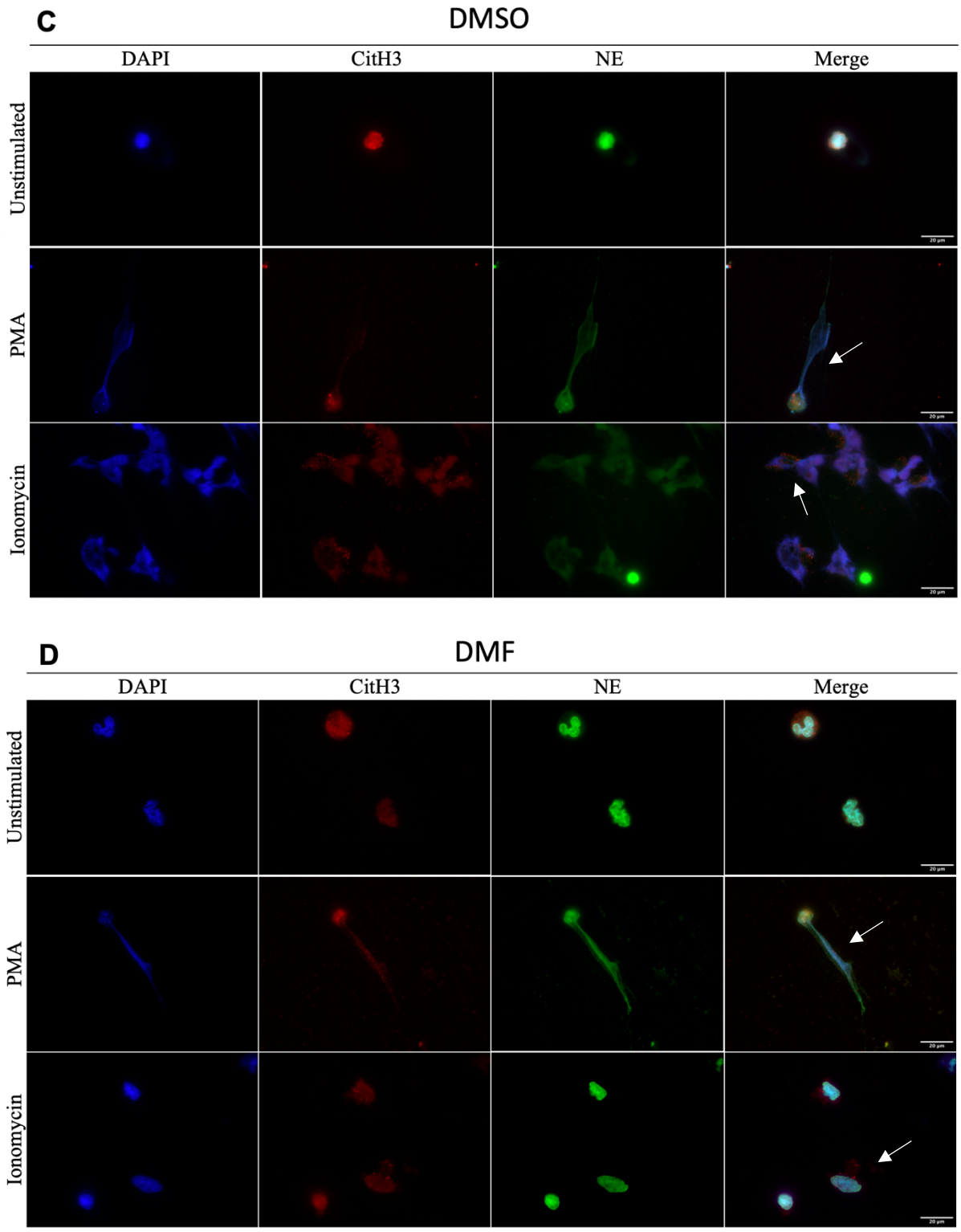


**Figure 4.2. NET formation in HL-60 cells.** HL-60 cells pre-treated with differentiation compounds or not (control) were stimulated with PMA or ionomycin (IO) compared to no stimulation, before fixed, stained with NET-identifying antibodies anti-CitH3 (red), anti-NE (green), counterstained with DNA-binding fluorescent compound DAPI (blue) and analyzed by fluorescent microscopy. Pre-treatment: **(A)** non-treated control cells **(B)** ATRA **(C)** DMSO **(D)** DMF. Images were acquired and analyzed by Zeiss AxioObserver Z1 microscope and ZEN 2012 (blue version) software and figures were made using ImageJ v.2.1.0 (Fiji). Scale bars: 20 µm.

Investigation by immunofluorescence showed that untreated control cells, unstimulated or stimulated, did not form NETs, neither did the cells pre-treated with ATRA (Fig. 4.2 A-B). However, both the DMSO and DMF pre-treated HL-60 cells extruded NETs or NET-like structures after stimulation with PMA or IO as compared to no NET formation without stimulation (Fig. 4.2 C-D). The cells pre-treated with DMF and stimulated with IO appeared to be in an early stage of NET formation, thus pre-NET structures (Fig. 4.2 D, arrow), compared to the cells pre-treated with DMSO and stimulated with PMA or IO and cells pre-treated with DMF and stimulated with PMA which generated structures similar to fully extruded NETs (Fig. 4.2 C and D, arrows).

## 4.2 CML cells and NET formation

After being trained in cell tissue culturing, microscopy, exposing of cells to different compounds, and optimizing the methods for cellular differentiation and visualization of NETs by immunofluorescence, the next step was to utilize these methods to investigate the capability of CML cells to form NETs. For this, the CML cell line Kcl-22 was used (Table 4.1).

### 4.2.1 Differentiation capability of Kcl-22 cells assessed by nuclear morphology and expression of cell surface markers

Kcl-22 cells were exposed to ATRA, DMSO, or DMF for five days as described for the HL-60 cells. Cell differentiation was assessed morphologically by MGG staining (Fig. 4.3 A) and differential counting (Fig. 4.3 B) as described for the HL-60 cells and additionally by quantifying cell surface-expressed cluster of differentiation (CD) markers by flow cytometry. Cells with a morphology similar to late stages in the granulocyte maturation process were counted as “differentiated” and cells with a round nuclear morphology were counted as “undifferentiated” as described in Figure 4.1 B. The differential counting showed low levels of differentiation compared to control cells. Kcl-22 cells treated with DMSO or ATRA resulted in the highest percentage of differentiated cells, but still, less than 40% of the cells were scored as differentiated. Kcl-22 cells treated with DMF showed little or no differentiation compared to control cells.

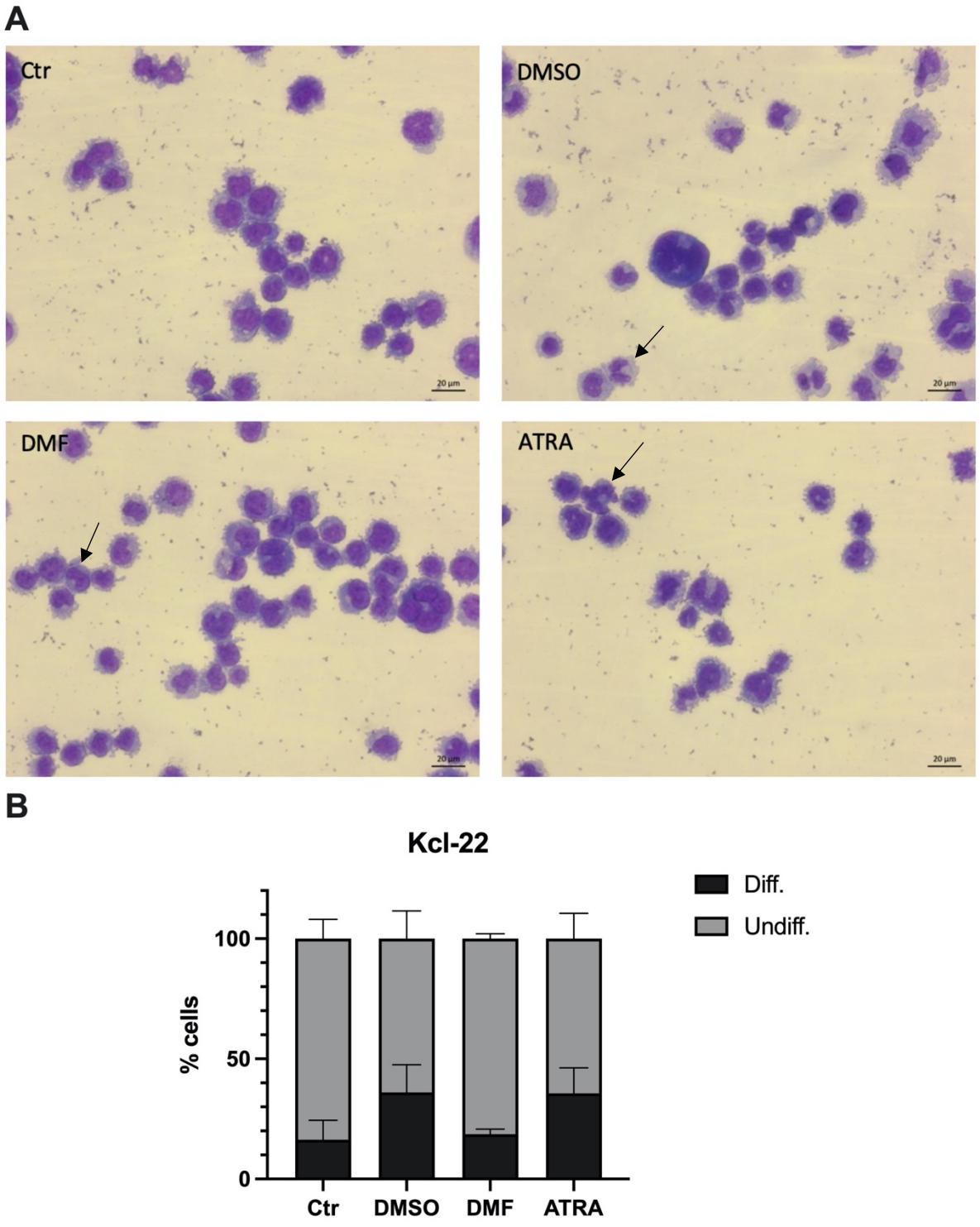


**Figure 4.3. Granulocytic differentiation of Kcl-22 cells.** Kcl-22 cells were treated or untreated with differentiation compounds for 5 days. **(A)** Ctr cells (untreated), DMSO, DMF, and ATRA treated cells after May-Grunwald Giemsa (MGG) staining and light microscopy (Zeiss Axio Vert A1, 40x objective, Scale bars: 20µm). Arrows point to "differentiated" cells. **(B)** Cell differentiating was assessed morphologically after MGG staining by counting the number of "differentiated" and "undifferentiated" cells. Percent differentiated (Diff) and undifferentiated (Undiff) Kcl-22 cells untreated (Ctr), DMSO, DMF, and ATRA treated cells when 100 cells from each condition were counted and scored in three separate experiments.

Measurement of cell surface-expressed cluster of differentiation (CD) markers allows for distinguishing neutrophils from other types of granulocytes and monocytes. By staining fixed cells with antibodies against CD markers of interest and running the samples through a flow cytometer expression of different CD markers on single cells can be detected and quantified. Analysis of the expression of specific CD markers can therefore be used as a tool to investigate and verify the differentiation state of cells after being exposed to differentiation compounds. Human neutrophils are identified by the expression of CD11b and CD33 and distinguished from eosinophils and monocytes based on the expression of CD15 and low or lack of expression of CD14 [7]. Therefore, these four CD markers were chosen to characterize their expression on Kcl-22 cells after treatment with ATRA, DMSO, or DMF compared to untreated cells. The cells were stained with pre-titrated volumes of directly fluorescent labelled antibodies against CD11b (PE), CD14 (AF488), CD15 (AF647), and CD33 (APC/Cyanine 7). In addition, cell samples from each condition were fixed but not stained for unstained controls. Compensation beads were stained with the four antibodies, one tube for each antibody.

The analysis of the flow cytometry data was done using FlowJo (10.8.1) and started with compensation of the four antibodies using the beads and the compensation tool in FlowJo. Gating for the live cell population using side and forward scatter was done, and cell doublets were excluded by gating on single cells using forward scatter area (FSC-A) on the x-axis, against forward scatter height (FSC-H) on the y-axis (Fig. 4.4 A). Then a gate was established for each CD marker based on negative (unstained cells) and positive (stained cells) cells (Fig. 4.4 A). This led to a quantification of CD14, CD11b, CD15, and CD33 expression of Kcl-22 cells after treatment with DMSO, DMF, or ATRA relative to untreated (Ctr) cells. The statistical analysis was performed in FlowJo, giving the median fluorescence intensity (MFI) based on three independent experiments (Fig. 4.4 B).

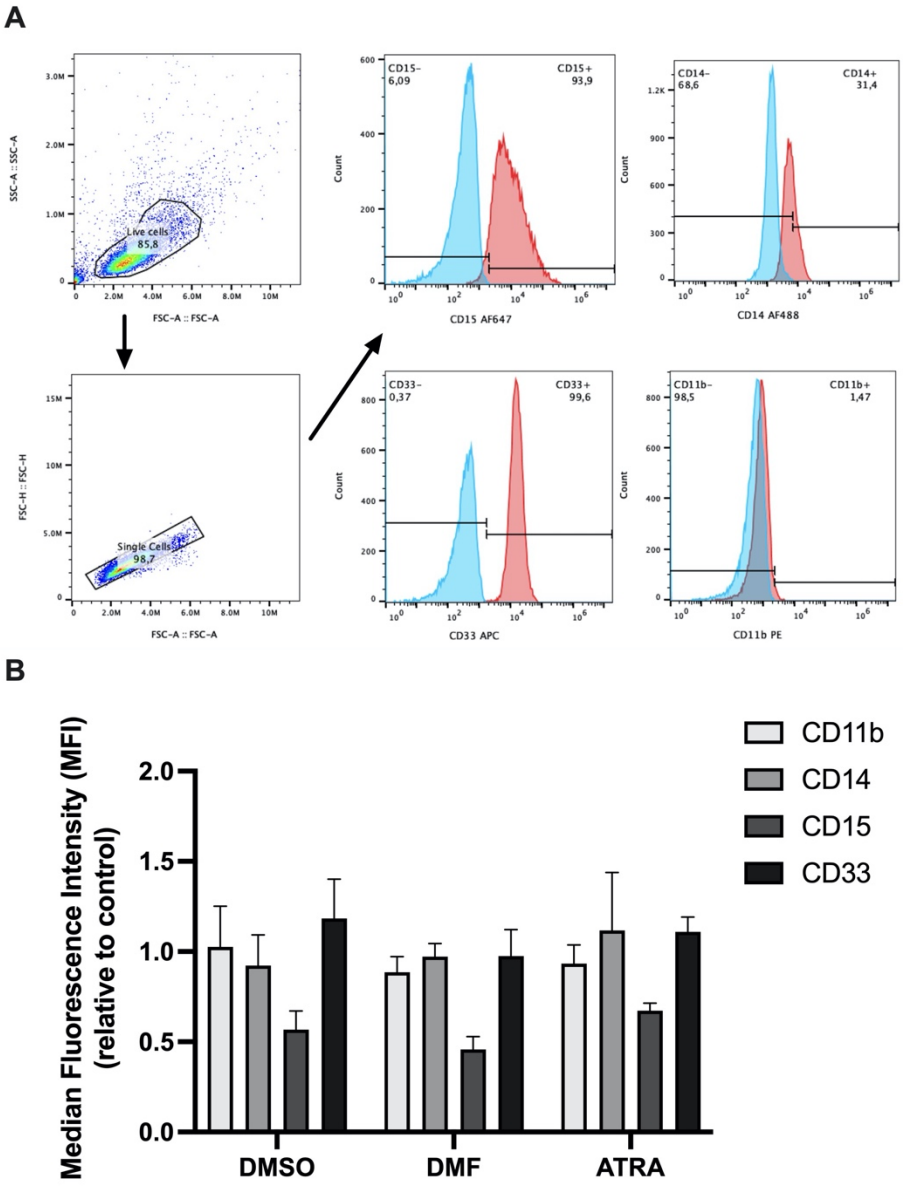


**Figure 4.4. Expression of CD markers on Kcl-22 cells (A)** Gating strategies for live cells and single cells and expression of CD15, CD33, CD14, and CD11b on untreated Kcl-22 cells where blue represents unstained cells and red antibody-stained cells. **(B)** Median fluorescence intensity (MFI) relative to control cells for DMSO, DMF, and ATRA treated Kcl-22 cells. Fluorochrome labelled antibodies against CD11b (PE), CD14 (AF488), CD15 (AF647), and CD33 (APC/Cyanine 7) were used.

These results showed that DMSO, DMF and ATRA treated Kcl-22 cells, from three separate experiments, only had minor differences with respect to expression of CD11b, CD14 and CD33, however, a reduction in CD15 expression was found for all three treatments. This could suggest that the treatment induced differentiation in another direction than neutrophils. The almost lack of nuclear morphology changes observed after MGG staining combined with the reduced CD15 expression could indicate that the Kcl-22 cells differentiated towards a mast

cell direction which then could be prone to generate mast cell extracellular traps (MCETs) [100].

### 4.2.2 Kcl-22 cells extrude NET-like structures

To investigate if ATRA, DMSO, or DMF treated Kcl-22 cells were able to generate extracellular traps (ETs) as compared to untreated Kcl-22 cells were attached to poly-l-lysine pre-coated coverslips in a 24-well plate and stimulated with PMA or IO for three hours. Cells were then assessed for induction of ETs by immunofluorescence, using antibodies against the ET components NE and CitH3, before counterstained with DAPI for visualization of the nucleus/DNA.

Investigation of ETs by fluorescence microscopy showed that ATRA, DMSO, and DMF treated Kcl-22 cells had more ET formation after stimulation compared to control (untreated) cells (Fig. 4.5). From imaging only, it was not evident to conclude that any of the differentiation compounds resulted in Kcl-22 cells more prone to extrude ETs, as all cells that had been exposed to a differentiation agent (DMSO, DMF, or ATRA) for five days extruded ET-like structures after stimulation with both PMA and IO. Fluorescence microscopy showed more ET-like structures in the pre-treated cells even though, as demonstrated earlier, Kcl-22 cells only minorly differentiated towards neutrophils, but the KCl-22 cells could have differentiated towards mast cells based on reduced CD15 expression and unchanged nuclear morphology, thereby these ETs could represent MCETs. PMA exposed cells showed in general more ETs compared to IO exposed cells.

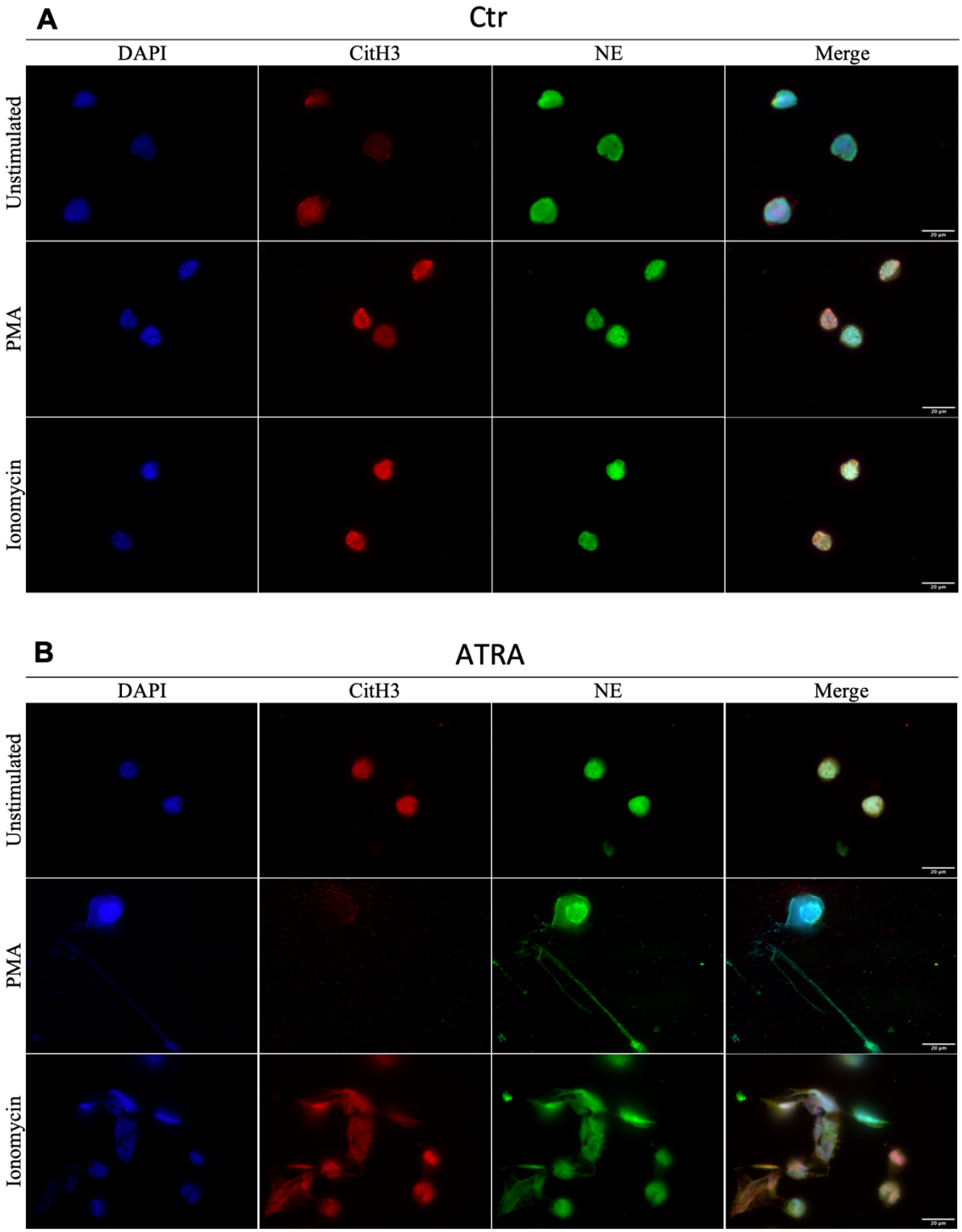
A
Ctr
DAPI
CitH3
NE
Merge
Unstimulated
PMA
Ionomycin
B
ATRA
DAPI
CitH3
NE
Merge
Unstimulated
PMA
Ionomycin

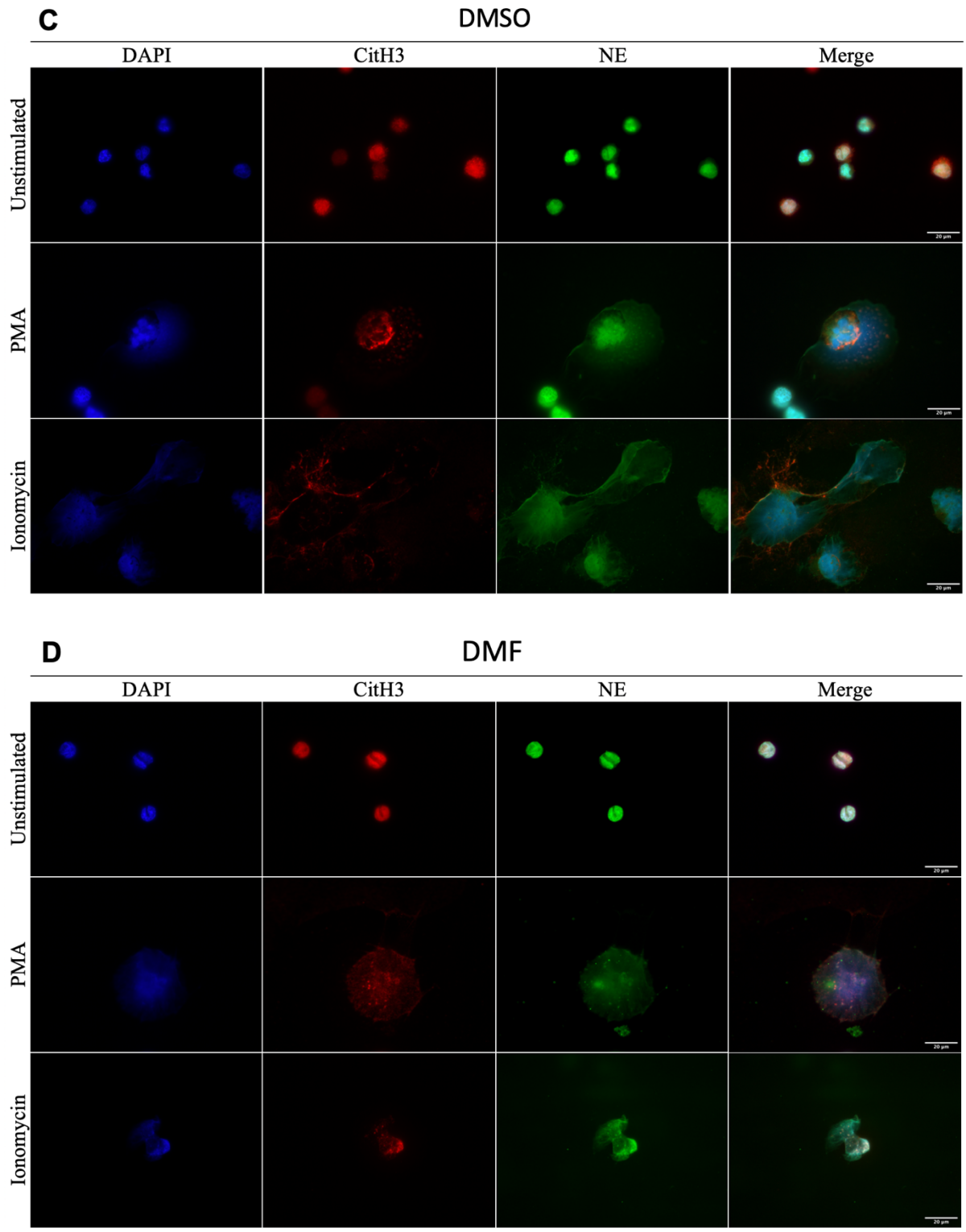


**Figure 4.5. Induction of ET formation in Kcl-22 cells.** Kcl-22 cells untreated or treated with differentiation compounds were not stimulated (unstimulated) or stimulated with PMA or ionomycin (IO), before being fixed and stained with the ET identifying markers anti-CitH3 (red) antibodies, anti-NE (green) antibodies, counterstained with DNA binding fluorescent compound DAPI (blue) and finally analyzed by fluorescent microscopy. Cells were pre-treated: **(A)** Non-treated (Ctr), **(B)** ATRA, **(C)** DMSO, **(D)** DMF. Images were acquired and analyzed by Zeiss AxioObserver Z1 microscope and ZEN 2012 (blue version) software and figures were made using ImageJ v.2.1.0 (Fiji). Scale bars: 20 µm.

### 4.2.3 Isolation of primary neutrophils and verification by MGG staining and flow cytometry

Since the Kcl-22 cells were not differentiated into neutrophils, NET formation was directly investigated in primary neutrophils derived and isolated from the blood of three CML patients and compared to neutrophils from the blood of two healthy donors (Table 4.1). The rare opportunity of examining NET formation in primary neutrophils from CML patients was through blood donated from these three CML patients included in the Bosupeg clinical trial (ClinicalTrials.gov Identifier: NCT03831776) at Haukeland University Hospital, whereas the blood from healthy individuals was donated through the Blood bank at Haukeland University Hospital. Primary neutrophils were isolated with Polymorphprep™ density gradient, from human venous blood from the three newly diagnosed CML patients and the two healthy donors.

**Table 4.1.** Primary samples and cell lines characteristics

| Sample | Gender | Age | Diagnosis | Treatment | CML phase | BCR-ABL1 fusion |
|---|---|---|---|---|---|---|
| CML 1 | M | 29 | CML | *De novo* | CP | e14-a2 (b3-a2) |
| CML 2 | M | 76 | CML | Hydroxyurea | CP | e13-a2 (b2-a2) |
| CML 3 | M | 74 | CML | *De novo* | CP | e14-a2 (b3-a2) |
| HD 1 | F | 26 | Healthy | NA | NA | NA |
| HD 2 | M | 56 | Healthy | NA | NA | NA |
| **Cell lines** | | | | | | |
| Kcl-22 | F | 52 | CML | NA | BP | e13-a2 (b2-a2) |
| KU-812 | M | 38 | CML | NA | BP | e14-a2 (b3-a2) |
| Molm-13 | M | 20 | AML | NA | NA | NA |
| HL-60 | F | 35 | APL | NA | NA | NA |

(CP: chronic phase, BP: blast phase, de novo: newly diagnosed, NA: not addressed)

After primary neutrophils were isolated using Polymorphprep™, the result of the isolation was assessed by flow cytometry for the expression of neutrophil-associated CD markers (CD11b, CD14, CD15, CD33) as described earlier for the Kcl-22 cells (Fig. 4.6 A-D). This also allowed for a comparison between the isolated neutrophils and the remaining mononuclear cell population (MCs). In addition, the isolated cells were morphologically examined by MGG staining (Fig. 4.6 E).

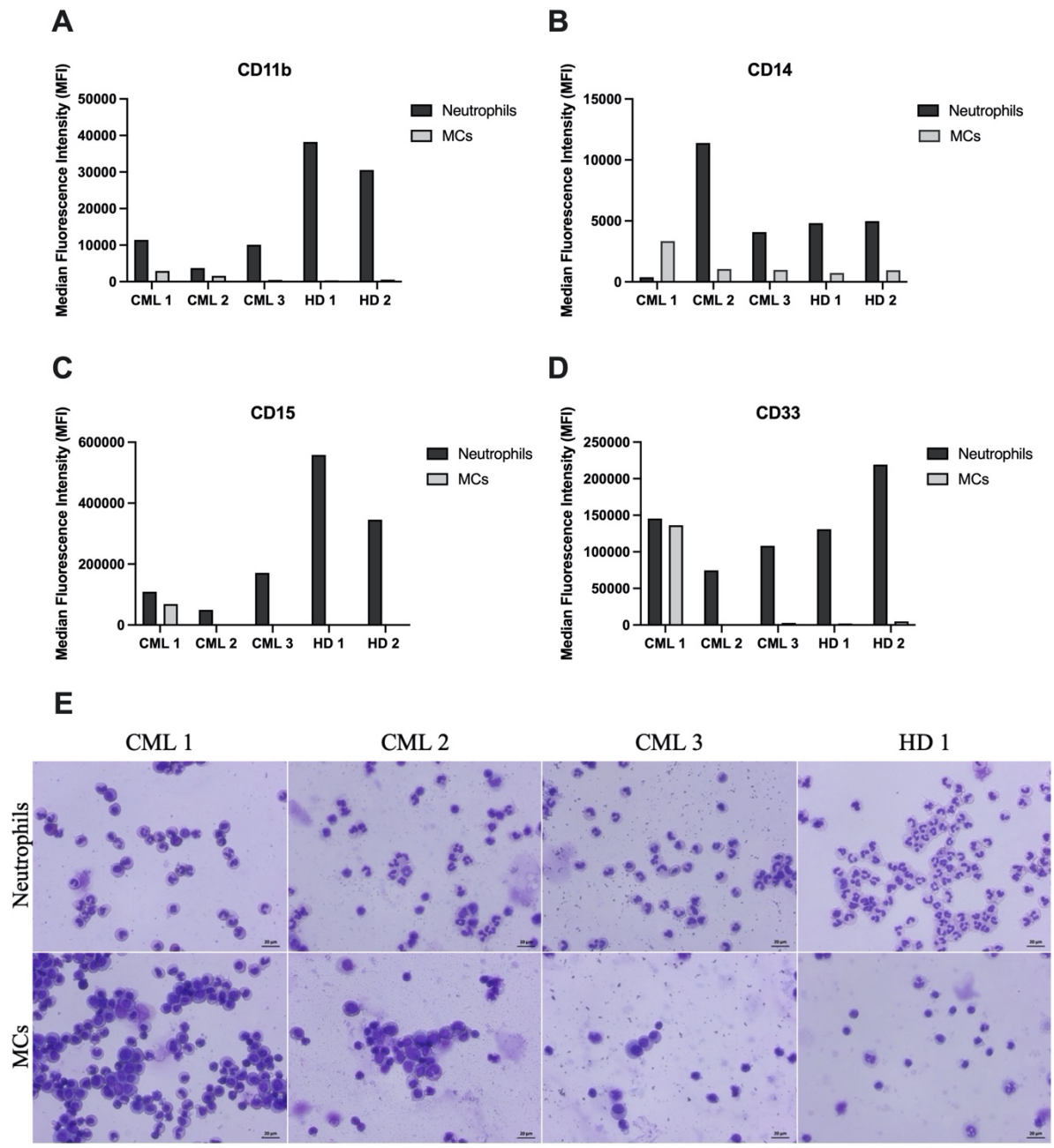


**Figure 4.6. Isolation of primary neutrophils.** Neutrophils and mononuclear cells (MCs) isolated from peripheral blood of three CML patients (CML 1, CML 2, CML 3) and two healthy donors (HD 2, HD 1) using density gradient Polymorphprep$^{TM}$. Median fluorescence intensity (MFI) of CD11b **(A)**, CD14 **(B)**, CD15 **(C),** and CD33 **(D)** acquired by flow cytometry and analysed in FlowJo. **(E)** Isolated neutrophils and MCs stained with May-Grunwald Giemsa, and images were acquired by light microscopy (Zeiss Axiovert A1, objective 40x). Scale bars: 20µm.

The median fluorescence intensity (MFI) (Fig. 4.6 A-D) showed in general higher expression of all four CD markers investigated in neutrophils compared to mononuclear cells (MCs). Morphological assessment after MGG staining, showed almost 100% nuclear segmented and banded neutrophils in the cells obtained from the neutrophil layer, demonstrating successful

isolation compared to the round appearance of the nuclei in the remaining mononuclear cells (MCs).

### 4.2.4 Induction of NET formation in primary neutrophils

After effectively inducing and visualizing NET-like structures in the HL-60 and Kcl-22 cell lines, the optimized method was used to investigate NET formation in the successfully isolated primary neutrophils. Isolated neutrophils were, stimulated with PMA or IO compared to non-stimulated, fixed, and stained by immunofluorescence, and assessed for NET formation by fluorescence microscopy (Fig. 4.7) as described for the HL-60 and Kcl-22 cells.

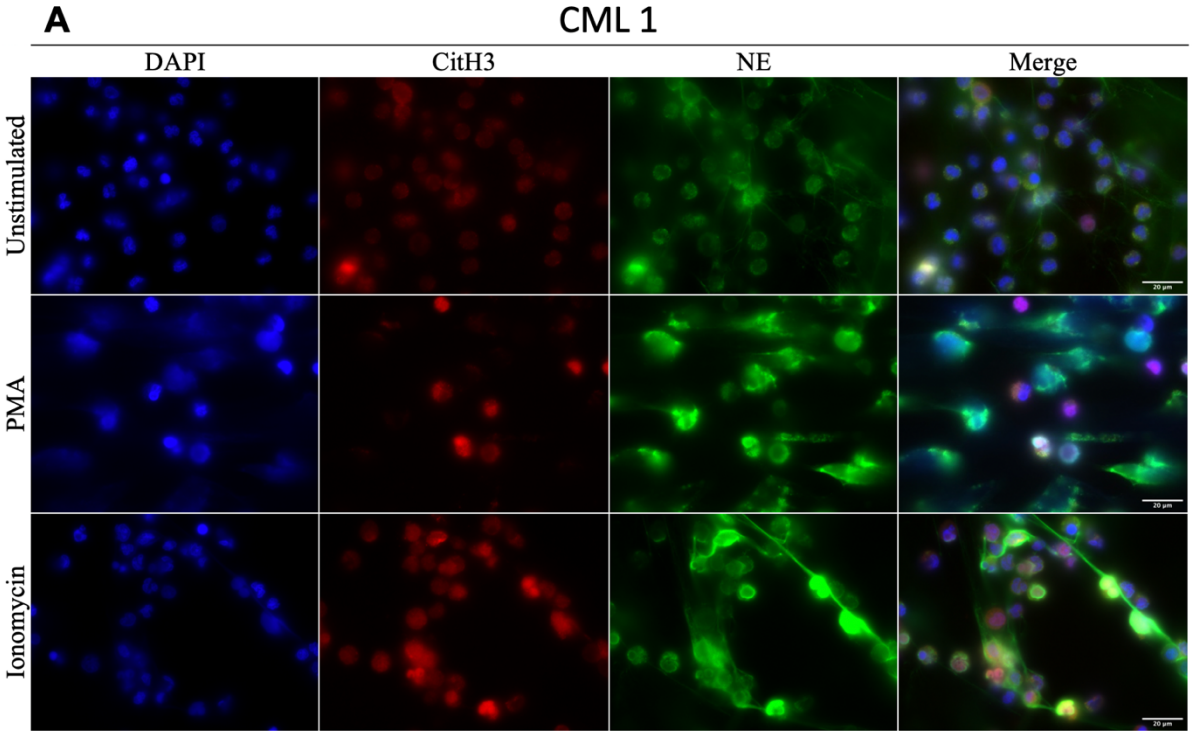

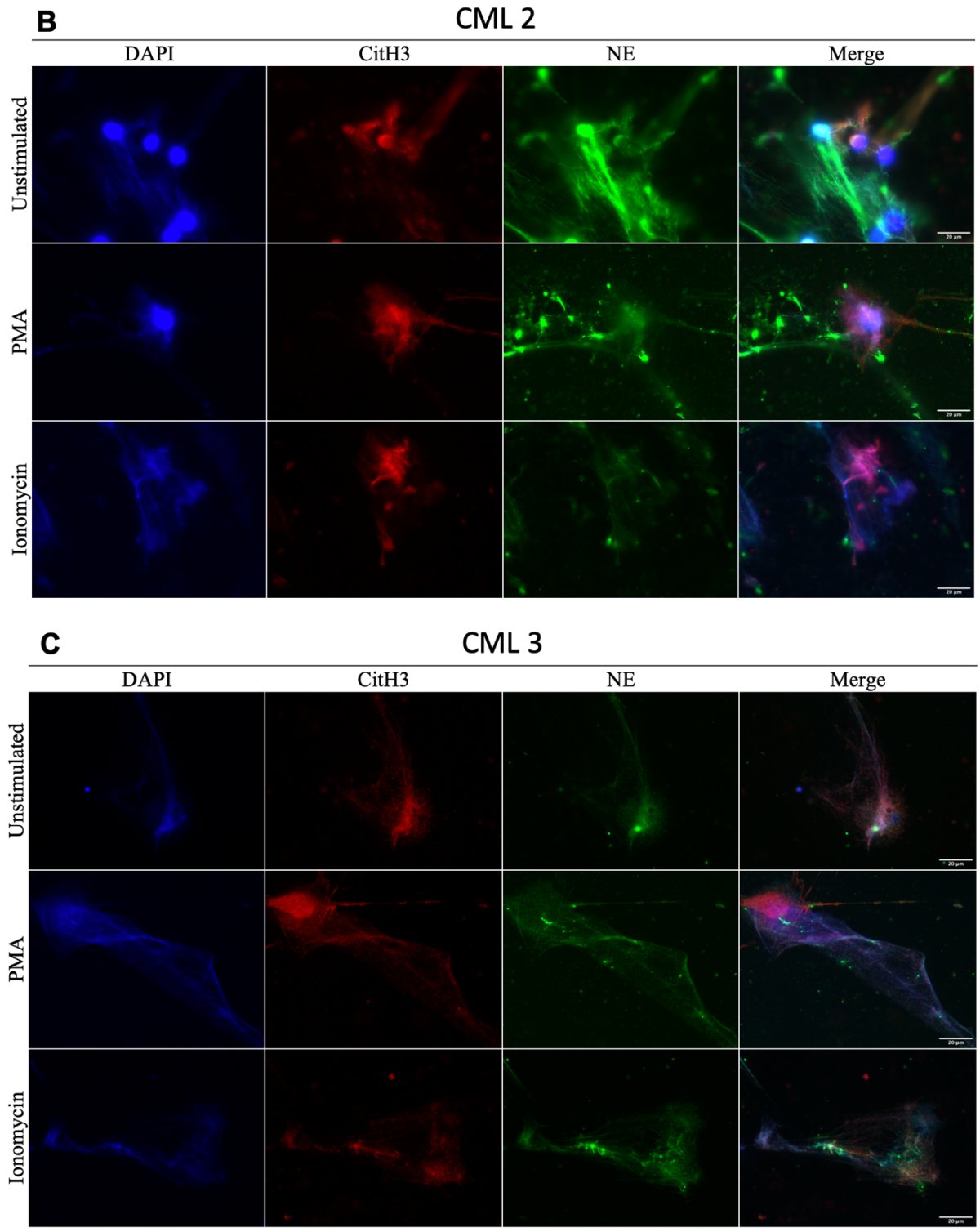
B
CML 2
DAPI
CitH3
NE
Merge
Unstimulated
PMA
Ionomycin
C
CML 3
DAPI
CitH3
NE
Merge
Unstimulated
PMA
Ionomycin

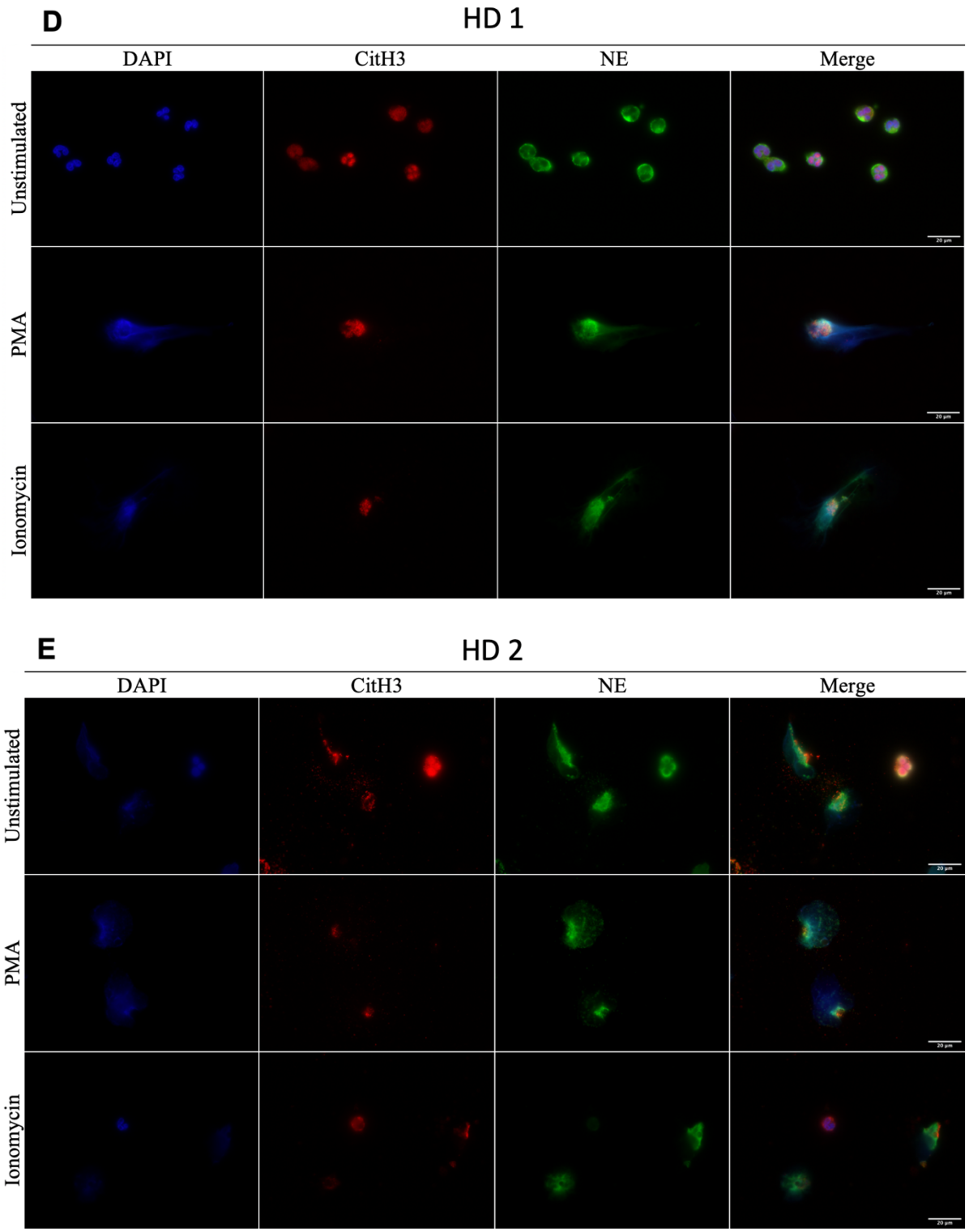


**Figure 4.7. NET formation in primary neutrophils.** Primary neutrophils isolated from venous blood of three CML patients and two healthy donors stimulated with PMA or ionomycin (IO) or unstimulated were fixed and stained with NET identifying markers; anti-CitH3 (red) antibodies, anti-NE (green) antibodies and counterstained with DNA binding fluorescent compound DAPI (blue) and analyzed by fluorescent microscopy. **(A)** CML 1, **(B)** CML 2, **(C)** CML 3, **(D)** HD 1, **(E)** HD 2. Images acquired by AxioObserver Z1 and ZEN 2012 (blue version) software and figures were made using ImageJ v.2.1.0 (Fiji), 63x oil objective. Scale bars: 20 µm.

NET formation appeared more excessive in neutrophils from all three CML patients (Fig. 4.7 A-C) compared to the two healthy donors (Fig. 4.7 D and E), where neutrophils derived from the CML patients formed longer structures, covering larger areas compared to the neutrophils from the healthy donors. In the unstimulated neutrophils from healthy donor 1 (Fig. 4.7 D), areas with fully intact neutrophils without any NETs were observed. This was never observed in either stimulated or unstimulated neutrophils derived from any of the CML patients.

The investigation of NETs in primary cells showed in general a higher degree of NET formation compared to the Kcl-22 cells (Fig. 4.5). Primary neutrophils extruded NET-like structures upon stimulation with PMA and IO, and without any stimulating agent. NETs released by primary neutrophils derived from these three CML patients formed longer structures covering substantial areas compared to the mast cells-like Kcl-22 cells which formed smaller ET-like structures possibly representing MCETs.

### 4.2.5 NET formation in neutrophils by live cell imaging

After investigating NETs in fixed cells by immunofluorescence, live cell imaging was performed to visualize the process of NET formation in real-time. Live cell imaging was performed on neutrophils isolated from the blood of all three CML patients and compared to neutrophils from one healthy donor and ATRA-treated Kcl-22 cells. After neutrophil isolation (primary cells) or five days of ATRA treatment (Kcl-22 cells), 0.1 x $10^6$ cells were seeded onto a µ-Slide 8-well tray (pre-coated with Poly-L-Lysine) and incubated for 1 hour for the cells to attach. Thereafter, cells were stained with hoechst 33342 (blue) and SYTOX Green (green), and stimulation agents (PMA or IO) were added simultaneously with start of live cell imaging. Hoechst 33342 binds to DNA and can penetrate the plasma membrane of intact cells, thereby visualizing all cells (both live and dead). SYTOX Green can only penetrate the cellular membrane of compromised cells and will only stain the DNA of cells without intact membranes. During imaging, one image was taken every five min for all conditions (unstimulated, PMA, or IO stimulated). All images acquired at the start, and then every 30 min are shown in the Appendix (Fig. 6.1-6.5). A selection of these images (taken at the start, at 60 min, and at 150 min) are shown in Figure 4.8.

One specific feature during NET formation is the decondensation of chromatin resulting in plasma membrane rupture and a significant increase in the total size of the DNA. This decondensed chromatin can be seen (Fig. 4.8 A, arrows) as enlarged green structures.

**A: CML patient 1, B: CML patient 2, C: CML patient 3, D: Healthy donor 2, E: Kcl-22 cells pre-treated with ATRA**

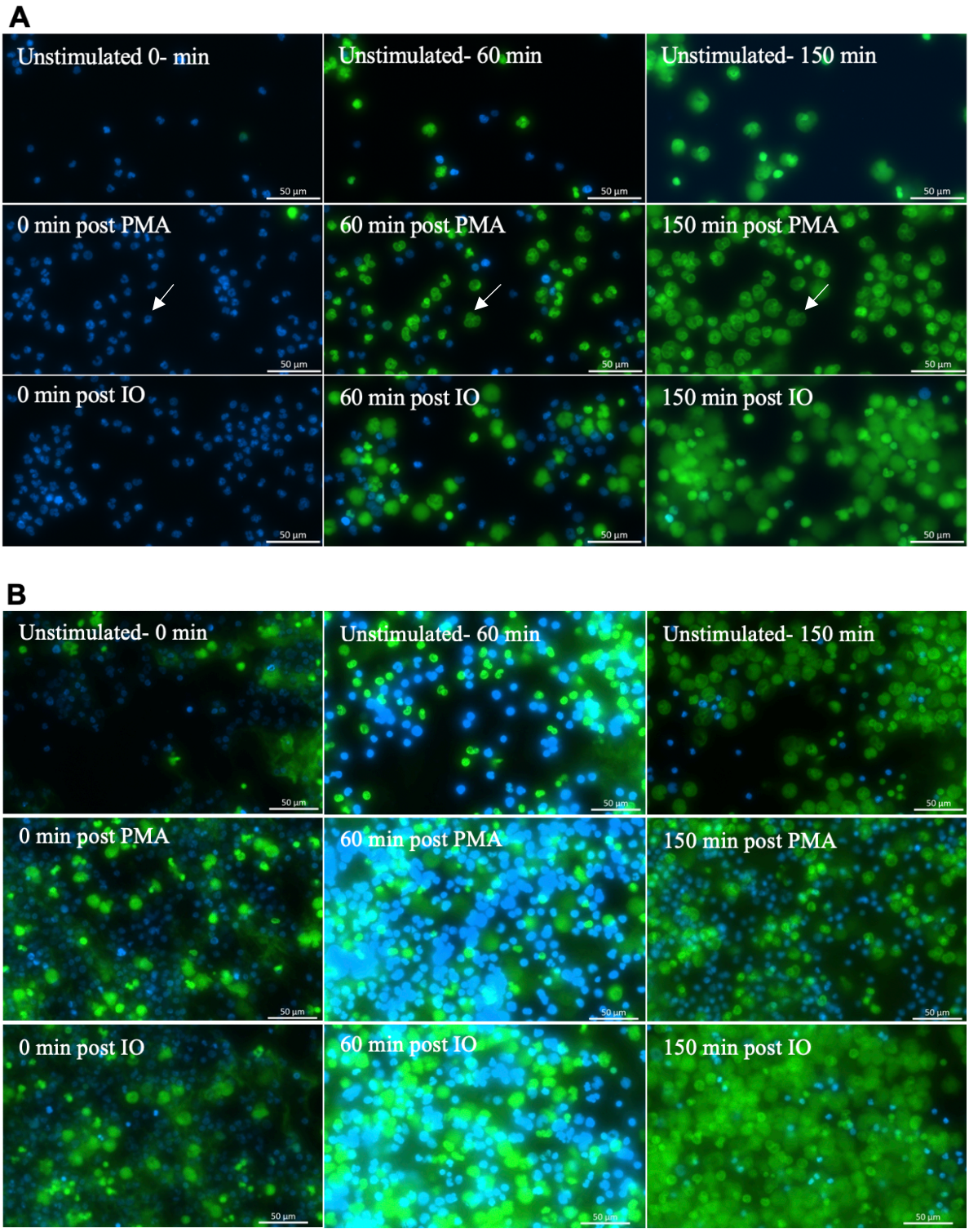

C

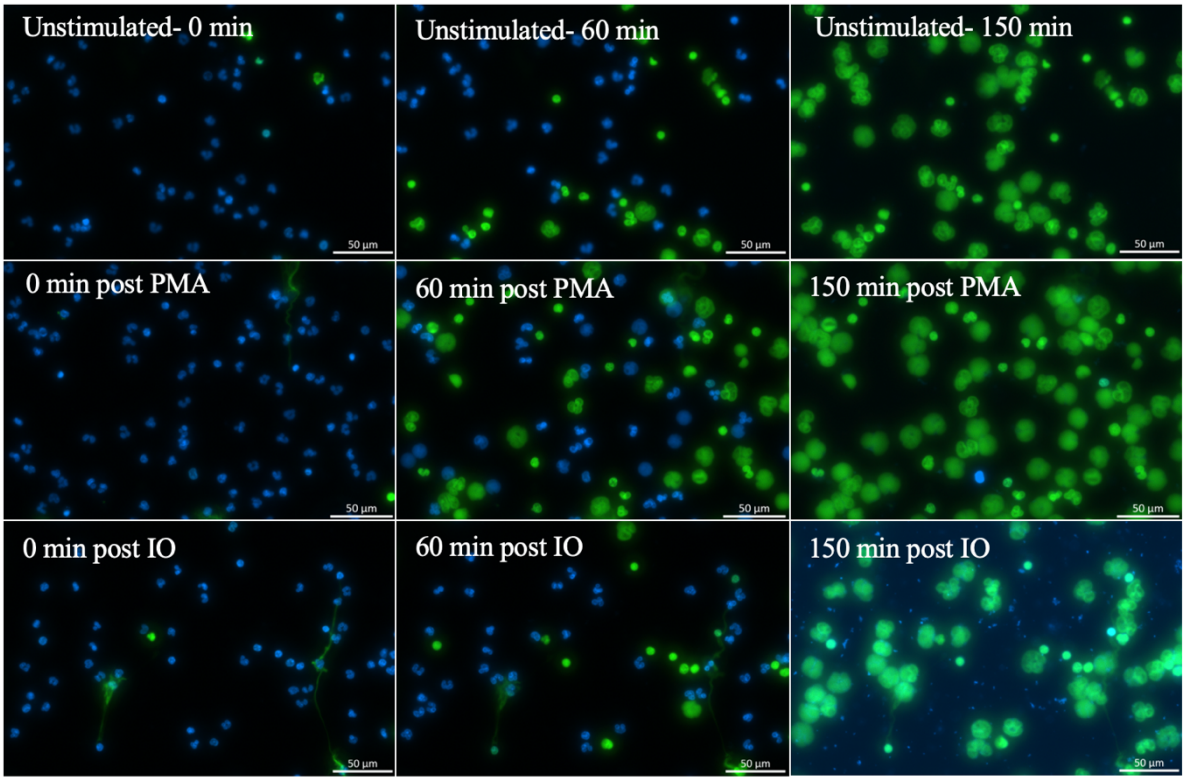
Unstimulated- 0 min
Unstimulated- 60 min
Unstimulated- 150 min
0 min post PMA
60 min post PMA
150 min post PMA
0 min post IO
60 min post IO
150 min post IO
50 µm

D

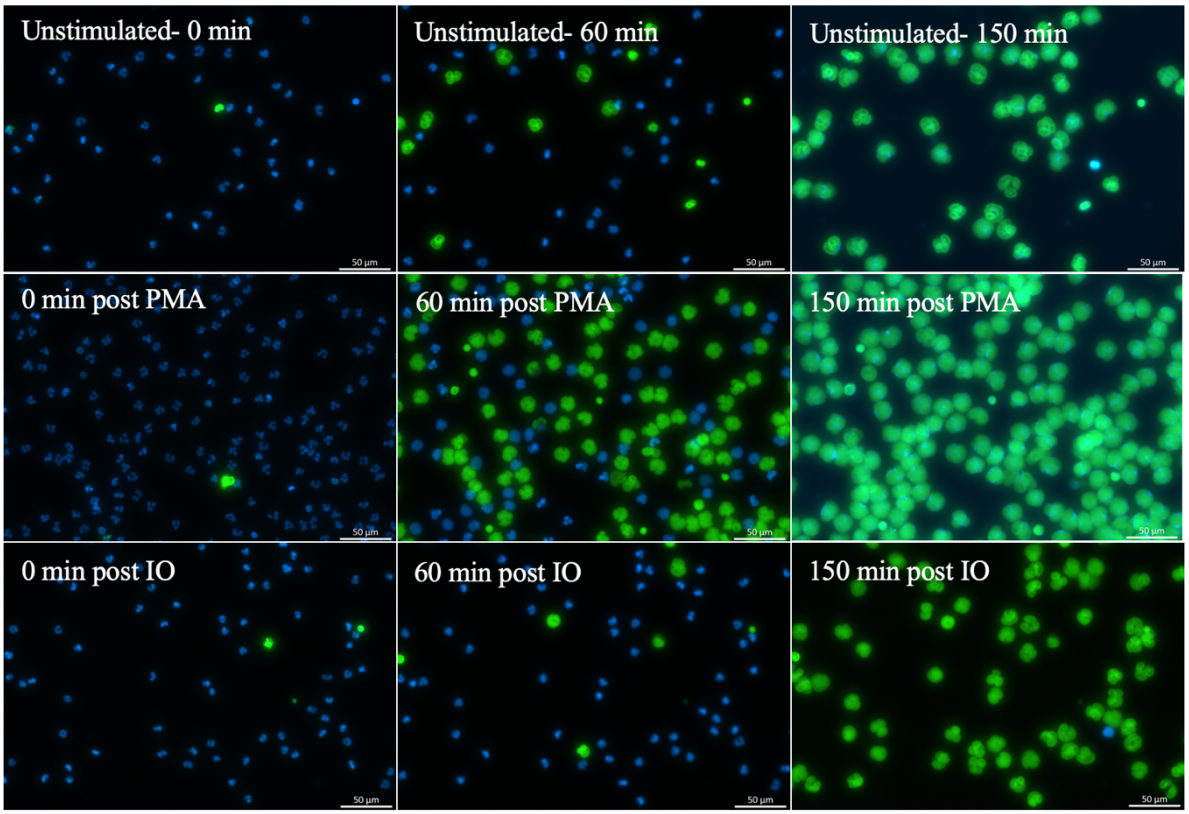
Unstimulated- 0 min
Unstimulated- 60 min
Unstimulated- 150 min
0 min post PMA
60 min post PMA
150 min post PMA
0 min post IO
60 min post IO
150 min post IO
50 µm

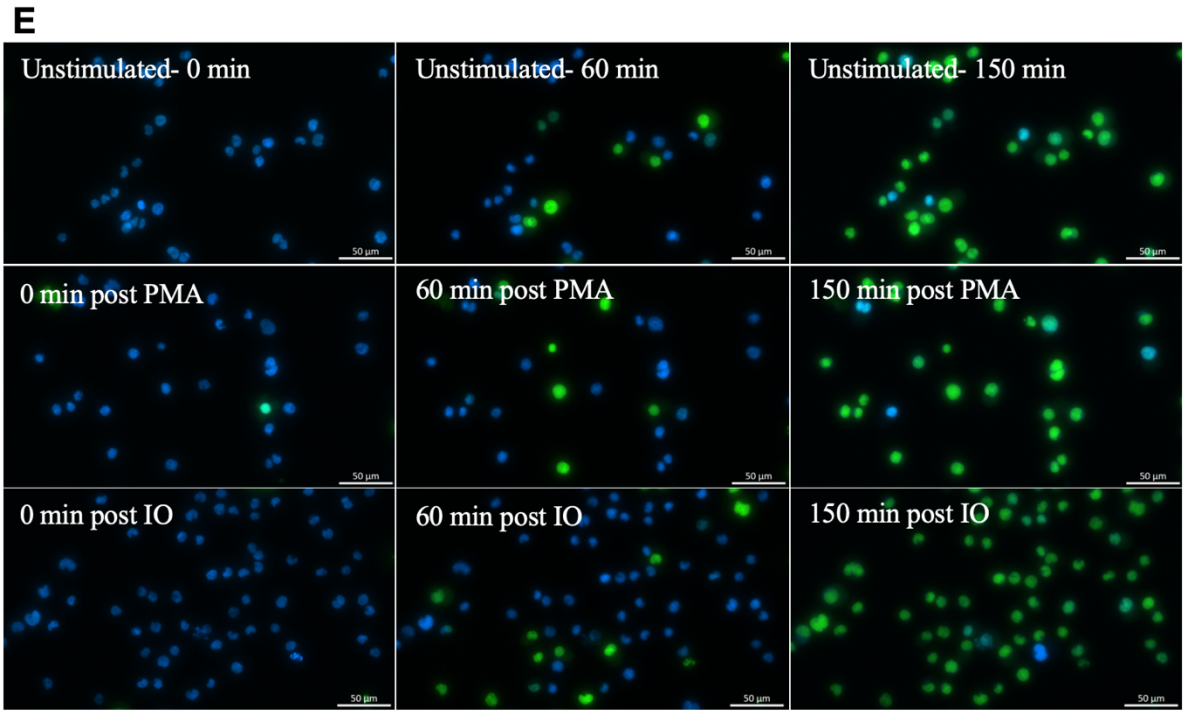


**Figure 4.8. Live cell imaging of neutrophils and Kcl-22 cells during NET formation.** Live cell imaging performed on cells stained live with Hoechst 33342 (blue) and SYTOX Green (green) before stimulated with PMA or IO, or not stimulated (unstimulated). Shown are merged images captured at 0 min, 60 min, and 150 min after stimulation. **(A)** CML 1, **(B)** CML 2, **(C)** CML 3, **(D)** HD 2, **(E)** ATRA pre-treated Kcl-22 cells. Live cell imaging by fluorescent microscope (Zeiss AxioObserver Z1 and ZEN 2012 (blue version) software and figures were made using ImageJ v.2.1.0 (Fiji), 10x objective). Scale bars: 50 µm.

Live cell imaging showed that the chromatin expanded for the neutrophils isolated from all three CML patients (Fig. 4.8 A-C) and the healthy donor (Fig. 4.8 D). In ATRA-treated Kcl-22 cells (Fig. 4.8 E) there was overall less visual chromatin expansion compared to primary cells. After three hours of live imaging, pictures were acquired for the quantification of cells with NETs and ETs by manual counting.

## 4.3 Quantification of ETs

After assessing NETs/ETs in primary CML neutrophils and Kcl-22 cells by immunofluorescence and visualizing the process of NET formation by live cell imaging, the next step was an attempt to quantify NETs/ETs in primary neutrophils and in Kcl-22 cells. Quantification of NETs was done by manual counting of NET-like structures through microscopy and by detecting and quantifying the NET component MPO in the cell supernatant by enzyme-linked immunosorbent assay (ELISA).

### 4.3.1 Quantification of NET-like structures by manual counting

Manual counting of NET-like structures was performed on isolated primary neutrophils derived from all three CML patients, healthy donor 2 (HD 2) and ATRA pre-treated Kcl-22 cells. Cells were stained with hoechst 33342 and SYTOX Green and counting was performed after stimulation for three hours with PMA or IO or without any stimulating agent. Counting of NET-like structures was performed on images acquired three hours after adding a stimulating agent (PMA or IO) and without any stimulation, thus following live cell imaging. NETs were counted in four different images captured at four different random areas in the µ-Slide 8 Well trays of stained cells.

As described earlier, decondensation of chromatin resulting in plasma membrane rupture is a feature of NET formation. This feature was used to quantify NETs and ETs, by counting the number of green structures with enlarged size. The percentage of NETs and ETs after manual counting is shown in Figure 4.9.

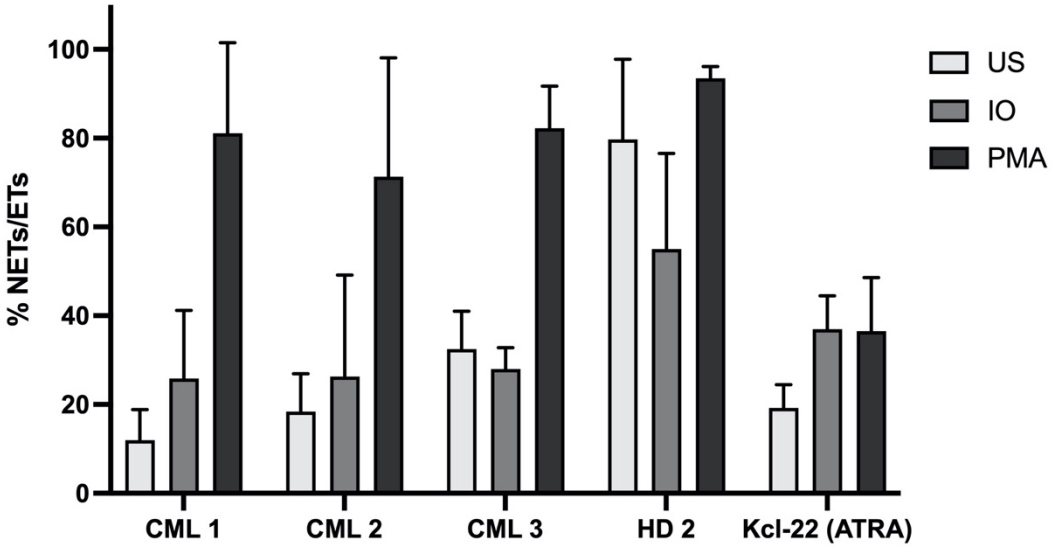


**Figure 4.9. Quantification of NETs by manual counting.** Cells were stained with hoechst 33342 and SYTOX Green followed by stimulation with PMA, IO or unstimulated (US). NETs and NET-like structures were manually counted by fluorescence microscopy (Zeiss AxioObserver Z1, objective 10x, ZEN 2012 (blue version) related to total number of cells per area counted as percentage of total cells in four different areas.

For the primary cells, PMA stimulation resulted in the highest number of NETs compared to IO stimulated cells and unstimulated cells. Neutrophils from all three CML patients had under 40% NET formation after IO stimulation, not very different from neutrophils without stimulation. Neutrophils from the healthy donor had a higher percentage of NETs for all

conditions (PMA, IO, and unstimulated) compared to neutrophils derived from the three CML patients. The healthy donor showed around 80% of NET formation in unstimulated neutrophils, indicating that the neutrophils might have been stressed and activated during handling prior to the experiment.

ATRA pre-treated Kcl-22 cells had an overall lower percentage of ET formation in PMA stimulated cells compared to primary neutrophils stimulated with PMA. This correlated with the results from immunofluorescence and live imaging, which also showed a lower number of ETs in Kcl-22 cells compared to primary neutrophils.

### 4.3.2 Quantification of NET components from primary neutrophils by ELISA

ELISA was done to quantify the amount myeloperoxidase (MPO) in the cell supernatants. Myeloperoxidase is a granular protein that is released during NET formation and is therefore a suitable marker for the quantification of NET components [101]. The quantification of NET components by ELISA was performed using the supernatants harvested from a 24-well plate with 0.2 x $10^6$ cells on coverslips after stimulation for three hours with PMA or with HBSS only (unstimulated) as control.

The concentrations of MPO in the supernatants after stimulation with PMA or without stimulation are shown in Figure 4.10, with the standard curve ranging from concentrations from 0 to 10 ng/mL (Fig. 4.10 A). The MPO concentration from undiluted supernatants from CML 1 and CML 2 were excessive, and out of range for the plate detector thus > 10 ng/mL, whereas CML 3 showed MPO concentrations within the standard curve, which increased after PMA stimulation (Fig. 4.10 B). The MPO concentration detected in the supernatant from HD 2 was higher in the unstimulated cells compared to PMA stimulated cells (Fig. 4.10 B). Interestingly, on the same MPO ELISA plate, supernatants from ATRA-pretreated Kcl-22 cells stimulated with PMA and unstimulated were added where no MPO was found (data not shown).

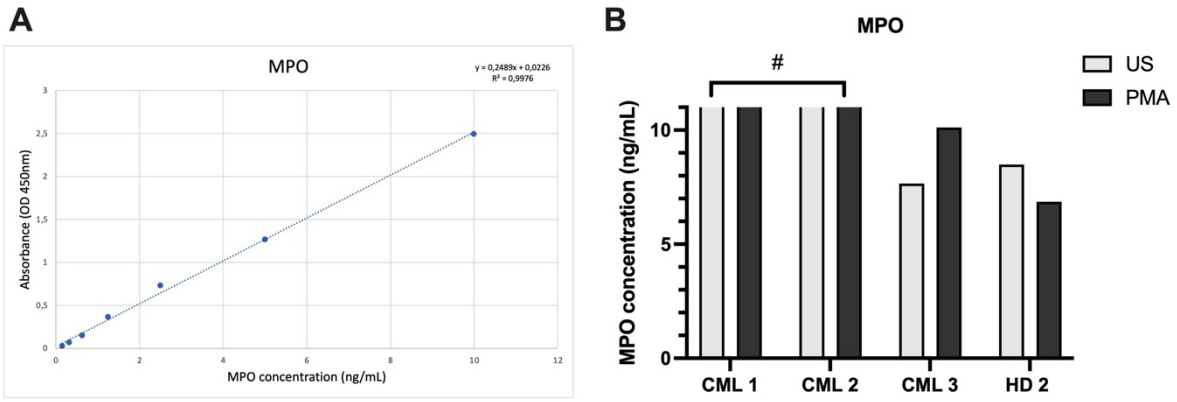


**Figure 4.10. Quantification of NETs by ELISA. (A)** Standard curve for MPO from 0 to 10 ng/mL. **(B)** Concentration (ng/mL) of MPO in supernatants from neutrophils isolated from three CML patients (CML 1, CML 2, CML 3) and one healthy donor (HD 2) after 3 hours of PMA stimulation or without stimulation (US). All concentrations are shown after blank reduction, and average of two replicates. # Values out of range for the standard curve.

## 4.4 The role of BCR-ABL1 in NET formation

All the previous experiments led to the last part of the thesis where the role of BCR-ABL1 in NET formation was investigated. This was done by treating Kcl-22 cells or cells derived from CML patients with specific tyrosine kinase inhibitors (TKIs) included in the current treatment for CML patients. These specific TKIs will turn off the kinase activity of the BCR-ABL1 protein and consequently the downstream signalling pathways. In this thesis, two different TKIs were used, the third-generation TKI ponatinib, which works through competitive binding in the ATP binding site, and the newly approved allosteric inhibitor ABL001 (Asciminib), which binds to the myristylation site, thereby locking BCR-ABL1 in an inactive state [85, 102].

### 4.4.1 Validation and mapping of *BCR-ABL1* in primary cells by RT-PCR

However, before treating cells with TKIs, reverse transcription polymerase chain reaction (RT-PCR) and agarose gel electrophoresis were performed in an attempt to confirm (at diagnosis the presence and type of fusion were determined as routine diagnostics at Haukeland University Hospital with cells derived from the bone marrow, see Table 4.1) the presence of *BCR-ABL1* and the *BCR-ABL1* fusion transcript in the blood cells derived from the three CML patients. RT-PCR amplifies cDNA made from mRNA transcripts, and gel electrophoresis allows for the visualization of these RT-PCR products. The *BCR-ABL1* gene is in most cases

transcribed into an mRNA with either the e13a2 or e14a2 junction with different sizes, therefore, allowing identification by agarose gel electrophoresis.

Primary isolated neutrophils (N) and the remaining mononuclear cells (M) were lysed directly after isolation (CML 2, CML 3, and HD 2 (4 x $10^6$ cells)) or directly after thawing cryopreserved previously isolated neutrophils and the remaining mononuclear cells for CML 1 (12 x $10^6$ cells). The *BCR-ABL1* positive cell lines Kcl-22 (e13a2) and Ku812 (e14a2) and the *BCR-ABL1* negative AML cell line Molm-13 were lysed as the primary cells. After lysis, total RNA was isolated and cDNA was synthesized by using oligo (dT) primers by reverse transcription, followed by PCR amplification of the cDNA sequence of interest using specific primers. Forward and reverse primers flanking the *BCR-ABL1* fusion were used to amplify this specific region resulting in different sizes of the PCR product dependent on fusion; e13a2: 314 bp, e14a2: 388 bp [103]. Beta-actin was used as a housekeeping gene. The sequences of the primers are shown in Table 3.1. After PCR, samples were run using agarose gel electrophoresis where PCR products were separated by size and visualized (Fig. 4.11).

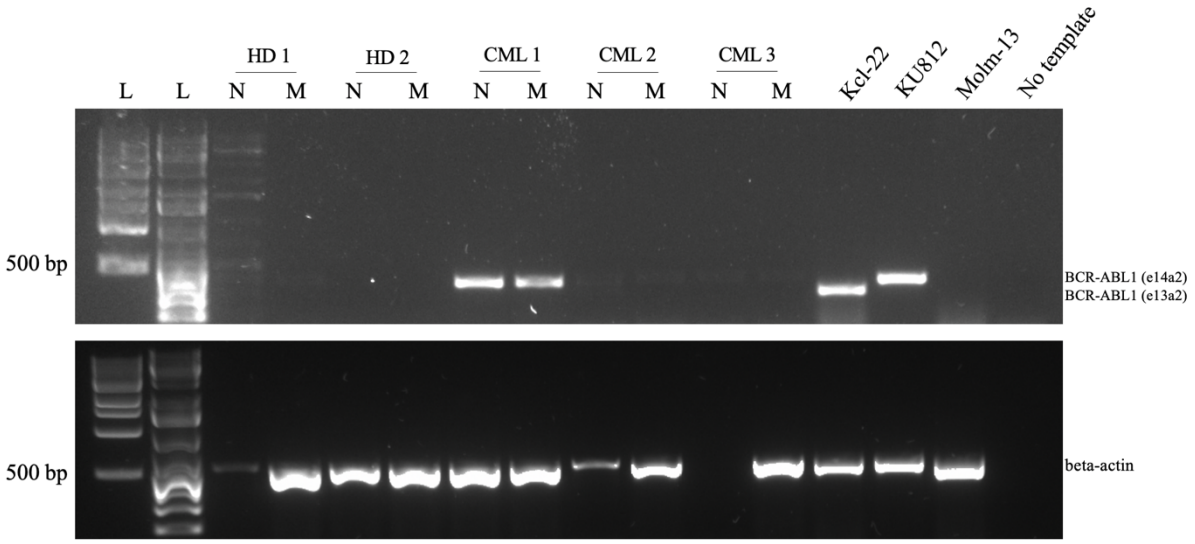


**Figure 4.11. RT-PCR products visualized by agarose gel electrophoresis.** L: molecular weight marker, base pair (bp), N: isolated neutrophils, M: remaining mononuclear cells, HD 1 and 2: healthy donor 1 and 2 (negative controls), CML 1, 2, and 3: cells from CML patient 1, 2 and 3. Kcl-22 (e13a2) and Ku812 (e14a2): *BCR-ABL1* positive controls, and Molm-13: *BCR-ABL1* negative control. No template: negative control for contamination of PCR mix and primers. Beta-actin is used as housekeeping gene where only half volume of PCR product was applied on the gel for the cell lines compared to the primary cells.

The *BCR-ABL1* positive CML cell lines Kcl-22 (e13a2) and Ku812 (e14a2) represented positive controls expressing two different fusions, whereas the *BCR-ABL1* negative AML cell line Molm-13 represented a negative control. *BCR-ABL1* was present in CML 1 in both the

isolated neutrophils (N) and the remaining mononuclear (M) cells as compared to no *BCR-ABL1* in HD 2 in either of these cell populations (Fig. 4.11). CML 1 contained the same size *BCR-ABL1* fusion as the Ku812 cell line which is e14a2. This confirmed the clinical information at diagnosis of this patient (Table 4.2). However, no clear *BCR-ABL1* bands were observed for CML 2 or CML 3. The housekeeping gene used was beta-actin, present in all RT-PCR reactions except in isolated neutrophils from CML patient 3 and the one with no added template (Fig. 4.11). Since no clear *BCR-ABL1* expression was found for CML 2 and CML 3, the agarose gel electrophoresis was repeated using RT-PCR products from CML 1 only, to clearly demonstrate the expression and type of fusion directly compared to positive and negative controls (Fig. 4.12). One difference between CML 1 and, CML 2 and CML 3 was the number of cells lysed for total RNA isolation, as explained above.

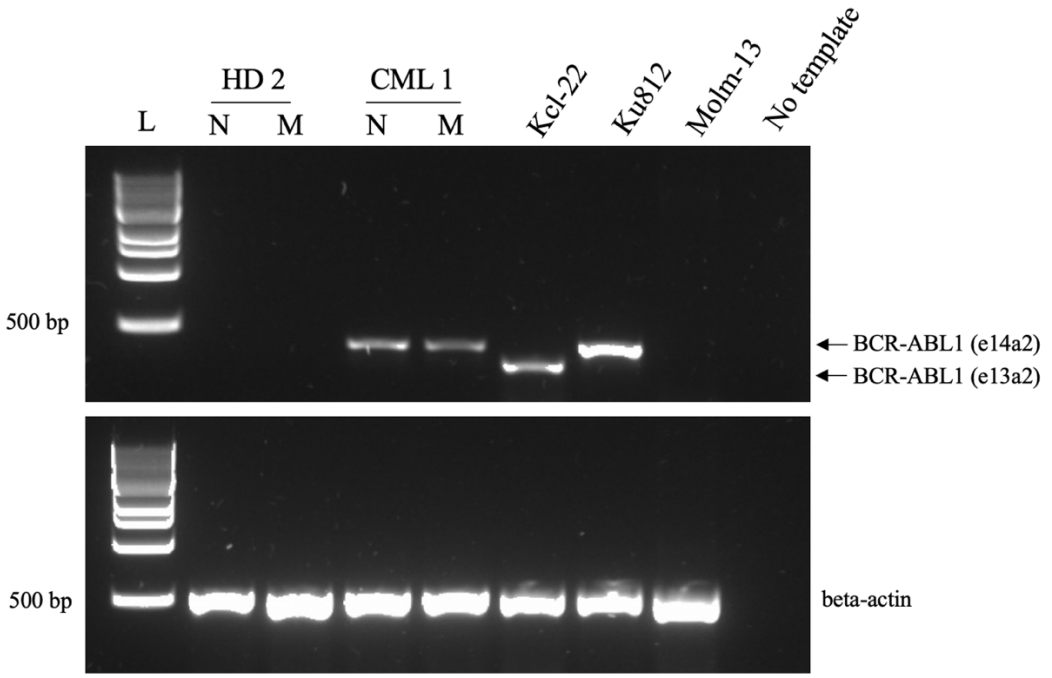


**Figure 4.12. RT-PCR products visualized by agarose gel electrophoresis.** L: molecular weight marker, base pair (bp), N: isolated neutrophils, M: remaining mononuclear cells, HD 1 and 2: healthy donor 1 and 2 (negative controls), CML 1, 2, and 3: cells from CML patient 1, 2 and 3. Kcl-22 (e13a2) and Ku812 (e14a2): *BCR-ABL1* positive controls, and Molm-13: *BCR-ABL1* negative control. No template: negative control for contamination of PCR mix and primers. Beta-actin is used as housekeeping gene where only half volume of PCR product was applied on the gel for the cell lines compared to the primary cells.

### 4.4.2 BCR-ABL1 protein expression in primary cells

In addition to the attempt to confirm the presence of *BCR-ABL1* with RT-PCR, immunoblot analysis was performed to corroborate the presence of BCR-ABL1 at the protein level. The

isolated neutrophils (N) and remaining mononuclear cells (M) derived from the three CML patients and healthy donor 2 were lysed with lysis buffer (SHIEH) and lysates were run on SDS-PAGE to separate the proteins by size. Proteins were then blotted onto a membrane and incubated with primary antibodies against the protein of interest and horseradish peroxidase (HRP)-conjugated secondary antibodies for visualization. BCR-ABL1 expression was investigated using an antibody binding to the C-terminal of c-Abl thereby also recognizing BCR-ABL and these two different proteins are easy to distinguish by size as BCR-ABL1 normally is 210 kDa protein whereas c-Abl is 135 kDa (clearly seen for Kcl-22 in Fig. 4.13). Following this, the blot was incubated with anti-COX-IV representing the loading control. No visual bands were detected for either BCR-ABL1 or c-Abl for CML 1, CML 2, or CML 3 or HD 2 as negative control. An additional attempt was done with higher amount of total proteins for all the primary cell lysates in the immunoblotting, however, still no expression of BCR-ABL1 or c-Abl was found. In order to detect BCR-ABL1 in the primary cells, where only a percentage of the cells most likely will express BCR-ABL1, a higher number of cells probably need to be lysed from the start, compared to the Kcl-22 cells, where each cell express BCR-ABL1.

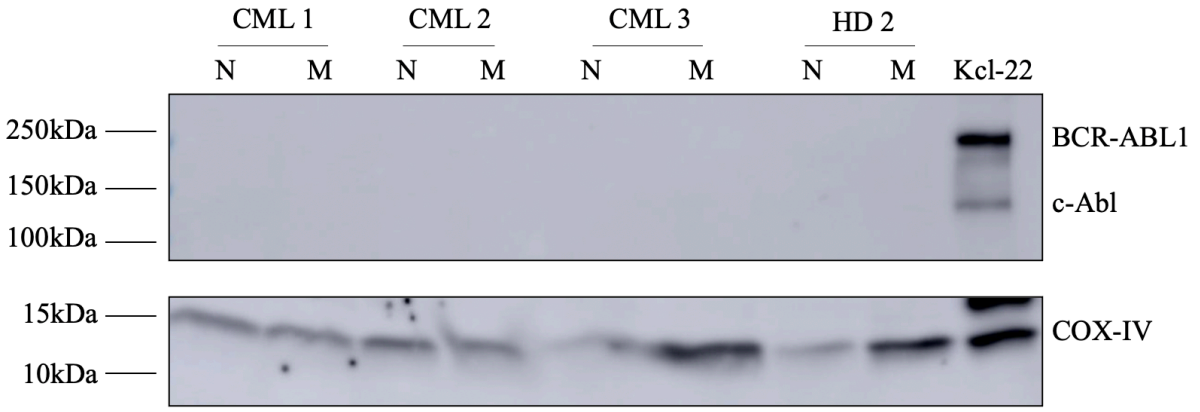


**Figure 4.13.** Immunoblot analysis of BCR-ABL1 expression in primary cells from three CML patients (CML 1, 2, and 3) and one healthy donor (HD 2). COX-IV represents loading control. N: isolated neutrophils, M: remaining mononuclear cells. CML cell line Kcl-22: positive control for BCR-ABL1 and c-Abl expression, healthy donor 2 (HD 2): negative control for BCR-ABL1 expression. (c-Abl antibody: (24-11) sc-23 mouse monoclonal $IgG_1$, Santa Cruz Biotechnology, COX-IV antibody: ab 16056, Abcam).

### 4.4.3 TKIs inhibit phosphorylation of BCR-ABL1 in Kcl-22 cells

To demonstrate and confirm the inhibiting effect of the TKIs on BCR-ABL1, Kcl-22 cells, untreated (control cells) or pre-treated with ATRA for five days, were treated for one hour

with either ponatinib or ABL001 (asciminib) to inhibit and block the phosphorylation and activity of BCR-ABL1. After one hour of TKI treatment, cells were lysed and immunoblot analysis was performed to investigate the expression of total BCR-ABL1, phospho-BCR-ABL1, and c-Abl using anti-phospho-c-Abl (Y412) and c-Abl antibodies. Immunoblot analysis of Kcl-22 cells treated with TKIs showed no phospho-BCR-ABL1 expression after treatment with either ponatinib or ABL001, irrespectively of ATRA treatment compared to control cells. Total BCR-ABL1 expression was similar or slightly increased after TKI treatments compared to control cells (Fig. 4.14 A). Quantification of phospho-BCR-ABL1 and total BCR-ABL1 expression was performed based on three independent experiments. The Immunoblot shown in Figure 4.14 A was the one with the clearest bands. All membranes from immunoblot analysis are shown in full size in the Appendix (Fig. 6.6). The band intensities were analysed using Image Lab (BioRad) and calculated relative to c-Abl expression (Fig. 4.14 B). This clearly demonstrated that both TKIs inhibited phosphorylation of BCR-ABL1 thereby inhibiting the activity of BCR-ABL1.

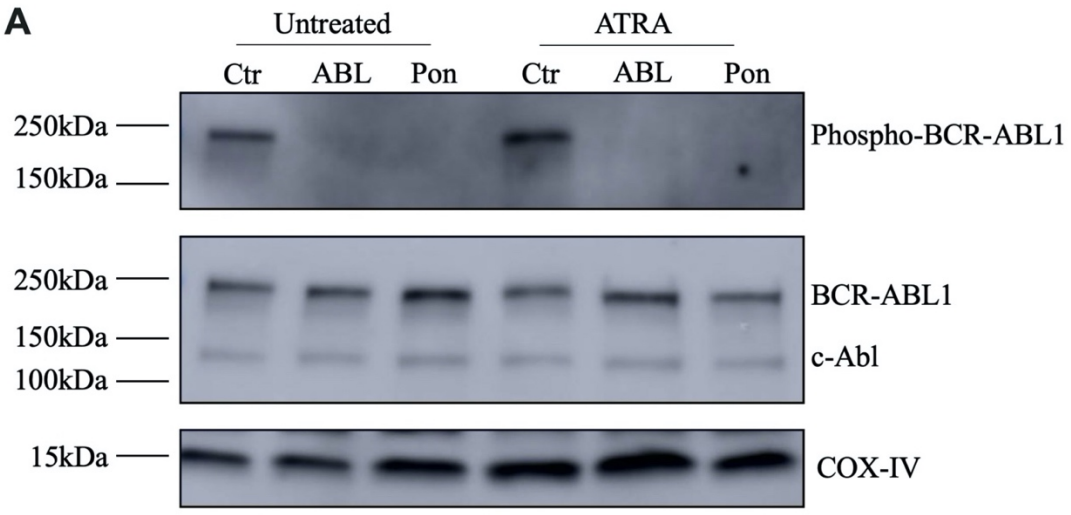


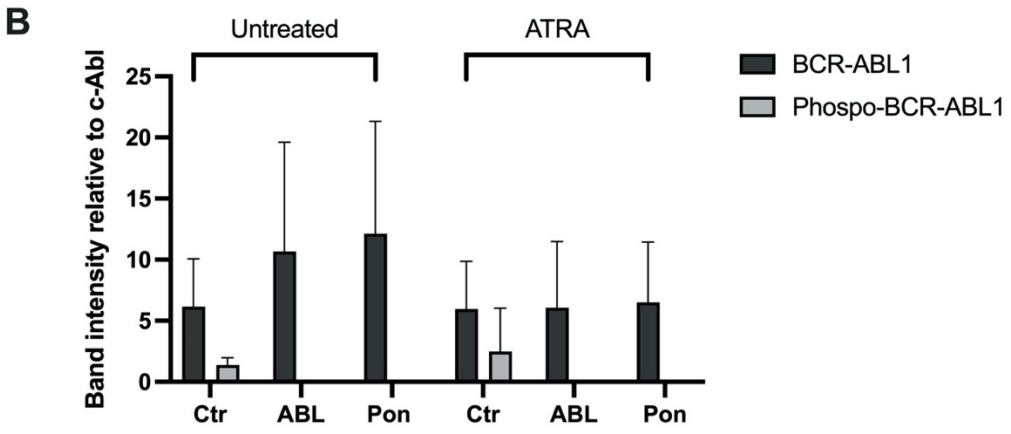

**Figure 4.14. TKI treatment of Kcl-22 cells.** The effect of TKIs on phospho-BCR-ABL1 in Kcl-22 cells untreated or pre-treated with ATRA for five days. **(A)** Immunoblot analysis of Kcl-22 cells (untreated or pre-treated with ATRA) was untreated (Ctr) or treated with the TKI ABL001 (ABL) or ponatinib (Pon) for 1 hour before cell lysis and immunoblotted with antibodies for phospho-c-Abl (Y412) (P-BCR-ABL1), anti-c-Abl (total BCR-ABL1 and c-Abl) and anti-COX-IV as loading control. **(B)** Quantification of phospho-BCR-ABL1 (Y412) and total BCR-ABL1 expression. Band intensity values of BCR-ABL1 and phospho-BCR-ABL1 relative to c-Abl were analysed using Image Lab (BioRad) based on three separate experiments.

### 4.4.4 Extracellular trap formation in Kcl-22 cells after TKI treatment

Immunofluorescence, as described earlier, was performed on Kcl-22 cells after TKI treatment to study if the affected BCR-ABL1 activity influenced the capability of these CML cells to form ETs. Control Kcl-22 cells or Kcl-22 cells pre-treated with ATRA for five days were treated for 1 hour with ponatinib or ABL001 or untreated. The cells were then stimulated with PMA for one hour compared to non-stimulated cells before fixed and stained using antibodies against neutrophil elastase (NE) and citrullinated histone H3 and counterstained with DAPI. Merged images are shown in Figure 4.15. The individual images are shown in the Appendix in Figure 6.7 and 6.8. There was no apparent increase or decrease of extracellular traps in the Kcl-22 cells after treatment with either of the TKIs.

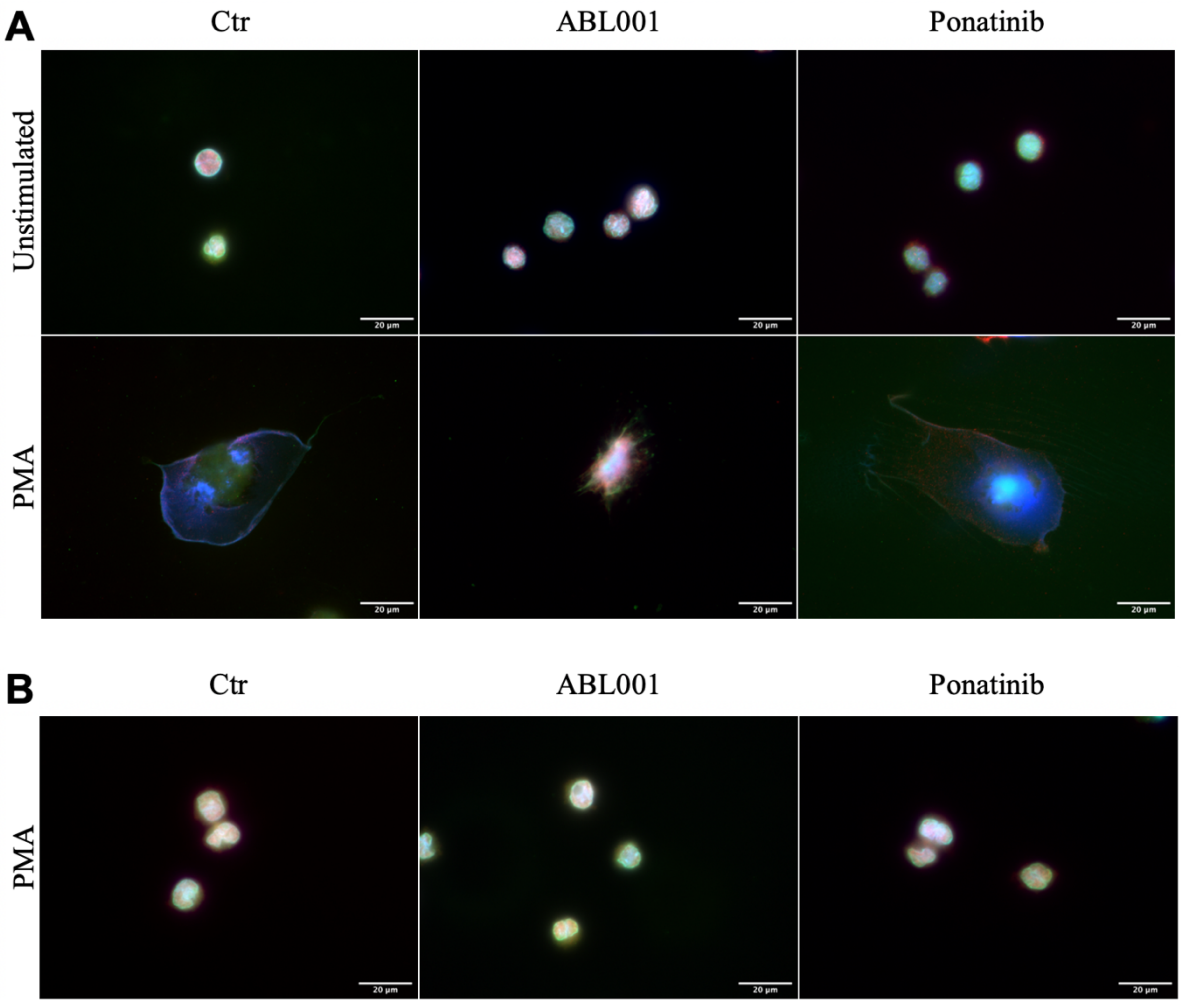


**Figure 4.15. Extracellular trap formation in Kcl-22 cells treated with TKIs. (A)** Kcl-22 cells pre-treated with ATRA, treated for one hour with the TKIs ABL001 or ponatinib or not treated (Ctr) followed by stimulation with PMA or not (unstimulated) **(B)** Kcl-22 cells not pre-treated with ATRA, treated for one hour with the TKIs ABL001 or ponatinib or not treated (Ctr) and stimulated with PMA. All cells were fixed and stained with ET identifying markers; anti-CitH3 (red) antibodies, anti-NE (green) antibodies and counterstained with DNA (blue) and analyzed by fluorescent microscopy Zeiss AxioObserver Z1 and ZEN 2012 (blue version) software and figures were made using ImageJ v.2.1.0 (Fiji), 63x oil objective. Merge images are shown. Scale bars: 20 µm.

### 4.4.5 NET formation after TKI treatment in primary neutrophils isolated form one CML patient

Primary neutrophils from CML 1 were treated with TKIs to investigate the effect of these on the NET formation. Neutrophils isolated from the blood of CML patient 1 that had been cryopreserved, were thawed, and incubated for one hour in media with ponatinib or ABL001 or without TKIs. Then the cells were seeded onto an IBIDI tray, stained with hoechst and SYTOX Green and stimulated or not with PMA. After 3 hours of stimulation, four live cells

images were acquired at four random areas from each condition, and NETs were quantified by manual counting showing that almost all the neutrophils formed NETs (Fig. 4.16). The manual counting of cells in NETosis showed no difference between TKI treated and untreated cells. In all three conditions slightly more NETs after PMA stimulation were observed compared to unstimulated cells. The unusually high percentage of NETs in these neutrophils could be due to stress during thawing and centrifugation, thus triggering NET formation, however, the treatment with ABL001 or ponatinib did not seem to have any effect on NET formation.

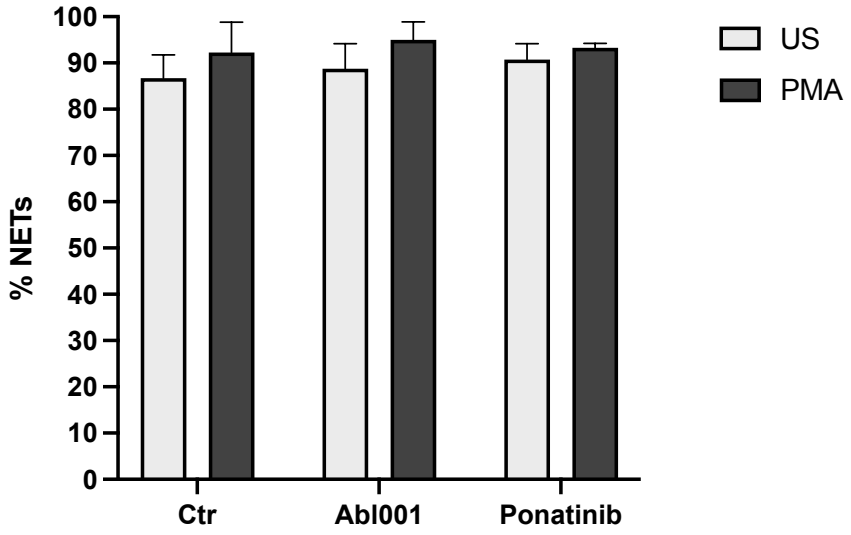


**Figure 4.16. NET formation in neutrophils from CML 1 after TKI treatment.** Manual counting of NET formation in CML 1 neutrophils after one hour of TKI treatment or untreated (Ctr), and unstimulated (US) or stimulated with PMA for three hours prior to counting. Manual counting was performed in images taken in four different areas for each condition after cells were stained with hoechst and SYTOX Green. Total number of cells was counted, and number of enlarged green cells was counted as cells forming NETs.

# 5. Discussion

Neutrophil extracellular traps (NETs) are one of several strategies possessed by neutrophils to eliminate pathogenic sources. They were first described by Brinkmann and colleagues in 2004 as extracellular fibers of nuclear and granule constituents extruded from the cells to trap, disarm, and kill bacteria extracellularly [5]. Today, NETs are recognized as extracellular structures composed of decondensed chromatin decorated with granule proteins like neutrophil elastase (NE), cathepsin G, and myeloperoxidase (MPO) with effective antimicrobial properties against several pathogens including bacteria, viruses, fungi, and parasites [9]. Unfortunately, NETs have also been linked to the pathogenesis of several diseases, including autoimmune diseases, cardiovascular diseases, infectious diseases, and cancer [49].

Increasing number of studies have revealed the pro-cancer effects of NETs. The role of NETs in cancer has been shown to contribute to cancer progression by assisting with metastatic spread, conditioning the pre-metastatic niche, and by indorsing awakening of cancer dormant cells [104]. These effects are, among others, mediated by interactions with other pro-cancer mechanisms and the establishment of an inflammatory microenvironment [105]. NETs have also been shown to promote tumor angiogenesis and cancer-associated thrombosis [106]. Cardiovascular complications are a major cause of morbidity and mortality for many cancer patients and thrombosis is the second most common cause of death in cancer patients [107].

Cancer-associated thrombosis has been shown to be linked to increased NET formation, also in myeloid malignancies [107, 108]. Demers and colleagues previously demonstrated that peripheral blood neutrophils were more prone to generate extracellular traps in a CML mouse model [107]. By stimulation of isolated neutrophils from mice with CML-like neutrophils using platelet-activating factor (PAF), they demonstrated a significant increase in NET formation compared to neutrophils from the control group. With a high dose of PAF, the majority of neutrophils from the mice with a CML-like disease, generated NETs, with only around 30% of them being BCR-ABL1 positive. This suggested that it was not only the BCR-ABL1 positive cells that were more prone to extrude NETs, but rather the entire cell population. This indicated as they described, that CML predisposes neutrophils in general to generate NETs through a systemically acting factor, and not through BCR-ABL1.

Recently, in December 2021, approximately five months after the start of the present thesis, Telerman and colleagues published an article demonstrating that NET formation was increased in neutrophils derived from CML patients and in a CML neutrophil induced cell line [93]. By assessing NETs morphologically and through quantification by measurement of PAD4 expression and its downstream product CitH3, and determining intracellular ROS levels in isolated neutrophils derived from eight CML patients, they discovered a significant increase in NET formation compared to age- and gender-matched healthy controls. In addition, they used a BCR-ABL1 transduced ER-HoxB8 cell line model with the ability to differentiate into neutrophils. They described that the HoxB8-BCR-ABL1 cell line had increased CitH3 and MPO expression with co-localization of DNA, a characteristic of NET formation, and further proposed based on their findings, that BCR-ABL1 is associated with increased NET formation in the HoxB8 cell system.

To further study whether NET formation is increased in CML, the present thesis has investigated the ability of neutrophils isolated from patients with newly diagnosed CML (treatment naïve) to extrude NETs compared to healthy controls and investigated the ability of the CML cell line Kcl-22 to undergo NET formation. Also, the role of BCR-ABL1 in extracellular trap formation has been explored.

The following discussion is divided into two main parts based on the cells used for the study of extracellular trap formation. The investigation of extracellular traps (ETs) in the Kcl-22 cell line and the investigation of neutrophil extracellular traps (NETs) in primary cells derived from CML patients.

## 5.1 Extracellular trap (ET) formation in Kcl-22 cells

The Kcl-22 cell line was in this thesis attempted utilized as a model system to study the capability of BCR-ABL1 expressing CML cells to form NETs. Therefore, the Kcl-22 cells were treated using the same differentiation agents (DMSO, DMF, ATRA) as successfully used for neutrophilic differentiation of the promyelocytic leukemia cell line HL-60 using the protocol described by Manda-Handzlik and colleagues [99]. However, after exposing Kcl-22 cells to DMSO, DMF, or ATRA it was evident just by examining the nuclear morphology after MGG staining (Fig. 4.3) that the Kcl-22 cells did not differentiate towards neutrophils. However, the Kcl-22 cells did extrude NET-like structures after pre-treatment with ATRA,

DMSO, or DMF and stimulation with PMA or IO (Fig. 4.5 B-D). The immunofluorescence analysis showed structures of DNA extending out of the cells embedded with citrullinated histone H3 and neutrophilic elastase (NE), all known markers of NETs. The pre-treatment was essential for these NET-like structures to be formed, as Kcl-22 cells not pre-treated, but stimulated with PMA or IO, produced little or no NET-like structures (Fig. 4.5 A). This indicated that the DMSO, DMF, and ATRA treatments did cause a change in these cells in a way that made them prone to extrude ETs.

This was further supported by the flow cytometry results where the most noticeable difference was the decreased expression of CD15 in all three conditions (DMSO, DMF, and ATRA) compared to untreated control cells (Fig.4.4 B). CD15 is a granulocytic marker, however, not, or weakly expressed on human mast cells [109]. Therefore, the observed decrease in CD15 expression could indicate that these cells had differentiated or started to differentiate towards mast cells instead of neutrophils. Also, the observed increased expression of CD33 for the pre-treated cells correlated with the theory of mast cell differentiation since mast cells are positive for CD33 [100]. The unsegmented nuclei observed after MGG staining further substantiated this and not differentiation in the direction of one of the other types of granulocytes, basophils or eosinophils, that both have banded or segmented nuclei morphology.

Interestingly, one study had previously reported that the Kcl-22 cells expressed a non-functional CEBPα (CCAAT enhancer-binding protein α), a transcription factor acting as a cell proliferation inhibitor and a regulator of differentiation [110]. In this publication, it was shown that CEBPα restoration in the Kcl-22 cells, by stable transfection, differentiated these cells towards neutrophils. Therefore, the lack of a functional CEBPα in Kcl-22 cells most likely explains why the cells were not differentiating in a neutrophilic direction when exposed to DMSO, DMF, or ATRA. This could also indicate that CEBPα is a key regulator of differentiation to granulocytes with banded or lobed nuclei, if indeed the Kcl-22 cells were differentiated into mast cells after exposure to DMSO, DMF, or ATRA. The Kcl-22 cells, together with all other patient-derived CML cell lines, are obtained from patients in blast crisis. The progression from chronic phase to blast crisis is a process occurring over several years, a transition poorly understood, but involves inhibition of granulocytic differentiation. Kcl-22 cells were reported not to express any CEBPα protein compared to myeloid progenitor cells and the progression from chronic phase to blast phase has been correlated with a reduction in CEBPα protein expression [110]. Based on this information, it would have been very

interesting to reproduce this and overexpress CEBPα in the Kcl-22 cells in order to obtain a CML cell line model system of neutrophils for the investigation of NET formation in CML. However, due to time limitations, this was not conducted in this thesis.

Another possibility could be to use the BCR-ABL1 transduced ER-HoxB8 murine cell line model with the ability to differentiate into neutrophils as reported by Telerman and colleagues. For future investigations, the Kcl-22 cell line transfected with CEBPα protein could represent the best choice because it is a human CML cell line, thereby most likely representing the disease more appropriately compared to the murine HoxB8 cell line, originally not derived from CML being only CML-like due to BCR-ABL1 transfection.

After investigation of ET formation, an attempt to quantify the concentration of MPO, a common marker used in the quantification of NETs, was performed using the cell supernatants of Kcl-22 cells pre-treated with ATRA followed by PMA stimulation. The results from the ELISA did not show any concentration of MPO, (the raw data (optical density values) from the ELISA is shown in Table 6.2 in the Appendix). MPO is a marker of neutrophils and NETs, thereby the lack of MPO detection in the supernatants is another indication that the Kcl-22 cells indeed were differentiated towards mast cells and that the ETs generated most likely represent MCETs. In a study of different types of extracellular traps, they used MPO as a marker for neutrophil and macrophage extracellular traps (NETs and METs), but not to identify mast cell-derived extracellular traps, which further suggests that MPO is not a marker of MCETs. Instead, they use tryptase for the identification of MCETs [111]. Therefore, it would be interesting to study the presence of tryptase instead of MPO, using ELISA, to investigate if the Kcl-22 cells indeed are differentiated towards mast cells and extruding MCETs.

### 5.1.1 BCR-ABL1 in ET formation in Kcl-22 cells

One aim of this thesis was to elucidate the role of BCR-ABL1 in the formation of NETs, or in the case of Kcl-22 cells, possibly another type of ETs. To study if BCR-ABL1 in any way contributed to the formation of ETs, cells were treated with two BCR-ABL1 specific TKIs. Both TKIs, ponatinib and ABL001, completely inhibited the phosphorylation activity of the BCR-ABL1 protein in Kcl-22 cells (control and pre-treated with ATRA) after one hour of treatment (Fig 4.14 A), resulting in a blockage of BCR-ABL1 downstream signalling. After TKI treatment, control Kcl-22 cells stimulated with PMA and ATRA pre-treated Kcl-22 cells

stimulated with PMA or unstimulated were stained and investigated by immunofluorescence for ETs after TKI treatment (Fig. 4.15). The results showed similar ETs formation after TKI treatment after PMA stimulation in ATRA pre-treated cells as compared to cells not treated by TKIs. This indicated that in the Kcl-22 cells, BCR-ABL1 does not have a direct role in the formation of ETs.

However, even though they are developed to be BCR-ABL1 specific, TKIs have been shown to cause a variety of side effects [112]. Therefore, it is known that TKIs influence the cells in other ways than just inhibiting BCR-ABL1 phosphorylation [113]. The use of TKIs is therefore questionable when specifically studying the role of BCR-ABL1. Another approach to study the role of BCR-ABL1 in NET formation could be to use a CML cell line that does differentiate towards neutrophils and to use CRISPR to turn off the oncogene. Thereafter, the difference between BCR-ABL1 positive and negative cells in NET formation could be investigated to elucidate the role of BCR-ABL1 protein in this process.

## 5.2 NET formation in primary neutrophils

NET formation was analysed in primary neutrophils isolated from the blood of three CML patients and two healthy donors. The isolation was confirmed by nuclear morphological assessment after MGG staining (Fig. 4.6) and flow cytometry (Fig. 4.6). Immunofluorescence is one of the best ways to investigate NET formation due to the use of NET specific markers [114]. In this thesis, NET formation was investigated by immunofluorescence using antibodies against the NET markers NE and CitH3.

In the results from immunofluorescence microscopy of primary neutrophils isolated from three CML patients following stimulation with PMA or IO, more excessive NET formation was observed compared to neutrophils isolated from the healthy donors. Also, the NET structures were larger and covered greater areas than the ones from the healthy donors. This correlated with the findings of Telerman and colleagues, that the NET formation capability is increased in neutrophils derived from CML patients compared to healthy controls [93]. In addition, unstimulated neutrophils from CML patients seemed to extrude a higher degree of NETs compared to unstimulated neutrophils from the healthy donors. This could indicate that the neutrophils from CML patients in general are more prone to form NETs compared to neutrophils from healthy individuals.

### 5.2.1 NET quantification in primary neutrophils

Following assessment of NET formation by immunofluorescence, attempts to quantify NETs were performed using manual morphological counting of NETs from live cell imaging and ELISA. Quantification will provide information on differences between NET formation in neutrophils from healthy donors compared to neutrophils derived from CML patients. In the context of this study, quantification by manual counting and ELISA was performed on neutrophils derived from the three CML patients, but compared to neutrophils from only one healthy donor (HD 2).

ELISA was performed to quantify the amount of myeloperoxidase in the supernatants of the neutrophils after PMA stimulation. MPO is a neutrophil-derived protein and is a widely used marker for NETs, and therefore quantifying MPO by ELISA represents a specific and objective quantification of NET formation. MPO concentrations in supernatants of neutrophils have been shown to correlate with the rate of NETs, represented by the presence of citrullinated histone H3, and patients with diseases involving NETosis as a driver of the pathogenesis have been shown to have elevated levels of MPO in their serum [101]. In this thesis, the cell supernatants were collected from different experiments, both from primary cells and the cell lines Kcl-22, and stored at -80 degrees before they were all run on the one MPO ELISA plate purchased. Therefore, a careful selection of supernatants was done, and no extra space was available to run dilutions of the different supernatants. The MPO ELISA showed the highest concentrations of MPO in cells from both CML patient 1 and 2, with concentrations ranging above the highest concentration of the standard curve (> 10 ng/mL) for both PMA stimulated and unstimulated neutrophils, indicating a high degree of NET formation. Further dilutions of the supernatant would have provided the exact concentrations and if there were any differences between the unstimulated and PMA stimulated. Cells from CML patient 3 showed a higher concentration of MPO in PMA stimulated neutrophils compared to unstimulated neutrophils, as expected. The MPO concentration measured in the supernatants of neutrophils derived from the healthy donor (HD 2) was lower after PMA stimulation compared to all three CML patients. However, the MPO concentration from unstimulated cells was higher than for the stimulated cells. The same was observed after manual counting of NETs, thus a higher degree of NET formation in the unstimulated cells compared to stimulated neutrophils from healthy donor 2. The opposite was observed in neutrophils isolated from all three CML patients.

Manual counting of NET-like structures was performed on cells stained with hoechst and SYTOX green from pictures acquired from live cell imaging after three hours of stimulation. Manual counting is a less objective way to quantify NETs than ELISA. However, morphological quantification gives a direct indication of the number of NETs. Manual counting showed more NET formation after PMA stimulation compared to IO and unstimulating in all three CML patients. The manual counting in neutrophils from healthy donor 2 revealed a higher number of NETs formed by unstimulated neutrophils compared to the neutrophils stimulated with PMA or IO. This may indicate that the handling or other stimuli influenced the cells, and the results cannot be considered valid. Because of this, the higher number of NETs in neutrophils from the one healthy donor compared to neutrophils from all three CML patients do not indicate that neutrophils from CML patients produce less NETs compared to healthy neutrophils. In order to obtain some preliminary conclusions if neutrophils isolated from CML patients make more or less NETs compared to neutrophils from healthy individuals, quantification needs to be performed and compared to neutrophils from at least three healthy donors. Optimally, the use of age- and gender-matched controls for each CML patient will give a more correct control for comparison.

It is also evident that the cells obtained and studied from only three CML do not represent the disease in general. Therefore, the study of neutrophils from additional CML patients plus age- and gender-matched controls will be necessary to make a conclusion with respect to NET formation capabilities. In the study by Telerman and colleagues, cells from eight CML patients and gender- and age-matched controls for each patient were used, providing a better opportunity for at least preliminary conclusions.

The variations in NET formation after PMA stimulation compared to stimulation with IO is remarkable in neutrophils from all three CML patients studied and revealed that PMA was the most potent NET inducer in CML-derived primary neutrophils. This variation in the number of NETs between PMA and IO stimulation was not observed for the Kcl-22 cells. PMA activates protein kinase C, while ionomycin stimulates the calcium influx [115]. In addition, it has been shown that the two stimulants induce NET formation in two different ways which can explain the differences observed between PMA and IO induced NET formation in primary CML neutrophils, but not in Kcl-22.

### 5.2.2 The role of BCR-ABL1 in NET formation in primary CML neutrophils

The role of BCR-ABL1 in NET formation was investigated in primary CML neutrophils after treating the cells with TKIs that blocked phosphorylation and thereby turned off the activity of the BCR-ABL1 protein, as shown in Kcl-22 cells. Due to excess cells following cell isolation from the blood of CML patient 1, this allowed for cryopreservation of cells and therefore neutrophils from this patient could be used for further experiments. In addition, BCR-ABL1 mRNA expression had been verified by RT-PCR in the neutrophils isolated from CML 1. NET formation after 1 hour of ponatinib or ABL001 treatment was investigated in comparison to untreated neutrophils derived from CML 1. Cells were either stimulated with PMA or unstimulated for 3 hours prior to manual counting of NET structures. The morphological counting showed no differences between cells treated with ponatinib or ABL001 compared to untreated cells (Fig. 4.16). This further substantiated what was observed for the Kcl-22 cell line. Therefore, currently, no evidence exists that BCR-ABL1 protein plays a direct role in the formation of extracellular traps.

However, the unusual high percent of NETs, shown in Figure 4.16, after morphological counting, most likely was due to the fact that these neutrophils had been cryopreserved prior to the experiment. The extra handling of these neutrophils, by thawing and centrifugation, probably triggered NET formation. This could explain the high number of NETs for both unstimulated and PMA stimulated cells. Therefore, unless novel procedures for thawing of neutrophils are discovered, freshly isolated CML neutrophils, instead of cryopreserved, will be essential for future NET formation studies.

Studying NETs is challenging as human neutrophils are terminally mature cells with a short lifespan and very easily activated by *ex vivo* handling and environmental factors therefore neutrophils need to be used shortly after they are derived and isolated from the donor as this thesis confirms. Studying NETs in CML enhances this challenge even further because CML is a rare disease and getting blood from treatment-naïve patients is fortunate. Therefore, the use of cell line models is more convenient as they are easier to handle and much more accessible. However, as this thesis describe, a cell line model for CML neutrophils is a challenge to obtain.

Although primary cells have limitations, they offer the most relevant and direct answer to how the cells behave *in vivo* in comparison to cell line models. As described earlier, using neutrophils derived from more CML patients and comparing them to age- and gender-matched controls would be the optimal way to get an indication of NET formation in CML and to answer the question if CML neutrophils make more or less NETs compared to neutrophils from healthy individuals.

## 5.3 Conclusions and future perspectives

In summary, this thesis provides preliminary results that NET formation seems to be enhanced in neutrophils from CML patients and that BCR-ABL1 does not play a direct role in the formation of NETs in CML. This thesis presents an approach to assess NETs *ex vivo* using isolated primary neutrophils and a proposal on how to investigate NET formation in a human CML cell line using CEBPα transduced Kcl-22 cells.

For future studies on the involvement of NETs in CML, the same type of experiments as described in this thesis should be performed, only with an increased number of donor samples from both CML patients and healthy individuals. This would most likely provide a conclusion as to whether CML neutrophils have a higher capability of NET formation compared with neutrophils from age- and gender-matched healthy individuals. Future development of biomarkers for ETs measurement *in vivo* is also important in order to establish correlations between symptoms and ET formation.

If neutrophils from CML patients do form more NETs and that NET formation is further enhanced by some of the TKI treatments, as described by Telerman and colleagues, the study and developments of anti-NET therapeutics will be very interesting and highly relevant. If indeed NET formation is enhanced in CML patients, anti-NET therapeutics interfering with NET formation can be of great value in a step to reduce the cardiovascular complications in CML patients as well as cancer patients in general. And if the increase in cardiovascular complications, especially thrombosis reported with the use of TKIs is due to NET formation, more information on the frequency and associated molecular mechanisms and regulation, will be essential for anti-NET therapy development.

# References


1. Abbas AK, Lichtman AH, Pillai S: **Cellular and Molecular Immunology**: Elsevier; 2018.
2. Granot Z: **Neutrophils as a Therapeutic Target in Cancer**. *Frontiers in Immunology* 2019, **10**(1710).
3. Hamam HJ, Palaniyar N: **Post-Translational Modifications in NETosis and NETs-Mediated Diseases**. *Biomolecules* 2019, **9**(8).
4. Mantovani A, Cassatella MA, Costantini C, Jaillon S: **Neutrophils in the activation and regulation of innate and adaptive immunity**. *Nature Reviews Immunology* 2011, **11**(8):519-531.
5. Brinkmann V, Reichard U, Goosmann C, Fauler B, Uhlemann Y, Weiss DS, Weinrauch Y, Zychlinsky A: **Neutrophil extracellular traps kill bacteria**. *Science* 2004, **303**(5663):1532-1535.
6. Betts G, Young KA, Wise JA, Johnson E, Poe B, Kruse DH, Korol O, Johnson JE, Womble M, DeSaix P: **Anatomy and Physiology** OpenStax; 2013.
7. **Neutrophil Cell Markers** [https://www.rndsystems.com/resources/cell-markers/immune-cells/granulocytes/neutrophil-cell-markers]
8. Lakschevitz FS, Hassanpour S, Rubin A, Fine N, Sun C, Glogauer M: **Identification of neutrophil surface marker changes in health and inflammation using high-throughput screening flow cytometry**. *Experimental Cell Research* 2016, **342**(2):200-209.
9. Papayannopoulos V: **Neutrophil extracellular traps in immunity and disease**. *Nature Reviews Immunology* 2018, **18**(2):134-147.
10. Papayannopoulos V, Zychlinsky A: **NETs: a new strategy for using old weapons**. *Trends in Immunology* 2009, **30**(11):513-521.
11. Mayadas TN, Cullere X, Lowell CA: **The multifaceted functions of neutrophils**. *Annu Rev Pathol* 2014, **9**:181-218.
12. Beiter K, Wartha F, Albiger B, Normark S, Zychlinsky A, Henriques-Normark B: **An Endonuclease Allows Streptococcus pneumoniae to Escape from Neutrophil Extracellular Traps**. *Current Biology* 2006, **16**(4):401-407.
13. Doolin T, Amir HM, Duong L, Rosenzweig R, Urban LA, Bosch M, Pol A, Gross SP, Siryaporn A: **Mammalian histones facilitate antimicrobial synergy by disrupting the bacterial proton gradient and chromosome organization**. *Nature Communications* 2020, **11**(1):3888.
14. Ramos-Martínez E, Hernández-González L, Ramos-Martínez I, Pérez-Campos Mayoral L, López-Cortés GI, Pérez-Campos E, Mayoral Andrade G, Hernández-Huerta MT, José MV: **Multiple Origins of Extracellular DNA Traps**. *Frontiers in Immunology* 2021, **12**.
15. Neubert E, Meyer D, Kruss S, Erpenbeck L: **The power from within – understanding the driving forces of neutrophil extracellular trap formation**. *Journal of Cell Science* 2020, **133**(5).
16. von Köckritz-Blickwede M, Nizet V: **Innate immunity turned inside-out: antimicrobial defense by phagocyte extracellular traps**. *Journal of Molecular Medicine* 2009, **87**(8):775-783.
17. Arazna M, Pruchniak MP, Demkow U: **Neutrophil extracellular traps in bacterial infections: Strategies for escaping from killing**. *Respiratory Physiology & Neurobiology* 2013, **187**(1):74-77.

18. Ríos-López AL, González GM, Hernández-Bello R, Sánchez-González A: **Avoiding the trap: Mechanisms developed by pathogens to escape neutrophil extracellular traps**. *Microbiological Research* 2021, **243**:126644.
19. Kristian SA, Datta V, Weidenmaier C, Kansal R, Fedtke I, Peschel A, Gallo RL, Nizet V: **d-Alanylation of Teichoic Acids Promotes Group A Streptococcus Antimicrobial Peptide Resistance, Neutrophil Survival, and Epithelial Cell Invasion**. *Journal of Bacteriology* 2005, **187**(19):6719-6725.
20. Peschel A, Otto M, Jack RW, Kalbacher H, Jung G, Götz F: **Inactivation of the dlt operon in Staphylococcus aureus confers sensitivity to defensins, protegrins, and other antimicrobial peptides**. *J Biol Chem* 1999, **274**(13):8405-8410.
21. Wartha F, Beiter K, Albiger B, Fernebro J, Zychlinsky A, Normark S, Henriques-Normark B: **Capsule and d-alanylated lipoteichoic acids protect Streptococcus pneumoniae against neutrophil extracellular traps**. *Cellular Microbiology* 2007, **9**(5):1162-1171.
22. Berends ETM, Horswill AR, Haste NM, Monestier M, Nizet V, von Köckritz-Blickwede M: **Nuclease Expression by Staphylococcus aureus Facilitates Escape from Neutrophil Extracellular Traps**. *Journal of Innate Immunity* 2010, **2**(6):576-586.
23. Seper A, Hosseinzadeh A, Gorkiewicz G, Lichtenegger S, Roier S, Leitner DR, Röhm M, Grutsch A, Reidl J, Urban CF *et al*: **Vibrio cholerae Evades Neutrophil Extracellular Traps by the Activity of Two Extracellular Nucleases**. *PLOS Pathogens* 2013, **9**(9):e1003614.
24. Kaplan MJ, Radic M: **Neutrophil Extracellular Traps: Double-Edged Swords of Innate Immunity**. *The Journal of Immunology* 2012, **189**(6):2689-2695.
25. Fuchs TA, Abed U, Goosmann C, Hurwitz R, Schulze I, Wahn V, Weinrauch Y, Brinkmann V, Zychlinsky A: **Novel cell death program leads to neutrophil extracellular traps**. *J Cell Biol* 2007, **176**(2):231-241.
26. Pilsczek FH, Salina D, Poon KK, Fahey C, Yipp BG, Sibley CD, Robbins SM, Green FH, Surette MG, Sugai M *et al*: **A novel mechanism of rapid nuclear neutrophil extracellular trap formation in response to Staphylococcus aureus**. *J Immunol* 2010, **185**(12):7413-7425.
27. Yipp BG, Petri B, Salina D, Jenne CN, Scott BN, Zbytnuik LD, Pittman K, Asaduzzaman M, Wu K, Meijndert HC *et al*: **Infection-induced NETosis is a dynamic process involving neutrophil multitasking in vivo**. *Nat Med* 2012, **18**(9):1386-1393.
28. Bayr H: **Reactive oxygen species**. *Critical Care Medicine* 2005, **33**(12):S498-S501.
29. Burg ND, Pillinger MH: **The Neutrophil: Function and Regulation in Innate and Humoral Immunity**. *Clinical Immunology* 2001, **99**(1):7-17.
30. Metzler KD, Goosmann C, Lubojemska A, Zychlinsky A, Papayannopoulos V: **A myeloperoxidase-containing complex regulates neutrophil elastase release and actin dynamics during NETosis**. *Cell Rep* 2014, **8**(3):883-896.
31. Papayannopoulos V, Metzler KD, Hakkim A, Zychlinsky A: **Neutrophil elastase and myeloperoxidase regulate the formation of neutrophil extracellular traps**. *Journal of Cell Biology* 2010, **191**(3):677-691.
32. Metzler Kathleen D, Goosmann C, Lubojemska A, Zychlinsky A, Papayannopoulos V: **A Myeloperoxidase-Containing Complex Regulates Neutrophil Elastase Release and Actin Dynamics during NETosis**. *Cell Reports* 2014, **8**(3):883-896.

33. Sprenkeler EGG, Tool ATJ, Henriet SSV, van Bruggen R, Kuijpers TW: **Formation of neutrophil extracellular traps requires actin cytoskeleton rearrangements**. *Blood* 2022, **139**(21):3166-3180.
34. Chen KW, Monteleone M, Boucher D, Sollberger G, Ramnath D, Condon ND, Pein JBv, Broz P, Sweet MJ, Schroder K: **Noncanonical inflammasome signaling elicits gasdermin D–dependent neutrophil extracellular traps**. *Science Immunology* 2018, **3**(26):eaar6676.
35. Bianchi M, Niemiec MJ, Siler U, Urban CF, Reichenbach J: **Restoration of anti-Aspergillus defense by neutrophil extracellular traps in human chronic granulomatous disease after gene therapy is calprotectin-dependent**. *Journal of Allergy and Clinical Immunology* 2011, **127**(5):1243-1252.e1247.
36. Clark RA, Klebanoff SJ: **Chronic granulomatous disease: Studies of a family with impaired neutrophil chemotactic, metabolic and bactericidal function**. *The American Journal of Medicine* 1978, **65**(6):941-948.
37. Khan MA, Palaniyar N: **Transcriptional firing helps to drive NETosis**. *Scientific Reports* 2017, **7**(1):41749.
38. Douda DN, Khan MA, Grasemann H, Palaniyar N: **SK3 channel and mitochondrial ROS mediate NADPH oxidase-independent NETosis induced by calcium influx**. *Proc Natl Acad Sci U S A* 2015, **112**(9):2817-2822.
39. Douda DN, Khan MA, Grasemann H, Palaniyar N: **SK3 channel and mitochondrial ROS mediate NADPH oxidase-independent NETosis induced by calcium influx**. *Proceedings of the National Academy of Sciences of the United States of America* 2015, **112**(9):2817-2822.
40. Neeli I, Khan SN, Radic M: **Histone deimination as a response to inflammatory stimuli in neutrophils**. *J Immunol* 2008, **180**(3):1895-1902.
41. Wang Y, Li M, Stadler S, Correll S, Li P, Wang D, Hayama R, Leonelli L, Han H, Grigoryev SA *et al*: **Histone hypercitrullination mediates chromatin decondensation and neutrophil extracellular trap formation**. *J Cell Biol* 2009, **184**(2):205-213.
42. Poon I, Baxter AA, Lay FT, Mills GD, Adda CG, Payne JA, Phan TK, Ryan GF, White JA, Veneer PK *et al*: **Phosphoinositide-mediated oligomerization of a defensin induces cell lysis**. *Elife* 2014, **3**:e01808.
43. Kawabata K, Hagio T, Matsuoka S: **The role of neutrophil elastase in acute lung injury**. *Eur J Pharmacol* 2002, **451**(1):1-10.
44. Xu J, Zhang X, Pelayo R, Monestier M, Ammollo CT, Semeraro F, Taylor FB, Esmon NL, Lupu F, Esmon CT: **Extracellular histones are major mediators of death in sepsis**. *Nat Med* 2009, **15**(11):1318-1321.
45. Abrams ST, Zhang N, Manson J, Liu T, Dart C, Baluwa F, Wang SS, Brohi K, Kipar A, Yu W *et al*: **Circulating histones are mediators of trauma-associated lung injury**. *Am J Respir Crit Care Med* 2013, **187**(2):160-169.
46. Thomas GM, Carbo C, Curtis BR, Martinod K, Mazo IB, Schatzberg D, Cifuni SM, Fuchs TA, von Andrian UH, Hartwig JH *et al*: **Extracellular DNA traps are associated with the pathogenesis of TRALI in humans and mice**. *Blood* 2012, **119**(26):6335-6343.
47. Massberg S, Grahl L, von Bruehl ML, Manukyan D, Pfeiler S, Goosmann C, Brinkmann V, Lorenz M, Bidzhekov K, Khandagale AB *et al*: **Reciprocal coupling of coagulation and innate immunity via neutrophil serine proteases**. *Nat Med* 2010, **16**(8):887-896.
48. Engelmann B, Massberg S: **Thrombosis as an intravascular effector of innate immunity**. *Nature Reviews Immunology* 2013, **13**(1):34-45.

49. Mutua V, Gershwin LJ: **A Review of Neutrophil Extracellular Traps (NETs) in Disease: Potential Anti-NETs Therapeutics**. *Clin Rev Allergy Immunol* 2021, **61**(2):194-211.
50. Pan L, Lu MP, Wang JH, Xu M, Yang SR: **Immunological pathogenesis and treatment of systemic lupus erythematosus**. *World J Pediatr* 2020, **16**(1):19-30.
51. Barnes BJ, Adrover JM, Baxter-Stoltzfus A, Borczuk A, Cools-Lartigue J, Crawford JM, Daßler-Plenker J, Guerci P, Huynh C, Knight JS *et al*: **Targeting potential drivers of COVID-19: Neutrophil extracellular trapsNeutrophil extracellular traps in COVID-19**. *Journal of Experimental Medicine* 2020, **217**(6).
52. Al-Kuraishy HM, Al-Gareeb AI, Al-hussaniy HA, Al-Harcan NAH, Alexiou A, Batiha GE-S: **Neutrophil Extracellular Traps (NETs) and Covid-19: A new frontiers for therapeutic modality**. *International Immunopharmacology* 2022, **104**:108516.
53. Zuo Y, Yalavarthi S, Shi H, Gockman K, Zuo M, Madison JA, Blair C, Weber A, Barnes BJ, Egeblad M *et al*: **Neutrophil extracellular traps in COVID-19**. *JCI Insight* 2020, **5**(11):e138999.
54. Chereda B, Melo JV: **Natural course and biology of CML**. *Annals of Hematology* 2015, **94**(2):107-121.
55. Arber DA, Orazi A, Hasserjian R, Thiele J, Borowitz MJ, Le Beau MM, Bloomfield CD, Cazzola M, Vardiman JW: **The 2016 revision to the World Health Organization classification of myeloid neoplasms and acute leukemia**. *Blood* 2016, **127**(20):2391-2405.
56. Höglund M, Sandin F, Simonsson B: **Epidemiology of chronic myeloid leukaemia: an update**. *Annals of Hematology* 2015, **94**(2):241-247.
57. Vuelta E, García-Tuñón I, Hernández-Carabias P, Méndez L, Sánchez-Martín M: **Future Approaches for Treating Chronic Myeloid Leukemia: CRISPR Therapy**. *Biology (Basel)* 2021, **10**(2):118.
58. Apperley JF: **Chronic myeloid leukaemia**. *The Lancet* 2015, **385**(9976):1447-1459.
59. **Leukemia - Chronic Myeloid - CML: Phases** [https://www.cancer.net/cancer-types/leukemia-chronic-myeloid-cml/phases]
60. Kantarjian HM, Keating MJ, Talpaz M, Walters RS, Smith TL, Cork A, McCredie KB, Freireich EJ: **Chronic myelogenous leukemia in blast crisis: Analysis of 242 patients**. *The American Journal of Medicine* 1987, **83**(3):445-454.
61. Cortes J, Pavlovsky C, Saußele S: **Chronic myeloid leukaemia**. *The Lancet* 2021, **398**(10314):1914-1926.
62. Nowell PC: **The minute chromosome (Phl) in chronic granulocytic leukemia**. *Blut* 1962, **8**:65-66.
63. Rowley JD: **A New Consistent Chromosomal Abnormality in Chronic Myelogenous Leukaemia identified by Quinacrine Fluorescence and Giemsa Staining**. *Nature* 1973, **243**(5405):290-293.
64. Hungerford D, Nowell P: **A minute chromosome in human chronic granulocytic leukemia**. *Science* 1960, **132**(3438):1488-1501.
65. Kurzrock R, Gutterman JU, Talpaz M: **The Molecular Genetics of Philadelphia Chromosome–Positive Leukemias**. *New England Journal of Medicine* 1988, **319**(15):990-998.
66. and SRH, Till JH: **Protein Tyrosine Kinase Structure and Function**. *Annual Review of Biochemistry* 2000, **69**(1):373-398.
67. Van Etten RA, Debnath J, Zhou H, Casasnovas JM: **Introduction of a loss-of-function point mutation from the SH3 region of the Caenorhabditis elegans sem-**

**5 gene activates the transforming ability of c-abl in vivo and abolishes binding of proline-rich ligands in vitro**. *Oncogene* 1995, **10**(10):1977-1988.
68. Puil L, Liu J, Gish G, Mbamalu G, Bowtell D, Pelicci PG, Arlinghaus R, Pawson T: **Bcr-Abl oncoproteins bind directly to activators of the Ras signalling pathway**. *Embo j* 1994, **13**(4):764-773.
69. Bedi A, Zehnbauer BA, Barber JP, Sharkis SJ, Jones RJ: **Inhibition of apoptosis by BCR-ABL in chronic myeloid leukemia**. *Blood* 1994, **83**(8):2038-2044.
70. Gordon MY, Dowding CR, Riley GP, Goldman JM, Greaves MF: **Altered adhesive interactions with marrow stroma of haematopoietic progenitor cells in chronic myeloid leukaemia**. *Nature* 1987, **328**(6128):342-344.
71. Score J, Calasanz MJ, Ottman O, Pane F, Yeh RF, Sobrinho-Simões MA, Kreil S, Ward D, Hidalgo-Curtis C, Melo JV *et al*: **Analysis of genomic breakpoints in p190 and p210 BCR–ABL indicate distinct mechanisms of formation**. *Leukemia* 2010, **24**(10):1742-1750.
72. Faderl S, Talpaz M, Estrov Z, O'Brien S, Kurzrock R, Kantarjian HM: **The Biology of Chronic Myeloid Leukemia**. *New England Journal of Medicine* 1999, **341**(3):164-172.
73. Baccarani M, Castagnetti F, Gugliotta G, Rosti G, Soverini S, Albeer A, Pfirrmann M, for the International BCRABLSG: **The proportion of different BCR-ABL1 transcript types in chronic myeloid leukemia. An international overview**. *Leukemia* 2019, **33**(5):1173-1183.
74. Jain P, Kantarjian H, Patel KP, Gonzalez GN, Luthra R, Shamanna RK, Sasaki K, Jabbour E, Romo CG, Kadia TM *et al*: **Impact of BCR-ABL transcript type on outcome in patients with chronic-phase CML treated with tyrosine kinase inhibitors**. *Blood* 2016, **127**(10):1269-1275.
75. Baccarani M, Cortes J, Pane F, Niederwieser D, Saglio G, Apperley J, Cervantes F, Deininger M, Gratwohl A, Guilhot F *et al*: **Chronic myeloid leukemia: an update of concepts and management recommendations of European LeukemiaNet**. *J Clin Oncol* 2009, **27**(35):6041-6051.
76. Hehlmann R: **Chronic Myeloid Leukemia in 2020**. *HemaSphere* 2020, **4**(5):e468.
77. Kantarjian HM, Giles F, Quintás-Cardama A, Cortes J: **Important Therapeutic Targets in Chronic Myelogenous Leukemia**. *Clinical Cancer Research* 2007, **13**(4):1089-1097.
78. Druker BJ, Tamura S, Buchdunger E, Ohno S, Segal GM, Fanning S, Zimmermann J, Lydon NB: **Effects of a selective inhibitor of the Abl tyrosine kinase on the growth of Bcr-Abl positive cells**. *Nat Med* 1996, **2**(5):561-566.
79. O'Brien SG, Guilhot F, Larson RA, Gathmann I, Baccarani M, Cervantes F, Cornelissen JJ, Fischer T, Hochhaus A, Hughes T *et al*: **Imatinib Compared with Interferon and Low-Dose Cytarabine for Newly Diagnosed Chronic-Phase Chronic Myeloid Leukemia**. *New England Journal of Medicine* 2003, **348**(11):994-1004.
80. Savage DG, Antman KH: **Imatinib Mesylate — A New Oral Targeted Therapy**. *New England Journal of Medicine* 2002, **346**(9):683-693.
81. Soverini S, Hochhaus A, Nicolini FE, Gruber F, Lange T, Saglio G, Pane F, Müller MC, Ernst T, Rosti G *et al*: **BCR-ABL kinase domain mutation analysis in chronic myeloid leukemia patients treated with tyrosine kinase inhibitors: recommendations from an expert panel on behalf of European LeukemiaNet**. *Blood* 2011, **118**(5):1208-1215.
82. Cortes J, Jabbour E, Kantarjian H, Yin CC, Shan J, O'Brien S, Garcia-Manero G, Giles F, Breeden M, Reeves N *et al*: **Dynamics of BCR-ABL kinase domain**

**mutations in chronic myeloid leukemia after sequential treatment with multiple tyrosine kinase inhibitors**. *Blood* 2007, **110**(12):4005-4011.

83. O'Hare T, Eide CA, Deininger MWN: **Bcr-Abl kinase domain mutations, drug resistance, and the road to a cure for chronic myeloid leukemia**. *Blood* 2007, **110**(7):2242-2249.
84. **Novartis recieves FDA Breakthrough Therapy designations for investigational STAMP inhibitor asciminib (ABL001) in chronic myeloid leukemia** [https://www.novartis.com/news/media-releases/novartis-receives-fda-breakthrough-therapy-designations-investigational-stamp-inhibitor-asciminib-abl001-chronic-myeloid-leukemia]
85. Hughes TP, Mauro MJ, Cortes JE, Minami H, Rea D, DeAngelo DJ, Breccia M, Goh Y-T, Talpaz M, Hochhaus A *et al*: **Asciminib in Chronic Myeloid Leukemia after ABL Kinase Inhibitor Failure**. *New England Journal of Medicine* 2019, **381**(24):2315-2326.
86. Hochhaus A, Baccarani M, Silver RT, Schiffer C, Apperley JF, Cervantes F, Clark RE, Cortes JE, Deininger MW, Guilhot F *et al*: **European LeukemiaNet 2020 recommendations for treating chronic myeloid leukemia**. *Leukemia* 2020, **34**(4):966-984.
87. Kujawski LA, Talpaz M: **The role of interferon-alpha in the treatment of chronic myeloid leukemia**. *Cytokine & Growth Factor Reviews* 2007, **18**(5):459-471.
88. Tura S, Baccarani M: **α-Interferon in the Treatment of Chronic Myeloid Leukemia**. *Blood* 1995, **85**(10):2999-3000.
89. Graham SM, Jørgensen HG, Allan E, Pearson C, Alcorn MJ, Richmond L, Holyoake TL: **Primitive, quiescent, Philadelphia-positive stem cells from patients with chronic myeloid leukemia are insensitive to STI571 in vitro**. *Blood* 2002, **99**(1):319-325.
90. Milojkovic D, Apperley J: **Mechanisms of Resistance to Imatinib and Second-Generation Tyrosine Inhibitors in Chronic Myeloid Leukemia**. *Clin Cancer Res* 2009, **15**(24):7519-7527.
91. Caldemeyer L, Dugan M, Edwards J, Akard L: **Long-Term Side Effects of Tyrosine Kinase Inhibitors in Chronic Myeloid Leukemia**. *Current Hematologic Malignancy Reports* 2016, **11**(2):71-79.
92. Zeng P, Schmaier A: **Ponatinib and other CML Tyrosine Kinase Inhibitors in Thrombosis**. *Int J Mol Sci* 2020, **21**(18):6556.
93. Telerman A, Granot G, Leibovitch C, Yarchovsky-Dolberg O, Shacham-Abulafia A, Partouche S, Yeshurun M, Ellis MH, Raanani P, Wolach O: **Neutrophil Extracellular Traps Are Increased in Chronic Myeloid Leukemia and Are Differentially Affected by Tyrosine Kinase Inhibitors**. *Cancers (Basel)* 2021, **14**(1):119.
94. Paech F, Mingard C, Grünig D, Abegg VF, Bouitbir J, Krähenbühl S: **Mechanisms of mitochondrial toxicity of the kinase inhibitors ponatinib, regorafenib and sorafenib in human hepatic HepG2 cells**. *Toxicology* 2018, **395**:34-44.
95. Böyum A: **Isolation of mononuclear cells and granulocytes from human blood. Isolation of monuclear cells by one centrifugation, and of granulocytes by combining centrifugation and sedimentation at 1 g**. *Scand J Clin Lab Invest Suppl* 1968, **97**:77-89.
96. Krafts KP, Pambuccian SE: **Romanowsky staining in cytopathology: history, advantages and limitations**. *Biotech Histochem* 2011, **86**(2):82-93.
97. Shieh SY, Ikeda M, Taya Y, Prives C: **DNA damage-induced phosphorylation of p53 alleviates inhibition by MDM2**. *Cell* 1997, **91**(3):325-334.

98. Bradford MM: **A rapid and sensitive method for the quantitation of microgram quantities of protein utilizing the principle of protein-dye binding**. *Anal Biochem* 1976, **72**:248-254.
99. Manda-Handzlik A, Bystrzycka W, Wachowska M, Sieczkowska S, Stelmaszczyk-Emmel A, Demkow U, Ciepiela O: **The influence of agents differentiating HL-60 cells toward granulocyte-like cells on their ability to release neutrophil extracellular traps**. *Immunol Cell Biol* 2018, **96**(4):413-425.
100. **Mast Cell Marker** [https://www.rndsystems.com/resources/cell-markers/immune-cells/granulocytes/mast-cell-markers ]
101. Masuda S, Nakazawa D, Shida H, Miyoshi A, Kusunoki Y, Tomaru U, Ishizu A: **NETosis markers: Quest for specific, objective, and quantitative markers**. *Clinica Chimica Acta* 2016, **459**:89-93.
102. Goldman JM: **Ponatinib for Chronic Myeloid Leukemia**. *New England Journal of Medicine* 2012, **367**(22):2148-2149.
103. Rapozzi V, Burm BEA, Cogoi S, van der Marel GA, van Boom JH, Quadrifoglio F, Xodo LE: **Antiproliferative effect in chronic myeloid leukaemia cells by antisense peptide nucleic acids**. *Nucleic Acids Res* 2002, **30**(17):3712-3721.
104. Cerezo-Wallis D, Ballesteros I: **Neutrophils in cancer, a love–hate affair**. *The FEBS Journal*, **n/a**(n/a).
105. Shao B-Z, Yao Y, Li J-P, Chai N-L, Linghu E-Q: **The Role of Neutrophil Extracellular Traps in Cancer**. *Frontiers in Oncology* 2021, **11**.
106. Cristinziano L, Modestino L, Antonelli A, Marone G, Simon H-U, Varricchi G, Galdiero MR: **Neutrophil extracellular traps in cancer**. *Seminars in Cancer Biology* 2022, **79**:91-104.
107. Demers M, Krause DS, Schatzberg D, Martinod K, Voorhees JR, Fuchs TA, Scadden DT, Wagner DD: **Cancers predispose neutrophils to release extracellular DNA traps that contribute to cancer-associated thrombosis**. *Proceedings of the National Academy of Sciences of the United States of America* 2012, **109**(32):13076-13081.
108. Wolach O, Sellar RS, Martinod K, Cherpokova D, McConkey M, Chappell RJ, Silver AJ, Adams D, Castellano CA, Schneider RK *et al*: **Increased neutrophil extracellular trap formation promotes thrombosis in myeloproliferative neoplasms**. *Sci Transl Med* 2018, **10**(436).
109. Valent P, Akin C, Hartmann K, Nilsson G, Reiter A, Hermine O, Sotlar K, Sperr WR, Escribano L, George TI *et al*: **Mast cells as a unique hematopoietic lineage and cell system: From Paul Ehrlich's visions to precision medicine concepts**. *Theranostics* 2020, **10**(23):10743-10768.
110. Tavor S, Park DJ, Gery S, Vuong PT, Gombart AF, Koeffler HP: **Restoration of C/EBPα Expression in a BCR-ABL+ Cell Line Induces Terminal Granulocytic Differentiation***. *Journal of Biological Chemistry* 2003, **278**(52):52651-52659.
111. Pertiwi KR, de Boer OJ, Mackaaij C, Pabittei DR, de Winter RJ, Li X, van der Wal AC: **Extracellular traps derived from macrophages, mast cells, eosinophils and neutrophils are generated in a time-dependent manner during atherothrombosis**. *J Pathol* 2019, **247**(4):505-512.
112. Hartmann JT, Haap M, Kopp HG, Lipp HP: **Tyrosine kinase inhibitors - a review on pharmacology, metabolism and side effects**. *Curr Drug Metab* 2009, **10**(5):470-481.
113. Lee H, Basso IN, Kim DDH: **Target spectrum of the BCR-ABL tyrosine kinase inhibitors in chronic myeloid leukemia**. *Int J Hematol* 2021, **113**(5):632-641.

114. de Buhr N, von Köckritz-Blickwede M: **Detection, Visualization, and Quantification of Neutrophil Extracellular Traps (NETs) and NET Markers**. In: *Neutrophil: Methods and Protocols.* edn. Edited by Quinn MT, DeLeo FR. New York, NY: Springer US; 2020: 425-442.
115. Ai W, Li H, Song N, Li L, Chen H: **Optimal method to stimulate cytokine production and its use in immunotoxicity assessment**. *Int J Environ Res Public Health* 2013, **10**(9):3834-3842.

# 6. Appendix

## 6.1 NET formation in neutrophils by live cell imaging

Live cell imaging performed on neutrophils isolated from the blood of all three CML patients and compared to neutrophils from one healthy donor and ATRA treated Kcl-22 cells stained with hoechst and SYTOX green. Cells were stimulated with PMA or IO and compared to not simulated. Images acquired at the start, and then every 30 min are shown in Figure 6.1-6.5.

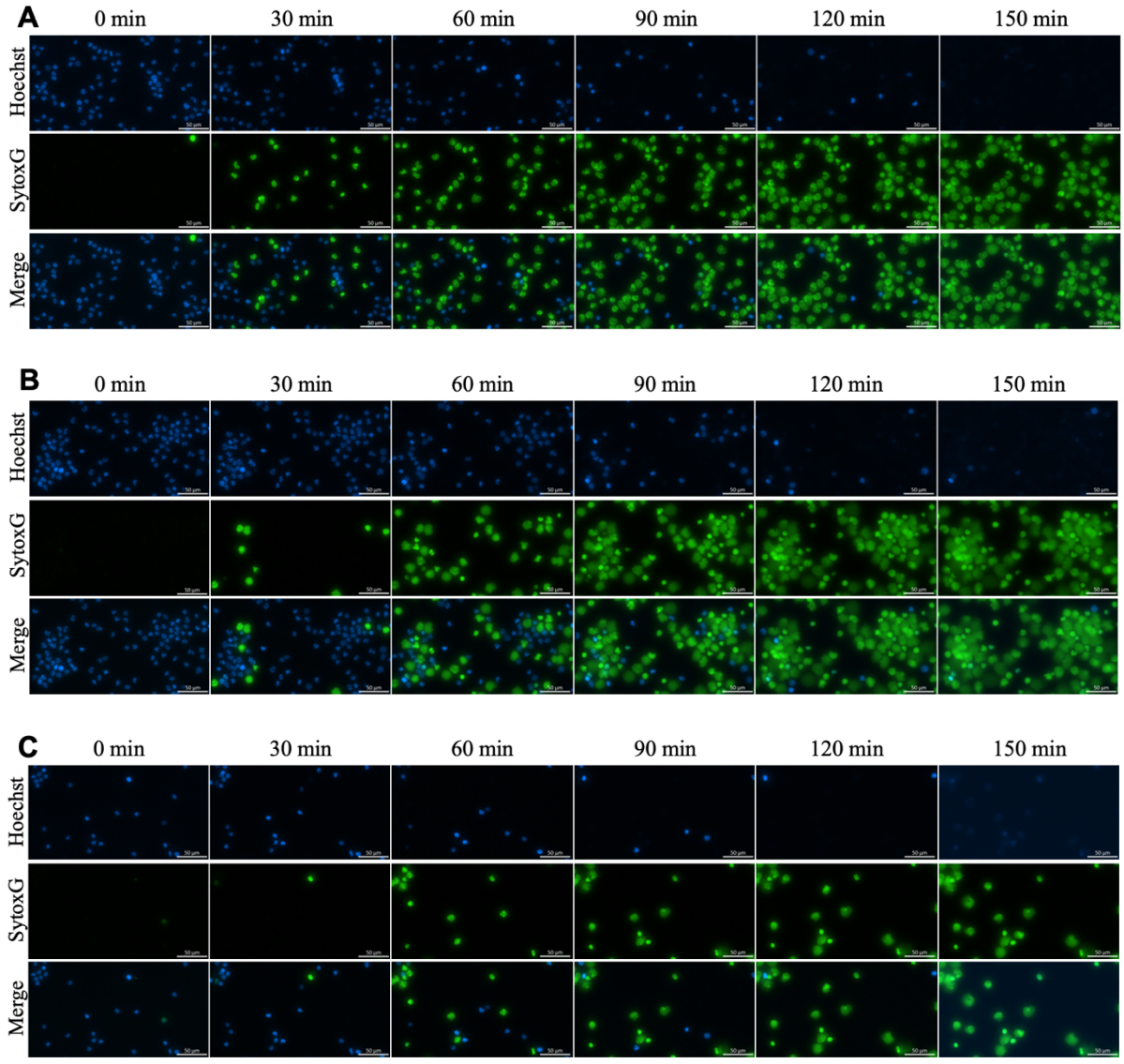


**Figure 6.1.** Live cell imaging of neutrophils isolated from the blood of CML patient 1 for the visualisation of cells during NET formation. Cells were stained with hoechst and SYTOX green and stimulated with PMA **(A)** or IO **(B)**, or not stimulated **(C)**. Shown are images captured at the start and every 30 min until 150 min after stimulation. Images were acquired

and analyzed by Zeiss AxioObserver Z1 microscope and ZEN 2012 (blue version) software and figures were made using ImageJ v.2.1.0 (Fiji). Scale bars: 50 µm.

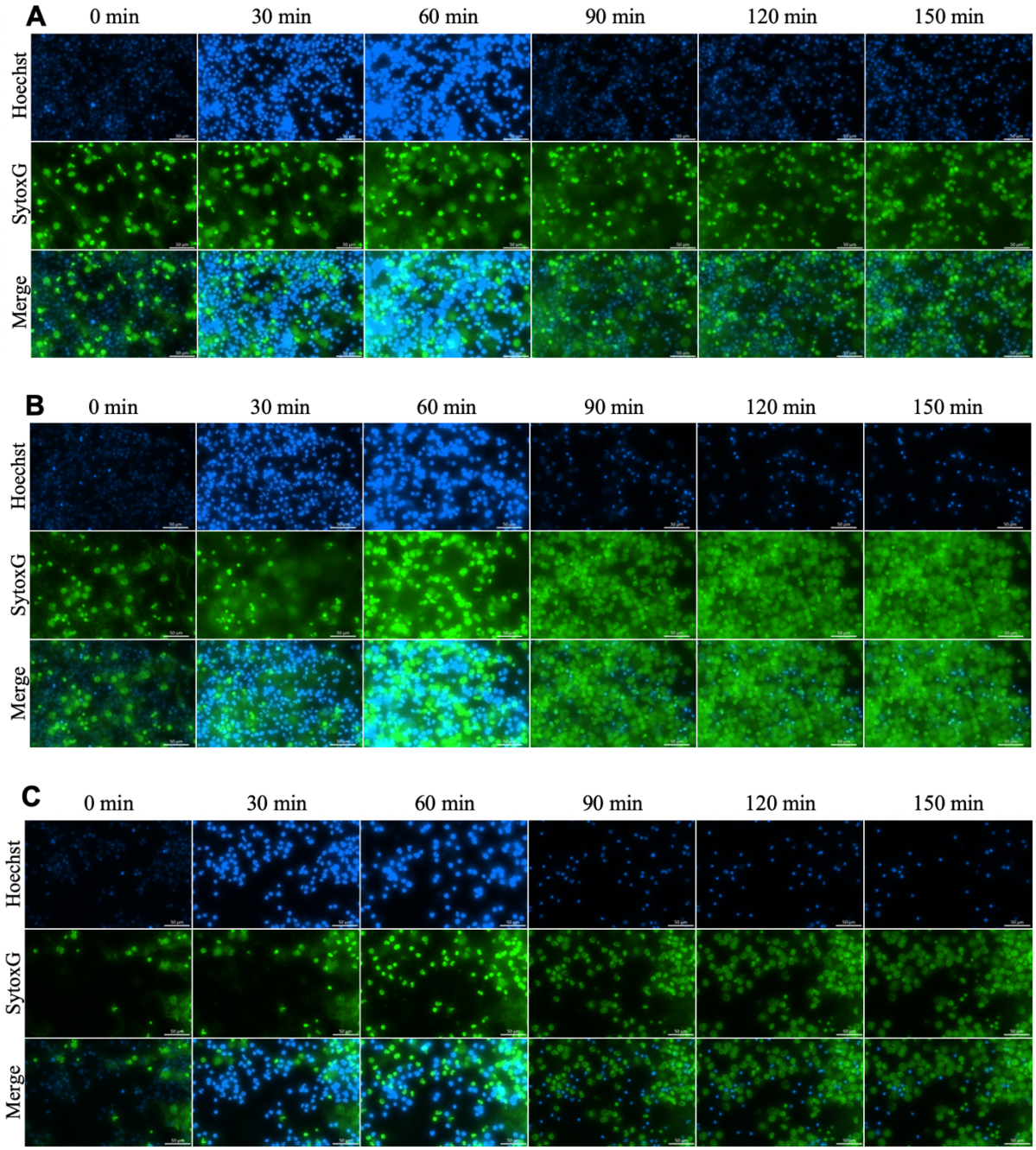


**Figure 6.2.** Live cell imaging of neutrophils isolated from the blood of CML patient 2 for the visualisation of cells during NET formation. Cells were stained with hoechst and SYTOX green and stimulated with PMA **(A)** or IO **(B)**, or not stimulated **(C)**. Shown are images captured at the start and every 30 min until 150 min after stimulation. Images were acquired and analyzed by Zeiss AxioObserver Z1 microscope and ZEN 2012 (blue version) software and figures were made using ImageJ v.2.1.0 (Fiji). Scale bars: 50 µm.

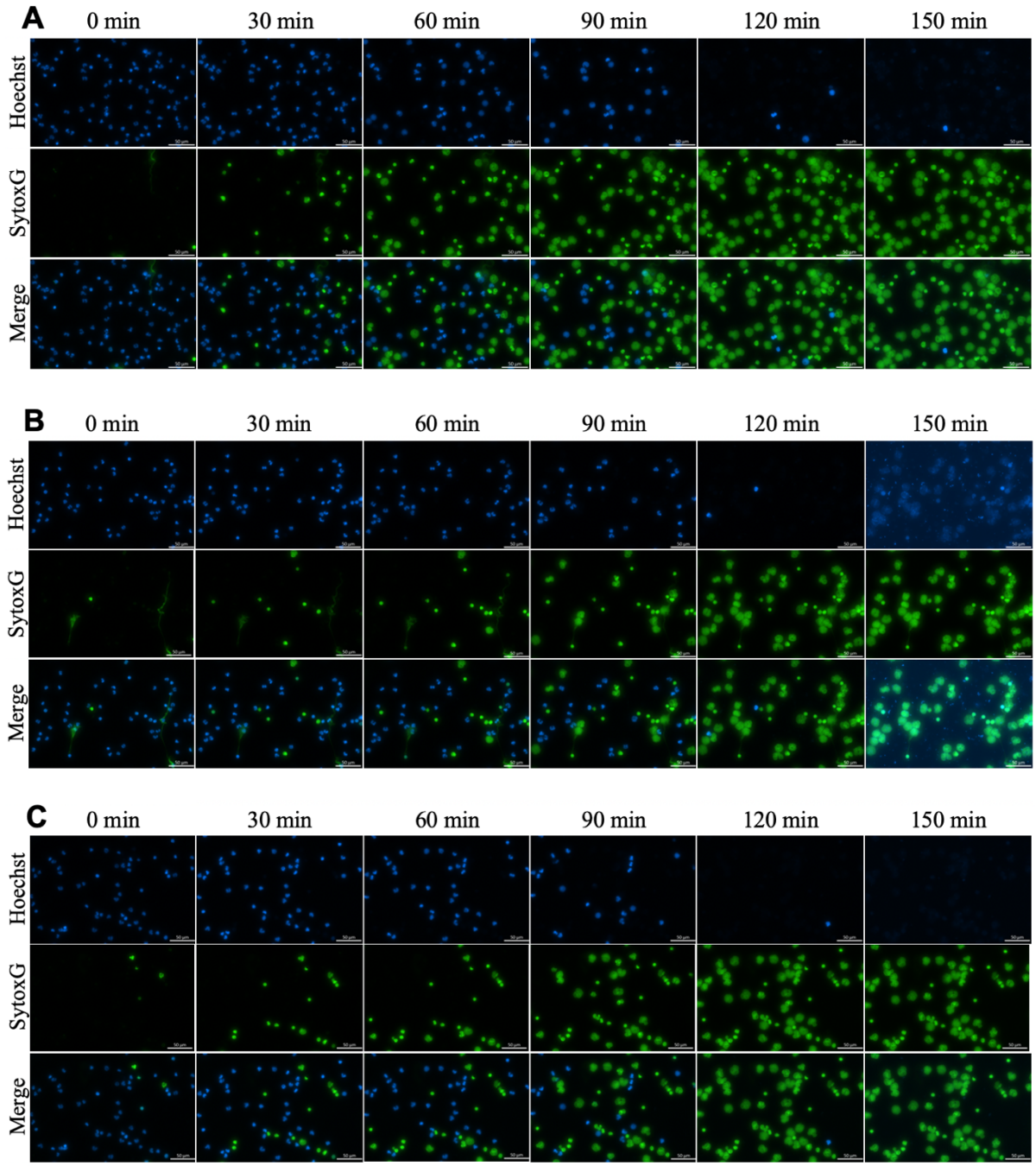


**Figure 6.3.** Live cell imaging of neutrophils isolated from the blood of CML patient 3 for the visualisation of cells during NET formation. Cells were stained with hoechst and SYTOX green and stimulated with PMA **(A)** or IO **(B)**, or not stimulated **(C)**. Shown are images captured at the start and every 30 min until 150 min after stimulation. Images were acquired and analyzed by Zeiss AxioObserver Z1 microscope and ZEN 2012 (blue version) software and figures were made using ImageJ v.2.1.0 (Fiji). Scale bars: 50 µm.

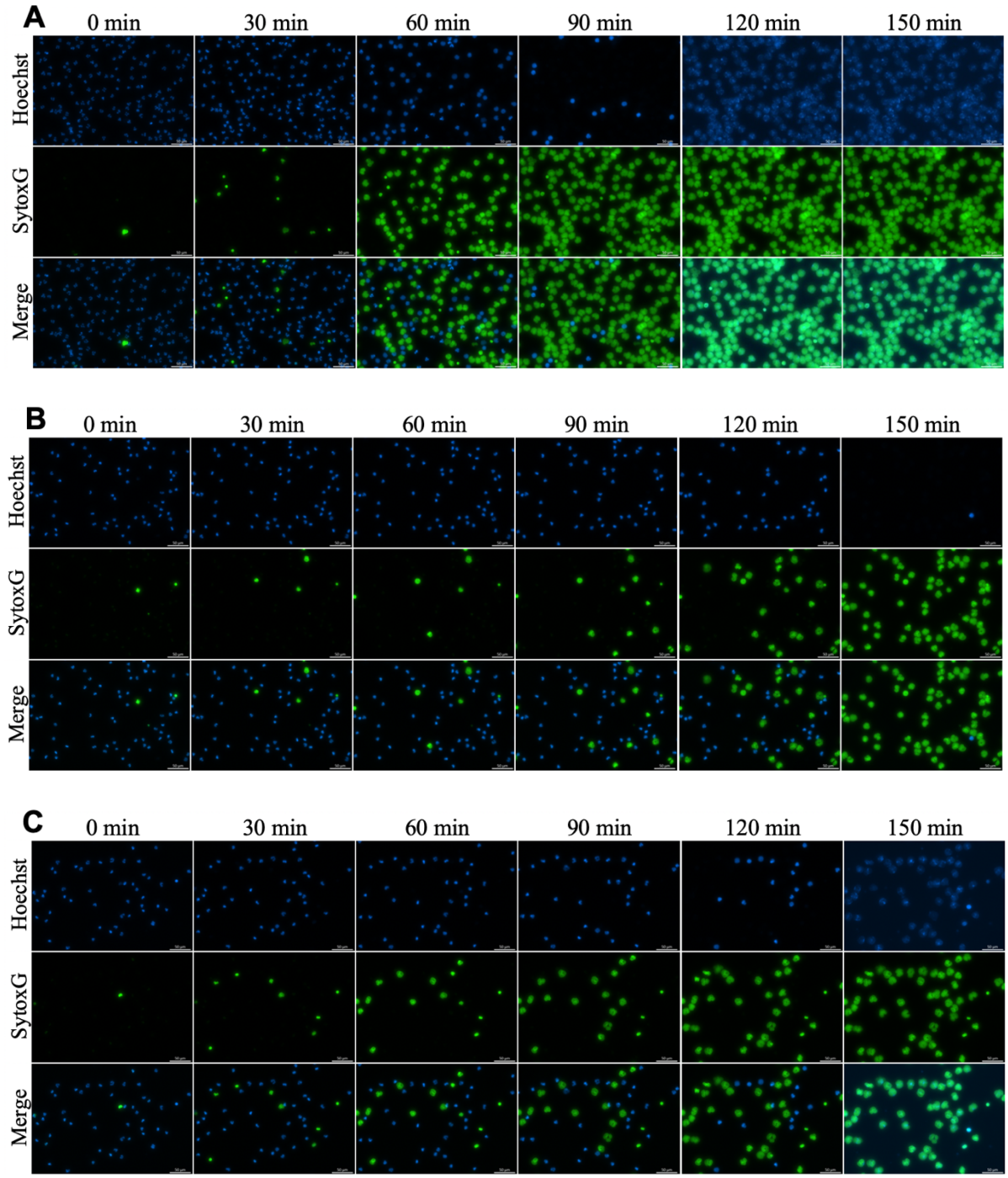


**Figure 6.4.** Live cell imaging of neutrophils isolated from the blood of healthy donor 2 for the visualisation of cells during NET formation. Cells were stained with hoechst and SYTOX green and stimulated with PMA **(A)** or IO **(B)**, or not stimulated **(C)**. Shown are images captured at the start and every 30 min until 150 min after stimulation. Images were acquired and analyzed by Zeiss AxioObserver Z1 microscope and ZEN 2012 (blue version) software and figures were made using ImageJ v.2.1.0 (Fiji). Scale bars: 50 µm.

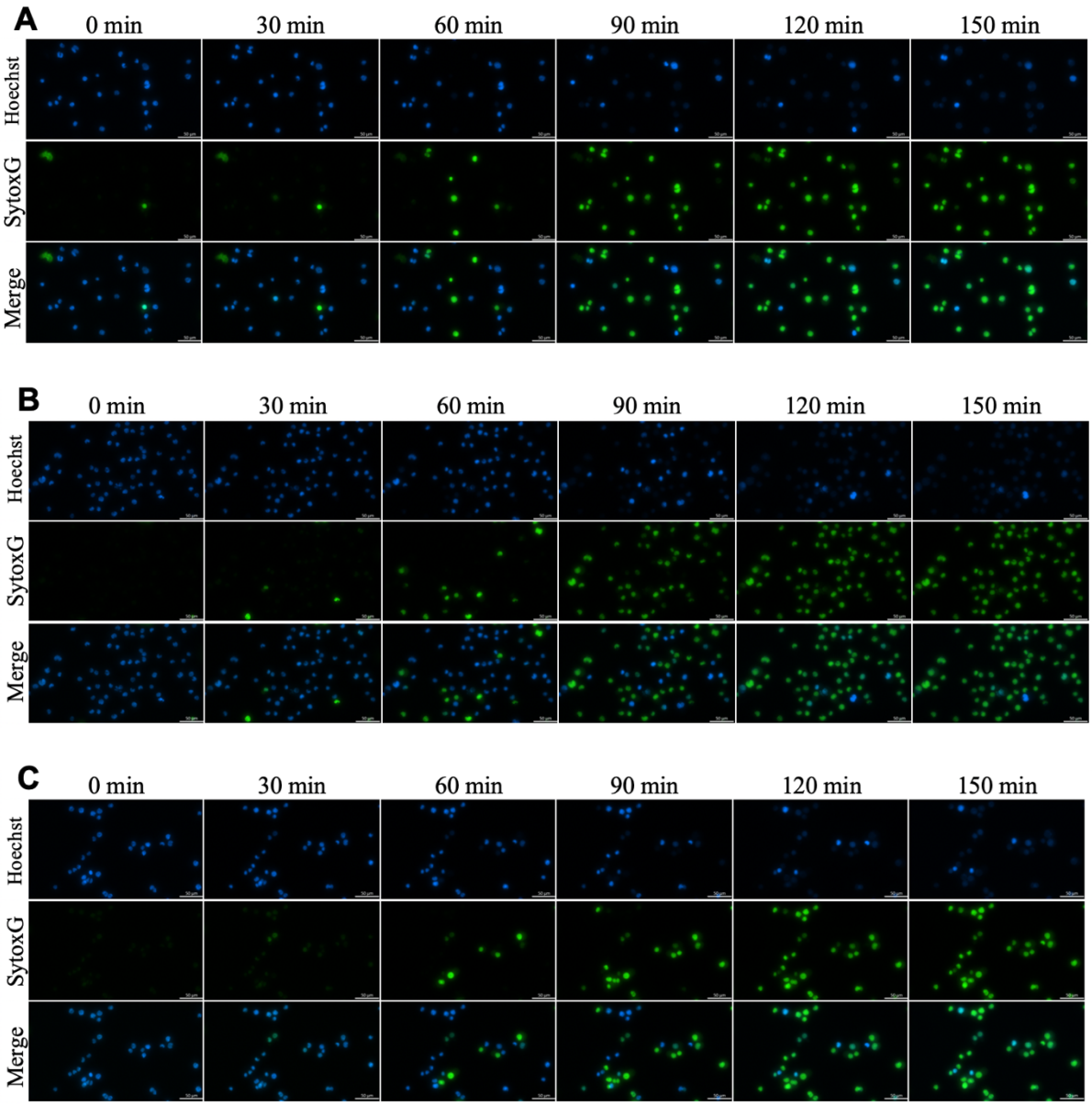


**Figure 6.5.** Live cell imaging of Kcl-22 cells pre-treated with ATRA for 5 days for the visualisation of cells during NET formation. Cells were stained with hoechst and SYTOX green and stimulated with PMA **(A)** or IO **(B)**, or not stimulated **(C)**. Shown are images captured at the start and every 30 min until 150 min after stimulation. Images were acquired and analyzed by Zeiss AxioObserver Z1 microscope and ZEN 2012 (blue version) software and figures were made using ImageJ v.2.1.0 (Fiji). Scale bars: 50 µm.

## 6.2 ELISA

**Table 6.1 ELISA plate layout**

| | | | | | | | | | | | |
|---|---|---|---|---|---|---|---|---|---|---|---|
| Blank | Blank | CML1 HBSS | CML1 HBSS | HD2 HBSS | HD2 HBSS | 1 Ctr HBSS | 1 Ctr HBSS | 2 Ctr HBSS | 2 Ctr HBSS | 3 Ctr HBSS | 3 Ctr HBSS |
| 0.156 ng/ml | 0.156 ng/ml | CML1 PMA | CML1 PMA | HD2 PMA | H23 PMA | 1 Ctr PMA | 1 Ctr PMA | 2 Ctr PMA | 2 Ctr PMA | 3 Ctr PMA | 3 Ctr PMA |
| 0.313 ng/ml | 0.313 ng/ml | CML2 HBSS | CML2 HBSS | HD2 HBSS | HD2 HBSS | 1 Abl HBSS | 1 Abl HBSS | 2 Abl HBSS | 2 Abl HBSS | 3 Abl HBSS | 3 Abl HBSS |
| 0.625 ng/ml | 0.625 ng/ml | CML2 PMA | CML2 PMA | HD2 PMA | HD2 PMA | 1 Abl PMA | 1 Abl PMA | 2 Abl PMA | 2 Abl PMA | 3 Abl PMA | 3 Abl PMA |
| 1.25 ng/ml | 1.25 ng/ml | CML3 HBSS | CML3 HBSS | 1 Ctr HBSS | 1 Ctr HBSS | 1 Pon HBSS | 1 Pon HBSS | 2 Pon HBSS | 2 Pon HBSS | 3 Pon HBSS | 3 Pon HBSS |
| 2.5 ng/ml | 2.5 ng/ml | CML3 PMA | CML3 PMA | 1 Ctr PMA | 1 Ctr PMA | 1 Pon PMA | 1 Pon PMA | 2 Pon PMA | 2 Pon PMA | 3 Pon PMA | 3 Pon PMA |
| 5 ng/ml | 5 ng/ml | CML3 HBSS | CML3 HBSS | 1 Abl HBSS | 1 Abl HBSS | 1 Pon HBSS | 1 Pon HBSS | 2 Abl HBSS | 2 Abl HBSS | 2 Pon HBSS | 2 Pon HBSS |
| 10 ng/ml | 10 ng/ml | CML3 PMA | CML3 PMA | 1 Abl PMA | 1 Abl PMA | 1 Pon PMA | 1 Pon PMA | 2 Abl P MA | 2 Abl PMA | 2 Pon PMA | 2 Pon PMA |

**Table 6.2 Raw data (optical density) for MPO concentrations**

| | | | | | | | | | | | |
|---|---|---|---|---|---|---|---|---|---|---|---|
| 0.0106 | 0.0115 | OverS | OverS | 2.1605 | 2.1347 | 0.0101 | 0.009 | 0.0105 | 0.0103 | 0.0149 | 0.0297 |
| 0.0434 | 0.0354 | OverS | OverS | 1.7375 | 1.7449 | 0.0091 | 0.0129 | 0.012 | 0.0079 | 0.0285 | 0.0896 |
| 0.0828 | 0.0805 | OverS | OverS | 0.8676 | 0.9339 | 0.013 | 0.0119 | 0.012 | 0.0108 | 0.0232 | 0.0338 |
| 0.1724 | 0.1476 | OverS | OverS | 0.0474 | 0.0444 | 0.0119 | 0.012 | 0.0099 | 0.0154 | 0.0157 | 0.0147 |
| 0.3785 | 0.3691 | 1.9244 | 1.9533 | 0.0164 | 0.0144 | 0.0144 | 0.0129 | 0.012 | 0.0134 | 0.0139 | 0.014 |
| 0.7741 | 0.7119 | 2.4279 | 2.6767 | 0.0064 | 0.0137 | 0.0147 | 0.013 | 0.0131 | 0.0133 | 0.0135 | 0.0126 |
| 1.1829 | 1.3673 | 1.696 | 1.7055 | 0.0136 | 0.0126 | 0.0131 | 0.0126 | 0.0129 | 0.0126 | 0.0117 | 0.0122 |
| 2.568 | 2.4365 | 0.1739 | 0.225 | 0.014 | 0.0133 | 0.0135 | 0.012 | 0.0125 | 0.0126 | 0.0115 | 0.0125 |

ELISA plate layout from supernatants from cells stimulated with PMA or unstimulated (HBSS). Blue – Standard. Green – Primary neutrophils isolated from CML 1, CML 2, CML 3, HD 2. Yellow – ATRA treated Kcl-22 cells (Numbers 1-3 represents the separate experiment). Grey – supernatants from coverslips treated with DNAse I.

## 6.3 Quantification of band size intensity after immunoblot analysis

After immunoblot analysis of Kcl-22 control or pre-treated with ATRA cells treated for one hour with the TKIs ponatinib or ABL001, the band size intensity was measured. Quantification of phospho-BCR-ABL1 and total BCR-ABL1 expression was performed based on three independent experiments after TKI treatment. The band intensities were analysed using Image Lab (BioRad) and calculated relative to c-Abl expression (Fig. 4.14 B). The band intensities were analysed for a total of three membranes (Fig. 6.6).

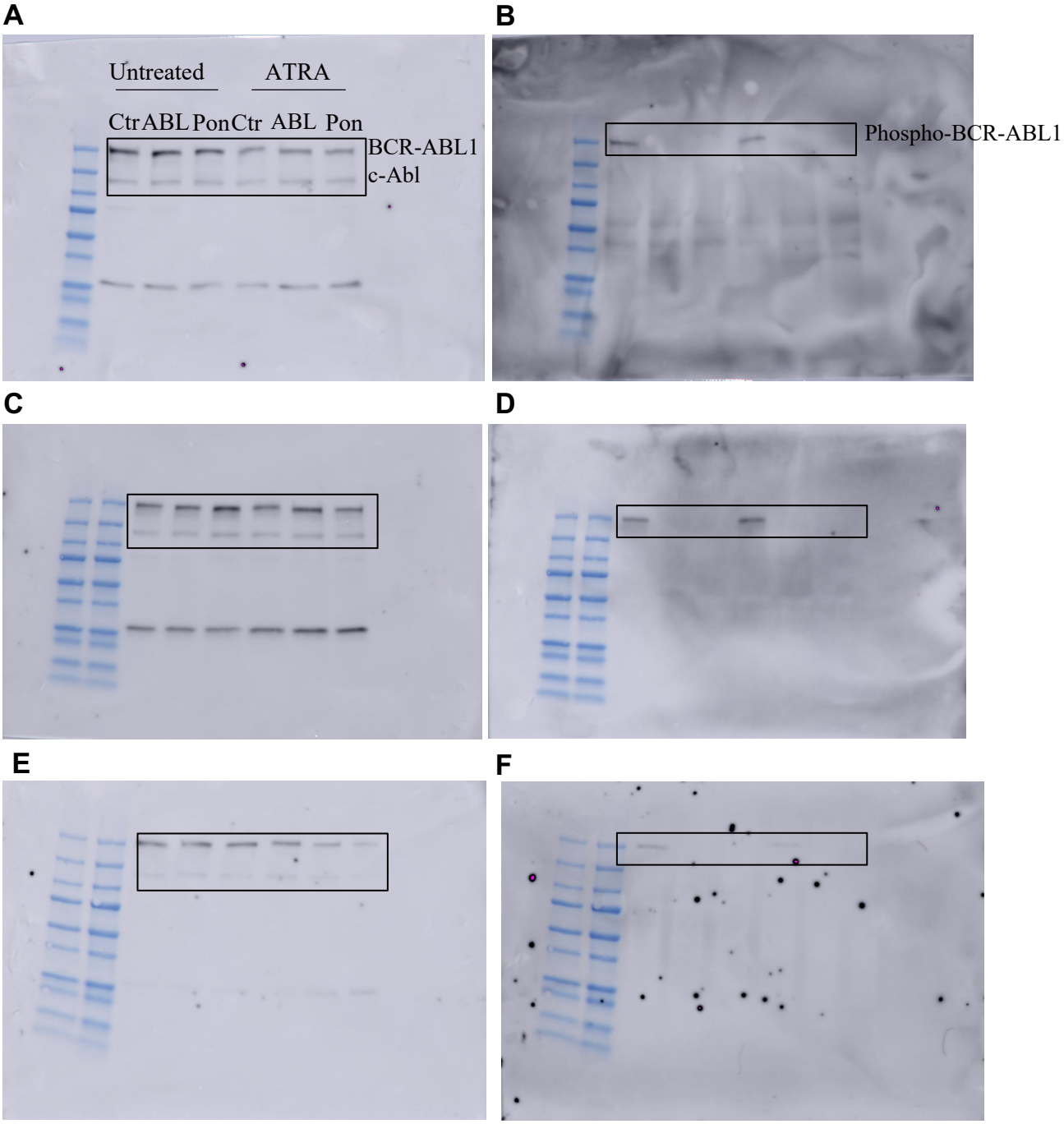


**Figure 6.6.** Full images of the immunoblots for BCR-ABL1, c-Abl and phosphor-BCR-ABL1 expression in Kcl-22 cells (control and pre-treated with ATRA) treated with TKIs. Boxes marks areas for band intensity quantification. Band intensity values of BCR-ABL1 and phospho-BCR-ABL1 relative to c-Abl were analysed using Image Lab (BioRad) based on three separate experiments. **(A, C, E)** BCR-ABL1 and c-Abl. **(B, D, F)** Phospho-BCR-ABL. (A and B are from experiment 1, C and D from experiment 2 and E and F from experiment 3).

## 6.4 NET formation in Kcl-22 cells after TKI treatment

Immunofluorescence was performed on Kcl-22 cells after TKI treatment to study if the affected BCR-ABL1 activity influenced the capability of these CML cells to form ETs. Control Kcl-22 cells or Kcl-22 cells pre-treated with ATRA for five days were treated for 1 hour with ponatinib or ABL001 or untreated. The cells were then stimulated with PMA for one hour compared to non-stimulated cells before fixed and stained using antibodies against neutrophil elastase (NE) and citrullinated histone H3 and counterstained with DAPI. Individual images are shown in Figure 6.7 and 6.8.

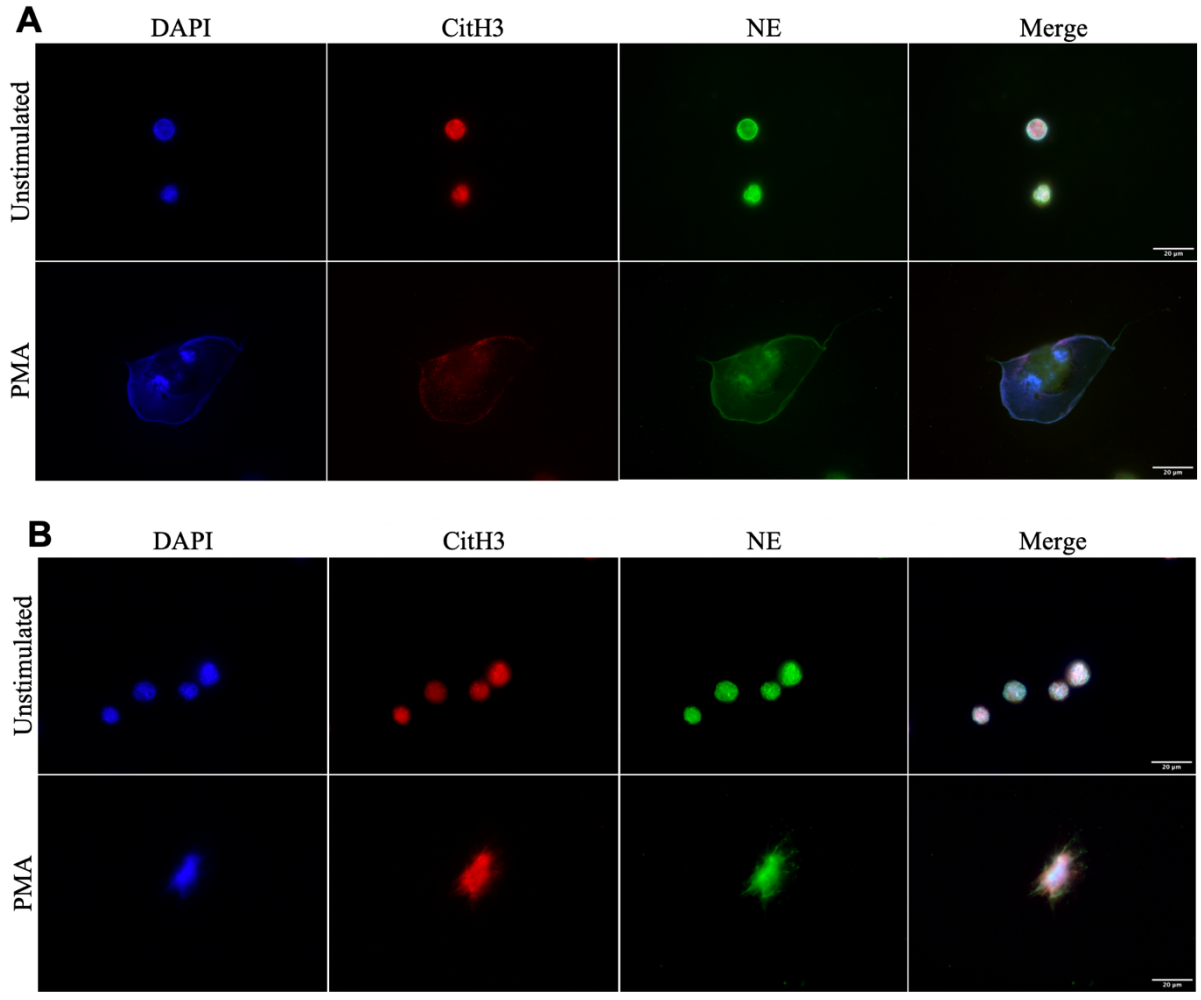

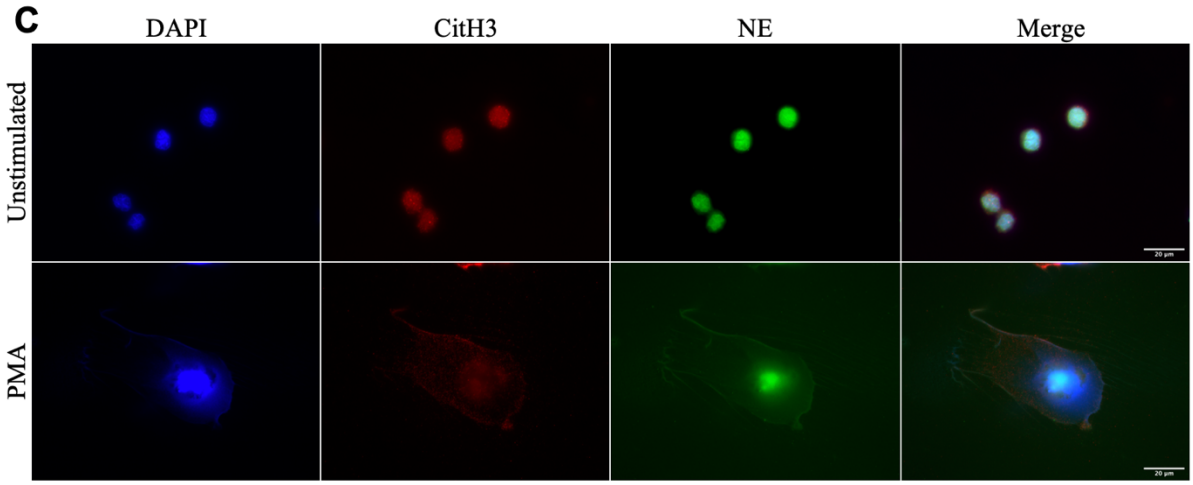


**Figure 6.7.** Induction of ET formation in ATRA pre-treated Kcl-22 cells treated for 1 hour with the tyrosine kinase inhibitors ABL001 **(B)** or ponatinib **(C)** or not treated with any TKI **(A)**. Cells were stimulated with PMA or not stimulated for 3 hours before they were fixed and stained with anti-H3 (red) antibodies, anti-NE (green) antibodies and counterstained with DNA binding fluorescence compound DAPI (blue). Images were acquired and analyzed by Zeiss AxioObserver Z1 microscope and ZEN 2012 (blue version) software and figures were made using ImageJ v.2.1.0 (Fiji). Scale bars: 20 µm.

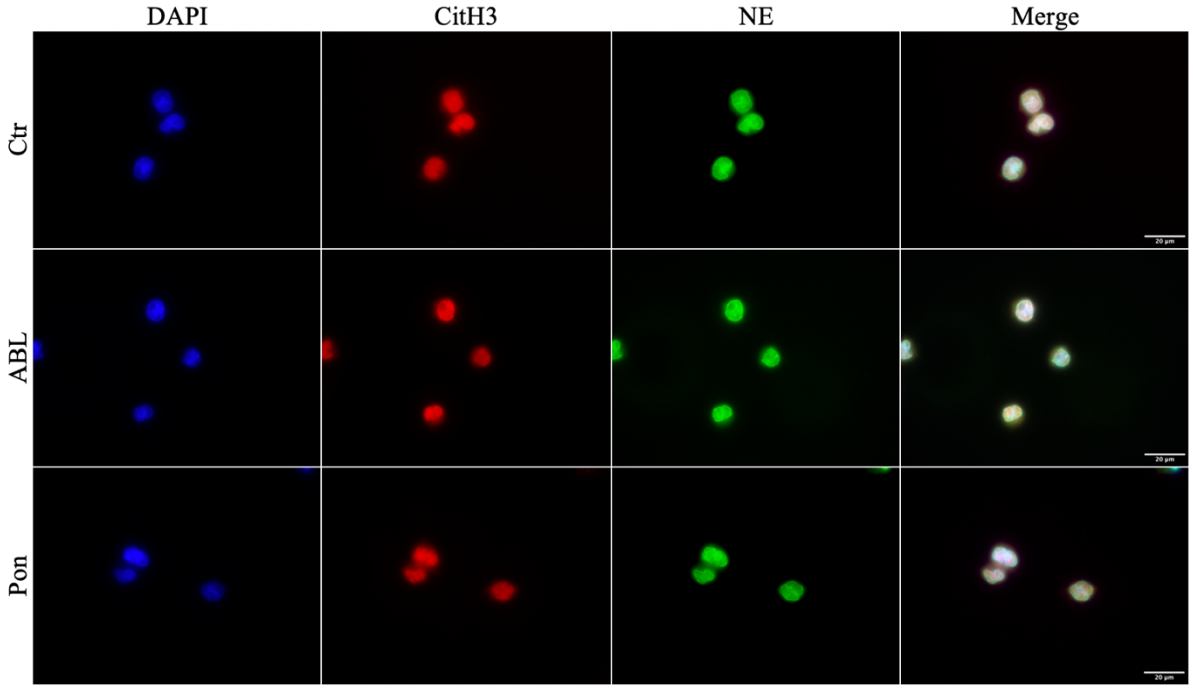


**Figure 6.8.** Induction of ET formation in Kcl-22 cells treated for 1 hour with the tyrosine kinase inhibitors ABL001 (ABL) or ponatinib (Pon) or not treated with any TKI (Ctr) and stimulated with PMA. Cells were fixed and stained with anti-H3 (red) antibodies, anti-NE (green) antibodies and counterstained with DNA binding fluorescence compound DAPI (blue). Images were acquired and analyzed by Zeiss AxioObserver Z1 microscope and ZEN 2012 (blue version) software and figures were made using ImageJ v.2.1.0 (Fiji). Scale bars: 20 µm.